Spring 2009

An exergy-based analysis of gasification and oxyburn processes

Ryan James Dudgeon
University of Iowa

AN EXERGY-BASED ANALYSIS OF GASIFICATION AND OXYBURN PROCESSES

by

Ryan James Dudgeon

A thesis submitted in partial fulfillment
of the requirements for the
Master of Science degree in Mechanical Engineering
in the Graduate College of
The University of Iowa

May 2009

Thesis Supervisor: Professor Lea-Der Chen

Graduate College
The University of Iowa
Iowa City, Iowa

CERTIFICATE OF APPROVAL

_____

MASTER'S THESIS

_____

This is to certify that the Master's thesis of

Ryan James Dudgeon

has been approved by the Examining Committee
for the thesis requirement for the Master of Science
degree in Mechanical Engineering at the May 2009 graduation.

Thesis Committee: _____
Lea-Der Chen, Thesis Supervisor

_____
Albert Ratner

_____
H.S. Udaykumar

ACKNOWLEDGMENTS

The author wishes to thank his family for their continued support during the writing of this thesis – his mother for her encouragement for continuing his education, his sisters for putting up with him spending two additional years as a student, and his late father, who never accepted anything less than an A from him in school. The author also wishes to thank Dr. L.D. Chen for his ideas, guidance, and endless patience.

ABSTRACT

An exergy analysis on gasification and oxyburn processes has been conducted. Equilibrium modeling in Aspen Plus© was used to develop a methodology for evaluating different fuels for gasification based on exergy analysis. The exergetic efficiency of gasifying a fuel strongly depended on the carbon boundary point, which is the equivalence ratio limit at which all carbon is converted to gaseous products in an adiabatic system. When evaluating a fuel for gasification, it is important to consider if the temperature of the carbon boundary point falls below 1050 K, which is also the temperature that the water-gas shift reaction begins to favor CO_2 and H_2. It was found that the rational efficiency, a common exergetic efficiency used in the literature, remained relatively unchanged at equivalence ratios past the carbon boundary point. A different exergetic efficiency, termed the gas efficiency, was proposed that showed better variance to the equivalence ratio and related better to the desired operation of the gasifier. It is shown that an oxyburn process can be used to decrease the energy requirement of capturing CO_2 if it is run closer to stoichiometric. Flue gas recirculation was investigated as a means to improve gasification efficiency, lower the reactor temperature of coal gasification, and capture CO_2. It was found that a higher percentage of flue gas must be recirculated back to the gasifier if flue gas from combustion with pure O_2 is used instead of air. Using flue gas recirculation allowed the gasifier equivalence ratio to be increased without solid carbon in the products. Increasing the equivalence ratio also resulted in a slight increase in the maximum achievable exergetic efficiency of the gasifier. Finally, an internal combustion engine model was developed based on closed-system thermodynamics and successfully integrated with the open-system realm of Aspen Plus.

TABLE OF CONTENTS

LIST OF TABLES

Table

LIST OF FIGURES

Figure

CHAPTER 1: INTRODUCTION

1.1 Motivation

Global climate change, which is largely a result of greenhouse gas emissions, as well as a global increase in demand and price of fossil fuels have recently become serious environmental and energy policy issues. Much of the electricity in the United States is generated by burning coal and natural gas. Coal contains significant amounts of sulfur and other toxins such as mercury, and natural gas is a valuable and often economically volatile finite natural resource; both emit large amounts of carbon dioxide into the atmosphere. Energy policy can become more environmentally-sustainable and a decreased amount of natural resources can be purchased from politically unstable foreign regions by developing renewable energy systems domestically. Biomass is one such renewable resource that has the potential to significantly replace coal and natural gas in smaller-scale energy applications. As a carbon-neutral fuel, biomass also contains less sulfur and toxins than its coal counterpart. Additionally, gasification is an energy conversion method that is gaining increased attention over direct combustion of solid fuels. Gasification can be integrated with combined heat and power plants and allows for the separation of undesirable components contained in solid fuels as well as the potential for carbon dioxide capture.

The University of Iowa has recently taken numerous steps to become a more sustainable campus. Chief among them is a bold initiative to make its Oakdale research campus completely powered by renewable energy in the near future. The purpose of the Oakdale Renewable Energy Plant would be to generate and supply steam, chilled water, and electricity to the research campus while demonstrating multiple, locally-based energy conversion technologies. These processes include gasification of biomass to produce syngas, production of biogas from anaerobic digesters, and capture and transport of biogas from the Iowa City landfill. In particular, the University of Iowa Utilities and

Energy Management has recently decided that an internal combustion engine of about 1.5 MW would be most appropriate for generating electricity from these combined gaseous fuels.

1.2 Specific Objectives

The main purpose of this research study was to use exergy analysis to develop a methodology for evaluating different fuels for gasification while comparing the effectiveness of gasifying three fossil fuels and three biomass fuels. A second objective was to develop an internal combustion engine model capable of predicting engine performance parameters that could be incorporated into the open system-based software Aspen Plus. A third objective was to perform an exergy analysis on oxyburn processes, including an investigation of flue gas recirculation and a comparison between two different gas separation processes for capturing CO_2.

CHAPTER 2: BACKGROUND

2.1 Biomass

Biomass is a biorenewable resource derived from organic material of biological origin (Brown, 2003). The cell walls of both woody and herbaceous (non-woody) biomass consist of lignocellulose, or fiber, which is composite structural material formed by plants that consists of variable amounts of cellulose, hemicellulose, and lignin.

The properties of biomass are defined by the material composition and heating value. The proximate analysis reports the moisture content, fixed carbon, volatile matter, and ash on a mass basis and is determined by heating the material under controlled conditions. Volatile matter is the fraction of substance that decomposes and escapes as gases upon heating at moderate (about 400°C) temperatures in a non-oxidizing environment. The remaining fraction is a mixture of fixed carbon and ash; the fixed carbon is determined by oxidation to carbon dioxide so that the non-combustible ash remains. The ultimate analysis reports the weight percent of carbon, hydrogen, nitrogen, oxygen, sulfur, chlorine, moisture, and ash of the substance.

The composition and heating value of biomass are vastly different from those of coal. Biomass contains about 35% less carbon than coal, and as a result, heating values of biomass are 20 – 30% lower than coal. Biomass also contains a larger percentage of oxygen, and in general, chemically bonded oxygen is partly responsible for the lower heating values of biomass (Brown, 2003).

The moisture and ash content of biomass are important factors when evaluating it as a fuel. In a gasification reactor, where drying is the first stage of conversion, biomass with high moisture content consumes otherwise useful heat to evaporate the liquid water, thereby causing less efficient gasification. Osowski and Fahlenkamp (2006) state that feedstocks with up to 50% moisture content can be successfully gasified. However, depending on the plant scale, the use of a dryer may be necessary prior to gasification for

feedstocks with higher moisture contents. Because ash is non-combustible material, feedstocks with higher ash contents have lower energy values. In addition, the specific composition of the ash is also important because it can affect the physical properties of the reactor and composition of the producer gas. Elements such as potassium, chlorine, sulfur, and heavy metals can cause high temperature corrosion of reactor components (Liao et al., 2007). In addition, elements such as chlorine and sulfur form acidic gases such as HCl and H_2S which must be cleansed from the product stream.

The heating value is the net energy released upon oxidizing a fuel under isothermal conditions. There are two heating values reported in the literature, the higher heating value (HHV) and lower heating value (LHV). The higher and lower heating values are often termed respectively the gross calorific value and net calorific value. The higher heating value pertains to reaction products containing condensed liquid water, while the lower heating value refers to products containing water vapor. The difference between the higher and lower heating values is the contribution of latent heat of vaporization of water.

2.2 Gasification

Gasification is a thermal process that converts a solid fuel into a combustible gas, often termed producer gas, which can be subsequently used to produce chemicals or liquid fuels or can be burned in a gas turbine or gas engine. In contrast to combustion, which occurs at fuel-lean conditions, gasification is a process that takes place at very fuel-rich conditions. Fuel-air equivalence ratios of 4 to 5 are typical, representing 20% to 25% of the theoretical amount of air required for complete combustion. The process is normally operated at temperatures in the range of 700 – 1000°C, and the produced gas, termed producer gas, is mainly composed of carbon monoxide, hydrogen, methane, nitrogen, and carbon dioxide. Other products exiting the gasifier include char and slag.

Char is un-reacted solid carbonaceous fuel, and slag is melted ash, although dry ash can also exit the gasifier if the temperature is low enough (Rezaiyan, 2005).

Thermal conversion in a gasification reactor occurs in a series of sub-processes, namely heating and drying, pyrolysis, solid-gas reactions, and gas-phase reactions (Higman, 2003). Because the fuel and oxidant typically enter the reactor from different locations, the fuel is first exposed to a high-temperature region deplete of oxygen. At this stage the fuel is quickly heated and dried as the moisture evaporates from the dry matter. Pyrolysis begins around 300°C, occurs in an absence of oxygen, and consists of the initial decomposition of long-chain organic matter into intermediate products (Brown, 2003). These products include char, gases such as hydrogen, carbon monoxide, carbon dioxide, and light hydrocarbons, as well as condensable vapors such as water, acetic acid, acetone, and heavier hydrocarbons known as tars. As these intermediate products move out of the pyrolysis region and become exposed to oxidant, solid-gas and gas-phase reactions occur in parallel, the most important of which are listen in Table 2-1. The first two reactions are highly exothermic and are important in supplying the heat required for drying, pyrolysis, and the two main endothermic reactions that produce CO and H_2.

The composition of the producer gas depends on several factors, one of them being the oxidant used. If air is the oxidizing agent, the producer gas will be diluted with nitrogen, thus lowering the heating value of the stream. Pure oxygen can be used as an oxidant, but separation of oxygen from air or water can be costly. Steam is often admitted to the gasifier in addition to air or pure oxygen in order to more directly control the producer gas composition through the water-gas shift reaction. Nitrogen dilution can be avoided through indirectly-heated gasification in which combustion and pyrolysis are separated. Char from the gasifier, an external fuel source, or a portion of the fuel is burned in a combustor, and the heat is transferred to the gasifier to supply the necessary energy for endothermic reactions (Phillips, 2007). In this way the products of combustion

that contain a large amount of nitrogen do not mix with the producer gas, and the heating value is increased.

Three common types of gasification reactors are updraft, downdraft, and fluidized bed. In an updraft, or countercurrent gasifier, fuel is admitted from the top of the reactor, oxidant from the bottom, and the product gas leaves through the top. Because the top of the reactor is mainly occupied by product gas, this region is deplete of oxygen and thus forms the pyrolysis zone. The area at the bottom of the reactor that contains more oxidant is the main site of exothermic gas-char reactions, which in turn produce heat for the endothermic reactions occurring at the center and top of the reactor. In a downdraft, or co-current gasifier, fuel and product gas move in the same downward direction. Fuel is again admitted from the top of the unit, oxidant enters at the middle, and the producer gas exits the bottom of the reactor. Again the top of the gasifier contains little oxygen thus forming a pyrolysis zone. The oxidant is typically admitted using an arrangement of nozzles in a converging throat region of the reactor. It is in this high-temperature region that exothermic reactions dominate, and as the primary pyrolysis products pass through, the heavier hydrocarbons and tars crack, or thermally decompose, into lighter gases and hydrocarbons. As a result, downdraft gasifiers emit the least amount of tars of the three. In a fluidized bed gasifier, oxidant flows upward through a region of floating particulate material consisting of the fuel and char. The fuel is typically added at the height of the bed, and the product gas is pushed out the top of the reactor. The fluidized bed is a region of high fluid turbulence that ensures the mixture is almost uniform in composition and temperature, and as a result, gasification occurs throughout the mixture, and there are no separate regions for pyrolysis, exothermic, and endothermic reactions. Fluidized bed gasifiers employ a freeboard space above the bed where additional char consumption and tar cracking occur, and secondary air is sometimes injected for these purposes.

2.3 Tar

Tar is loosely defined as organic condensable compounds formed in thermochemical reactions (Kinoshita, 1994). Tars are a major problem for gasification because they condense downstream from the gasifier, leading to fouling and plugging of filters, valves, heat exchangers, and other plant components (Cao et al., 2006). Tar contained in producer gas is normally reported in grams per standard cubic meter (g/m^3) or as a weight percent of biomass feed (Devi et al., 2003).

Much interest has been shown in the literature to adopt a universally-accepted classification system to more accurately describe tars. Evans and Milne (1987) suggested classifying tar as primary, secondary, and tertiary. They defined primary tars as cellulose-, hemicellulose-, and lignin-derived compounds; these are the products that are initially broken down at lower gasification temperatures. Secondary tars were characterized by phenolics and olefins and appear at intermediate gasification temperatures. Tertiary products included polycyclic aromatic hydrocarbons (PAH) and methyl derivatives of aromatics that are formed at higher gasification temperatures.

Van Paasen and Kiel (2004) developed a more detailed classification system consisting of five classes. They defined Class 1 tars as undetectable compounds but hypothesized that they mostly consist of primary and secondary tar species. Class 2 consisted of heterocyclic components with high water solubility such as phenol, pyridine, and cresol. Class 2 was made up of 1-ring PAH and light hydrocarbons that are not important in condensation and water solubility issues. Examples include xylene, styrene, and toluene. Class 4 consisted of 2- and 3-ring light PAH. These compounds, such as naphthalene, fluorene, and phenanthrene, condense at relatively high concentrations and intermediate temperatures. Class 5 consisted of heavy PAH with four or more rings that condense at higher temperatures and low concentrations (van Paasen, 2004).

Elliot (1988) reviewed biomass pyrolysis products and gasifier tars and proposed a general tar formation pathway as shown in Figure 2-1. The mechanism in Figure 2-1 is

in agreement with the primary, secondary, and tertiary classification system of Evans and Milne. The initial formation of primary tars at low temperatures leads to secondary tars at intermediate temperatures. Secondary tars finally form tertiary tars at the higher gasification temperatures.

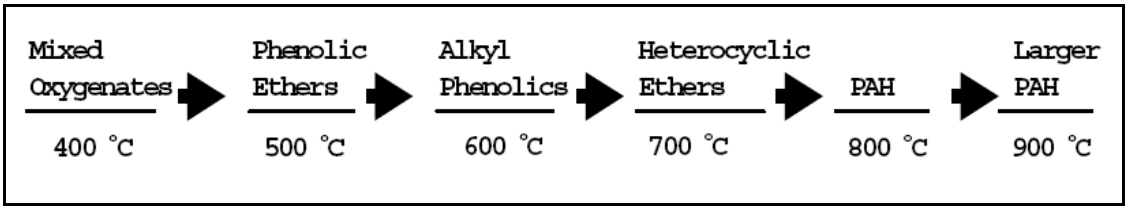

Figure 2-1: General temperature-dependent tar formation pathway.

Source: Elliot, D.C. 1988. "Relation of reaction time and temperature to chemical composition of pyrolysis oils," ACS Symposium Series 376, Pyrolysis Oils from Biomass. Edited by E.J. Soltes and T.A. Milne. Denver, CO. April 1987.

Evans and Milne (1997) studied the effects of time, temperature, and oxygen content on the maturation of tar products. When increasing the temperature from 500 to 1000°C, they found that the primary tar products were destroyed before the tertiary products appeared. The primary tar level was at a maximum at 500°C, and the tertiary tar level was at a maximum at 1000°C. They also found that the level of secondary tars peaked at about 750°C, at which point the primary and tertiary tars were at a minimum. These results complement those of Elliot (1988) in describing the temperature effects of tar formation.

The amount of tar contained in producer gas depends on the gasifier type and a variety of conditions. A review of biomass gasification studies by the National Renewable Energy Laboratory found a vast range of reported tar levels that spanned two

orders of magnitude (Milne et al., 1998). One reason for the spread in data can be attributed to the many definitions of tar being used in the literature and differences in sampling procedures. As a result, there has been a strong initiative in the scientific community to adopt a universally-accepted standard for tar definition and sampling procedures. There does appear to be a trend in tar levels with respect to gasifier type, with updraft gasifiers having the lowest levels of tar, updraft the highest, and fluidized beds in between. Milne et al. (1998) stated very general tar levels of 100 g/m^3 for updraft gasifiers, 10 g/m^3 for fluidized bed gasifiers, and 1 g/m^3 for downdraft gasifiers.

Kinoshita et al. (1994) used a bench-scale fluidized bed biomass gasifier to measure tar formation against temperature and equivalence ratio. They found that tar yields and tar concentrations increased from 700 to 750°C but then declined as the temperature was further raised to 900°C. Oxygen-containing compounds, of which phenol was most abundant, existed in significant quantities only at temperatures below 800°C. Increasing the temperature increased the amounts of three- and four-ring compounds, while the levels of one- and two-ring compounds decreased. Two exceptions to this trend were benzene and naphthalene, both of which increased with increasing temperature. The study concluded that higher temperatures favor the formation of fewer aromatic tar species without substituent groups.

Morf et al. (2002) studied tar formation in the absence of oxygen with a laboratory reactor. They produced a pyrolysis gas with a high content of primary tar and sent it through a reactor to study the effects of temperature on homogeneous tar conversion. They found that the total tar yield after homogeneous tar conversion increased from 500°C to 600°C. It peaked at 600°C before steadily decreasing as the reactor temperature increased to 1000°C. They observed that yields of primary tars decreased with increasing reactor temperature and found that acetol and acetic acid were the most abundant of these compounds. A definitive trend was not observed for secondary tar compounds, but phenol and cresol were quantitatively the most abundant

species of this group. Negligible amounts of tertiary tars were present at temperatures below about 800°C, but levels of these compounds increased substantially with further increasing temperature. In addition, naphthalene was found to be the most dominant of the tertiary tar compounds.

The major problem with tar species is their condensation downstream of the gasifier which leads to fouling of other components. Van Paasen and Kiel (2004) discussed the tar dewpoint as being the most important factor in handling producer gas. They combined experimental results from a fluidized bed wood gasifier with a model for the calculation of tar dewpoints to propose a different method of evaluating gasification tar. Using vapor/liquid equilibrium data from 29 common tar compounds, they found that the tar species with the highest dewpoints were the heavy PAH that have 4 or more rings. As a result, the most important factor influencing tar condensation was the concentration of the heaviest tar compounds, namely those of Classes 4 and 5, and not necessarily the total concentration of tar contained in the producer gas. As the temperature increased from 759 to 955°C, the total tar concentration in the producer gas decreased from 54.1 to 11.8 g/m^3. However, the tar dewpoint increased from 194 to 220°C, owing to an increase in concentration of heaviest Class 5 tar compounds from 466 to 1522 mg/m^3.

2.4 Producer Gas Cleanup

When producer gas exits the gasifier, the combustible portion of the gas is contaminated with particulate matter, acidic and toxic gases, and tar. For almost all end-use gas applications, these substances must be removed through gas cleaning processes.

The size of particulate matter exiting the gasifier covers a wide distribution of diameters and is typically reported in milligrams per standard cubic meter (mg/m^3). Fine particulate matter is a respiratory health hazard, making it stringently environmentally regulated. In addition, end-use applications of producer gas cannot tolerate high levels of

particulates. Hasler and Nussbaumer (1999) cited maximum particulate loading of producer gas of 50 mg/m^3 for internal combustion engines and 30 mg/m^3 for gas turbines. Many stable toxic gases emitted from the gasifier are also environmentally regulated, including ammonia (NH_3), hydrogen sulfide (H_2S), hydrogen cyanide (HCN), hydrochloric acid (HCl), nitrogen oxides (NO_x), and sulfur oxides (SO_x) (Cummer and Brown, 2002). Some of these gases, especially alkali vapors, can also be corrosive to equipment downstream of the gasifier. The fouling of equipment by condensing tars has already been mentioned, but there are also restrictions on tar levels for utilization in gas engines and gas turbines. Hasler and Nussbaumer (1999) stated a maximum tar concentration of 100 mg/m^3 for internal combustion engine use. Milne et al. (1998) suggested that tar levels be less than 10 mg/m^3 for gas engines and less than 5 mg/m^3 for gas turbines.

2.5 Internal Combustion Engines Fueled by Producer Gas

Internal combustion engines can be economically more attractive for producing power than gas turbines in smaller gasification plants. Unfortunately little progress has been made in the last couple decades in optimizing internal combustion engines for producer gas (Porpatham et al., 2007). Producer gas can be substituted in an engine designed for either gaseous fuels such as methane or liquid fuels such as gasoline, although the former is more common. Two companies that have specifically targeted the market for producer gas-fueled engines are Caterpillar and GE, which now owns the Jenbacher engine line. Caterpillar manufactures a line of engines designed for low-energy gases, and Jenbacher is widely known for their engines that run on a wide range of fuels from producer gas to digester-derived biogas.

The two most important factors that change the operation of engines fueled by producer gas are the heating value and the combustion kinetics of the fuel. Producer gas has a heating value of 3 to 6 MJ/m^3, while natural gas has a heating value of about 36

MJ/m^3. The combustion kinetics determine the laminar flame speed and the autoignition delay time of the fuel-air mixture, which are two of the most important thermochemical properties affecting engine performance and pollutant emissions. The laminar flame speed is the velocity of the unburned gases entering the combustion zone in the direction normal to the combustion zone (Heywood, 1988). At a temperature of 298 K and pressure of 1 atm, hydrogen, methane, and carbon monoxide have laminar burning velocities of approximately 190, 40, and 25 cm/s, respectively (Ilbas et al., 2006; Frassoldati et al., 2007). Given the disparity between the burning velocity of hydrogen and that of carbon monoxide and methane, the flame in an internal combustion engine will propagate much faster for a syngas mixture than for natural gas. The autoignition delay time is the time required for a mixture to spontaneously ignite at some prescribed conditions (Hernandez et al., 2006). Dependant only on chemical kinetics, the autoignition delay time is commonly measured using a fixed volume of fuel-air mixture.

Hernandez et al. (2005) used an equilibrium gasification model to determine producer gas compositions of biomass based on five gasification equivalence ratios ranging from 3.0 to 5.0. The producer gas compositions were then used as input to the chemical kinetics software Chemkin to study the laminar flame speed of fuel-air mixtures as a function of gasifier and engine equivalence ratio, temperature, and pressure. The simulations were computed using the GRI-Mech 3.0 chemistry set, which has been verified in the literature to accurately model the combustion kinetics of producer gas mixtures. The computational results were verified through comparison to experimental results obtained from pressure-development data of a spherical combustion bomb. It was found that the laminar flame speed increased with increasing temperature, decreased with increasing pressure, and showed a maximum for a gasifier equivalence ratio of 3.5, where the H_2 and CO mole fractions were highest. In addition, it was found that increasing amounts of water vapor in the producer gas decreased the laminar flame speed. Finally,

under typical engine conditions, the laminar flame speed of producer gas mixtures was found to be greater than that of methane and less than that of isooctane.

Hernandez et al. (2006) used the same producer gas compositions as Hernandez et al. (2005) in Chemkin to study the autoignition delay time of fixed-volume fuel-air mixtures based on gasifier and engine equivalence ratios, temperature, pressure, and fuel composition. The autoignition delay time was found to decrease exponentially with increasing temperature. The minimum autoignition delay time occurred with a gasification equivalence ratio of 3.5, at which point the concentration of H_2 in the fuel was at a maximum.

Natarajan et al. (2007) studied the effects of composition, equivalence ratio, and CO_2 dilution on the laminar flame speed of H_2-CO mixtures. Experimental data of premixed flames were compared to computational results of GRI-Mech 3.0 and a H_2/CO mechanism. The laminar flame speed was found to increase linearly with increasing equivalence ratios. H_2:CO ratios of 5:95, 50:50, and 95:5 were studied, and results showed that the laminar flame speed increased with increasing H_2 fraction. In addition, the laminar flame speed decreased by as much as 25% as the percentage of CO_2 dilution was increased from 0 to 20%.

The literature contains limited research concerning the operation of engines running on syngas. Sridhar et al. (2001) experimentally studied the effects of compression ratio on performance of a spark-ignited engine running on producer gas. They modified a direct injection diesel engine with a rated output of 28 kW and a compression ratio of 17 into a spark ignition engine that could operate at compression ratios of 11.5, 13.5, 14.5 and 17. The fuel had a volume composition of 19% H_2, 19% CO, 2% CH_4, 12% CO_2, and the remainder N_2. Results showed that both the work output and fuel-to-electricity efficiency increased with increasing compression ratio. Maximum power was obtained for equivalence ratios in the range of 1.00 – 1.06, although higher overall efficiencies could have been achieved by operating at leaner

conditions. It was found that the optimum spark timing decreased by 10 degrees before top-dead-center as the compression ratio increased from 11.5 to 17. It was also determined that a higher fraction of hydrogen in the fuel had a significant effect on the spark timing, since increasing the fraction of hydrogen increased the burn rate, which meant that the spark timing had to be closer to top-dead-center. Sridhar et al. (2001) concluded that it was technically feasible to operate spark-ignited engines on producer gas at higher compression ratios while avoiding knocking because producer gas is diluted with inert CO_2 and N_2.

Tinaut et al. (2006) developed a two-zone thermodynamic engine model to predict performance of a producer gas-fueled spark ignited engine. They presented a factor called the Engine Fuel Quality (EFQ) that is dependent on heating value, stoichiometric air-fuel ratio, and volume correction factor that can be used to quantitatively predict engine performance. The EFQ factor for a typical producer gas was about two-thirds of that of either a liquid fuel such as isooctane or gaseous fuel such as methane, and thus an engine fueled with producer gas would have a power output of two-thirds that of a primary fuel.

Munoz et al. (2000) experimentally investigated the operation of a gasoline spark-ignited engine running on producer gas. The engine under consideration had a compression ratio of 8.2 and maximum power of 6.6 kW at 3600 RPM. The producer gas came from a downdraft gasifier fed with agricultural and forestry residues and contained 14% H_2, 22% CO_2, 3% CH_4, and 47% N_2. It was found that although the producer gas had a lower heating value that was about one-tenth that of gasoline, the reduction in power was only about a factor of one-half.

Ahrenfeldt (2006) experimentally compared the performance of a spark-ignited engine running on producer gas and natural gas. Tar-free producer gas was generated from a downdraft gasifier fed by wood chips, and the fuel was fed to a 3-cylinder, high compression ratio, 17.5 kW spark-ignited engine. The study found that the lean burn

limit of the engine running on natural gas occurred at an excess air ratio of 1.8, while the lean burn limit for producer gas was 3, suggesting that producer gas is an excellent lean burn fuel. The effects of ignition retarding on performance and NO_x emissions were also investigated. At all load conditions, retarding the ignition resulted in increased power and efficiency, as well as decreased NO_x emissions. Furthermore, a combustion analysis was performed using in-cylinder pressure measurements to determine the variation of pressure curves and mass burn fractions for consecutive cycles. The slope of mass burn fraction, representing faster combustion, was found to be steepest for fuel mixtures with the highest H_2 content. The variation in maximum mass burn fractions for consecutive cycles was also determined to be relatively small, suggesting that producer gas can be successfully used at higher compression ratios.

2.6 Exergy

An exergy analysis is a fundamental tool for evaluating processes and systems. Exergy analysis is a combination of the First and Second Laws of Thermodynamics and accounts for irreversibilities. Exergy, or availability, can be defined as the potential to do work (Moran, 1989). More particularly, exergy is the maximum amount of work that can be achieved as a state of matter comes into equilibrium with its environment. The environment is assumed to be large and homogeneous in temperature, pressure, and composition, and it acts as a source or sink of internal energy without change to its intensive properties (Moran and Shapiro, 2008). The environment is represented by temperature T_∞ and pressure p_∞, and is also referred to as the dead state. Exergy is generally divided into two parts, the thermomechanical contribution and the chemical contribution. Thermomechanical exergy, or physical exergy, is the maximum amount of work that can be achieved by a state of matter as it comes into thermal and mechanical equilibrium with the environment. Neglecting kinetic and potential energy contributions,

the molar specific physical exergy of a species at temperature T and pressure p is defined by

$$\bar{e}^{ph} = \left[\bar{h}(T) - \bar{h}(T_\infty)\right] - T_\infty\left[\bar{s}(T, p) - \bar{s}(T_\infty, p_\infty)\right] \quad (2\text{-}1)$$

where $\bar{h}$ and $\bar{s}$ are the molar specific enthalpy and molar specific entropy, and the subscript ∞ denotes the state of the environment.

Chemical exergy is the maximum work potential of a substance at the dead state as it comes into chemical equilibrium with the environment (Moran, 1989). Because it is evaluated at the dead state, chemical exergy does not have a thermal component to it, thus differentiating it from physical exergy. Additionally, specification of chemical exergy requires that the chemical composition of the environment be specified as well. Szargut et al. (1988) defined the process for choosing the reference state for evaluation of chemical exergy. For every element, a reference species should be chosen that is most abundant and most stable in the environment. For example, the reference species for carbon is CO_2, the reference species for hydrogen is H_2O, the reference species for sulfur is SO_2, etc. In addition, the reference species fall into three groups: gaseous components of the atmosphere, solid substances of the Earth's crust, and ionic and nonionic substances of the oceans. For oxidation reactions relating to combustion and gasification, the composition of the atmosphere is most important, and the mole fractions of each reference species in the environment must be specified. The composition of the atmosphere varies with location and altitude, but the partial pressures of the reference species are easily measured, and average values near the Earth's surface are typically used. However, the amount of water vapor in the atmosphere is a continually changing parameter. Szargut et al. (1988) presented a mean partial pressure of water vapor based on a mean relative humidity of 0.7 at 298.15 K. At these conditions and with a dead state pressure of 101.325 kPa, the resulting mean partial pressure of water vapor in the environment was 2.2 kPa.

The chemical exergy of a substance can be defined by considering a reaction in which the substance at the dead state reacts with species contained in the environment such that the products consist solely of species found in the environment (Moran and Shapiro, 2008). Once all chemical elements of the substance are contained in species found in the environment, all the chemical potential of the substance to perform work has been liberated. The chemical exergy is thus the change between the chemical potential of the original substance and the chemical potential of the products. An example for a substance containing only C, H, N, and O is illustrated by Equation 2-2, where the reactant oxygen is supplied by the environment.

$$C_\alpha H_\beta N_\delta O_\zeta + \left(2\alpha + \frac{\beta}{2} - \zeta\right) O_2 \rightarrow \alpha CO_2 + \frac{\beta}{2} H_2O + \frac{\delta}{2} N_2 \tag{2-2}$$

The derived molar specific chemical exergy $\bar{e}^{ch}$ of the substance results in Equation 2-3

$$\bar{e}^{ch} = -\Delta G_{rxn}(T_\infty, p_\infty) + \bar{R} T_\infty \ln\left[\frac{\left(y_{\infty,O_2}\right)^{(2\alpha+\beta/2-\zeta)}}{\left(y_{\infty,CO_2}\right)^{\alpha}\left(y_{\infty,H_2O}\right)^{\frac{\beta}{2}}\left(y_{\infty,N_2}\right)^{\frac{\delta}{2}}}\right] \tag{2-3}$$

where ΔG_{rxn} is the change in Gibbs free energy of the reaction, $\bar{R}$ is the molar universal gas constant, and y is the mole fraction.

Components of an ideal gas that are also a part of the environment, such as N_2, CO_2, and O_2, also have a chemical exergy that is dependant on their partial pressure and the partial pressure of the component in the environment. For such gases, the molar chemical exergy is given by Equation 2-4 (Szargut et al., 1988).

$$\bar{e}_j^{ch} = \bar{R} T_\infty \ln \frac{p_j}{p_j^\infty} \tag{2-4}$$

where p_j is the partial pressure of species j.

The temperature and pressure of the environment vary by location and time. As a result, the concept of standard chemical exergy was introduced by Szargut et al. (1988) so that chemical exergy values could be compiled and used for multiple exergy analyses.

The standard chemical exergy is computed with Equation 2-4 with standard temperature and pressure (298.15 K and 101.325 kPa) as the environment conditions. Table 2-2 lists several species pertinent to this work and their standard chemical exergies. The chemical exergy of a gas stream of multiple components can be computed by summation of their partial chemical exergies, as given by Equation 2-5.

$$\bar{e}^{ch} = \sum y_j \bar{e}_j^{ch} + \bar{R} T_\infty \sum y_j \ln y_j \tag{2-5}$$

It should be noted that the chemical exergy of the mixture is always lower than the sum of its components, since the second term of Equation 2-5 represents the entropy of mixing and is always negative.

Equation 2-3 cannot be applied to many solid technical fuels such as biomass and coal because of lack of thermochemical property data. Szargut et al. (1988) proposed a statistical method for representing the chemical exergy of fuels. They used regression equations to approximate the ratio ψ between the specific chemical exergy and the lower heating value of fuels based on the O/C, H/C, N/C, and S/C ratios of the substance, as used in Equation 2-6.

$$\psi = \frac{e^{ch}}{LHV} \tag{2-6}$$

Two ratios relevant to this work are presented in Equations 2-7 and 2-8. Equation 2-7 is applicable to solid C, H, O, N compounds, and Equation 2-8 is applicable to bituminous coal, lignite, coke, and peat (Szargut et al., 1988).

$$\psi = \frac{1.044 + 0.0160\frac{H}{C} - 0.3493\frac{O}{C}\left[1 + 0.0531\frac{H}{C}\right] + 0.045\frac{N}{C}}{1 - 0.4124\frac{O}{C}} \tag{2-7}$$

$$\psi = 1.0437 + 0.1896\frac{H}{C} - 0.2499\frac{O}{C} + 0.0428\frac{N}{C} \tag{2-8}$$

The dependence of the ratio ψ on the S/C ratio could not be found for solid organic compounds, but Szargut et al. (1988) proposed a modification to the correlation using the

standard chemical exergy of sulfur. Accounting for the moisture and ash content as well, the standard specific chemical exergy of a solid fuel was proposed as

$$e^{ch} = (LHV_{fuel} + \Delta H_{vap,H_2O} z_{H_2O})\psi + (e_S^{ch} - HHV_S) z_S + e_{ash}^{ch} z_{ash} + e_{H_2O}^{ch} z_{H_2O} \qquad (2\text{-}9)$$

where $\Delta H_{vap,H_2O}$ is the enthalpy of water vaporization, z_{H_2O} is the water mass fraction in moist fuel, e_S^{ch} is the standard specific chemical exergy of solid sulfur, HHV_S is the higher heating value of sulfur, z_S is the sulfur mass fraction, z_{ash} is the ash mass fraction, and e_{ash}^{ch} is the chemical exergy of the ash, which is typically neglected (Szargut et al., 1988).

2.7 Exergy Analysis of Combustion and Gasification Processes

Many studies in the literature have focused on exergy analyses of power and chemical production plants consisting of complex systems of processes. Fewer studies have focused on the exergy analysis of the gasification process alone. Prins et al. (2003) studied the exergetic efficiency of an adiabatic equilibrium reactor model fed by a generic biomass. They computed the physical and chemical exergy of the product gas as well as any leftover char. They introduced the carbon boundary point, which is the temperature or equivalence ratio at which all solid carbon is oxidized into the gaseous state, leaving no solid carbon in the product stream. It was found that the optimum point of operation was located at the carbon boundary point. In addition, it was found that gasification using atmospheric-pressure steam is more efficient than using air when the exergetic losses of generating steam are not considered.

Prins and Ptasinski (2005) studied the exergetic losses of an adiabatic equilibrium reactor model of solid carbon reacting with air. They used equilibrium constants to compute equilibrium products and quantified the exergetic losses associated with product mixing, chemical reactions, heating of the fuel, and heating of the air. They found that the exergetic efficiency again peaked at the carbon boundary point, and losses

contributed by heating the fuel and mixing of the products were insignificant. The losses associated with the chemical reactions and heating of the air were more significant, and as the system became more fuel-lean, more air had to be heated to the reactant temperature, and as a result the overall efficiency decreased. The exergetic losses of the gasifier were plotted against the air-to-fuel ratio, as shown in Figure 2-2. These results concluded that reaction of solid carbon at rich conditions was more efficient than at lean conditions, making gasification a much more efficient conversion process than combustion.

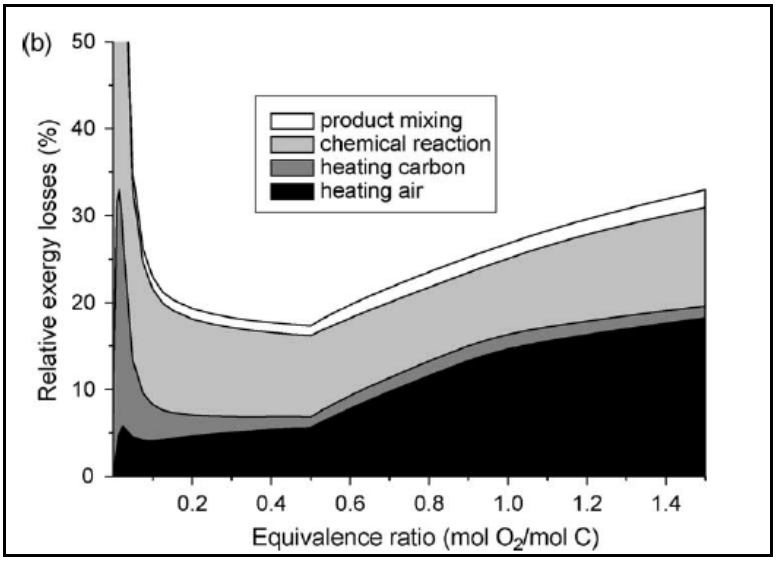

Figure 2-2: Exergy losses of adiabatic carbon reactor vs. equivalence ratio.

Source: Prins, M.J. and Ptasninski, K.J. (2005). Energy and exergy analyses of the oxidation and gasification of carbon. *Energy 30,* 982 – 1002.

Prins et al. (2007) used an equilibrium gasification model to study the effects of biomass and coal composition on the exergetic efficiency of a plant. The gasifier was

oxidized by mixtures of pure oxygen and steam, and the plant included a cryogenic separator for oxygen production, heat recovery system, and electricity production. The results showed that fuels with high oxygen-to-carbon (O/C) ratios resulted in larger exergy losses because of their high ratio of chemical exergy to lower heating value. In addition, these fuels had to be over-oxidized in the gasifier to reach the desired temperature. As a result, more oxygen was used than necessary for complete gasification, thereby causing thermodynamic losses. The effects of hydrogen-to-carbon (H/C) ratio were much less significant than the O/C ratio. It was also recommended that a gasification temperature of 927°C and fuel with O/C ratio less than 0.4 be used for high efficiency atmospheric pressure gasification.

Ptasinski et al. (2007) compared the exergetic gasification efficiency of coal, vegetable oils, straw, treated and untreated wood, grass/plants, sludge, and manure. They simulated the gasification process with an adiabatic equilibrium model, and special attention was paid to the O/C ratio of each fuel. The results showed that fuels with higher O/C ratios produced the lowest exergetic efficiencies because of the large amount of oxygen that had to be added to the gasifier to reach a temperature higher than that of the carbon boundary point. In terms of gasification efficiency based on lower heating value, all groups of biomass except sludge and manure could match the efficiency of coal. Sludge and manure had the lowest exergetic efficiencies because of their high moisture contents (33% and 44% respectively). As a result, more oxygen had to be added to generate heat to evaporate the moisture of the fuel. Ptasinski et al. (2007) then investigated the use of product gas enthalpy to dry very wet biomass fuels prior to gasification. They incorporated a dryer into the model and dried the sludge from 33% moisture to values from 30% to 11%. It was found that by drying the sludge to 19% moisture content, it was possible to reach gasification conditions in which no more oxygen was added than necessary for complete carbon oxidation. Although drying the

wet feedstock resulted in decreased physical exergy of the producer gas, the larger increase in chemical exergy resulted in increased exergetic efficiencies overall.

Table 2-1: Major gasification reactions and standard heats of reaction.

Reaction	Standard Enthalpy of Reaction
$C + \frac{1}{2}O_2 \leftrightarrow CO$	$\Delta H_{RXN} = -110.5\ kJ/mol$
$C + 2H_2 \leftrightarrow CH_4$	$\Delta H_{RXN} = -74.8\ kJ/mol$
$C + CO_2 \leftrightarrow 2CO$	$\Delta H_{RXN} = 172.4\ kJ/mol$
$C + H_2O \leftrightarrow H_2 + CO$	$\Delta H_{RXN} = 131.3\ kJ/mol$
$CO + H_2O \leftrightarrow H_2 + CO_2$	$\Delta H_{RXN} = -206.1\ kJ/mol$
$CO + 3H_2 \leftrightarrow CH_4 + H_2O$	$\Delta H_{RXN} = -41.1\ kJ/mol$

Table 2-2: Standard chemical exergy values of some common species.

Species	Standard Chemical Exergy (kJ/mol)
C (carbon graphite)	410.26
CO	275.10
CO_2	19.87
CH_4	831.65
H_2	236.1
H_2O (vapor)	9.5
H_2O (liquid)	0.9
N_2	0.72
O_2	3.97

CHAPTER 3: ASPEN PLUS© MODEL DEVELOPMENT

3.1 Introduction to Aspen Plus©

Modeling of the gasification process and combined heat and power simulations were performed using Aspen Plus©. Aspen© is a software suite composed of several chemical and thermodynamic process simulators. The main platform of this package is Aspen Plus©, which contains an extensive library of chemical and thermodynamic property data, as well as a wide array of unit operations.

Calculations in Aspen Plus© are performed by unit operation blocks. The Aspen Plus© Model Library contains several standard unit operations such as heat exchangers, separators, pumps, compressors, and reactors. In addition, Aspen Plus© allows for the capability to build custom unit operation models using Microsoft Excel© spreadsheets and Fortran code. Unit operation blocks are connected by material, heat, and work streams. Simulating a process involves three main steps. The first step requires setup of the flowsheet, in which the unit operation blocks are laid out and connected by desired streams. The second step consists of defining the chemical components of the simulation and specifying the temperature, pressure, flow, and composition of all streams. Finally, the operating conditions of the unit operation blocks are defined.

After all required input has been entered by the user, Aspen Plus© uses a sequential-modular method to solve material and energy balances. The software also offers many numerical methods and convergence options that the user can specify for more rigorous calculations. In addition, flowsheets can accommodate recycle streams, called “tear streams”, for which Aspen Plus© uses iterative numerical methods to converge on material and energy balance solutions.

3.2 Gasification Modeling

Gasification is a process that involves many complex reactions that depend on chemical kinetics, reactor geometry, and many other parameters. As a result, the

complexity of simulating gasification is simplified by modeling the process based on thermodynamic and chemical equilibrium. Equilibrium is a good assumption provided the residence time is long enough; however, in the case of most real world gasifiers this is not the case (Mathieu, 2002).

A reacting system is at its most stable composition at chemical equilibrium (Atkins, 2006). This state is achieved when the entropy of the system is maximized and its Gibbs free energy is minimized. Minimization of the Gibbs free energy of the products is the method used to calculate equilibrium in this work.

Aspen Plus© provides a unit operation model called RGIBBS that calculates chemical and thermodynamic equilibrium based on minimizing the Gibbs free energy of the system. The model allows specification of pressure, temperature, and heat duty so that constant pressure, adiabatic or constant temperature, constant pressure conditions can be specified. This gasification equilibrium model is considered to be zero-dimensional because the reactor is assumed to be perfectly mixed with no consideration of spatial parameters nor time. In actuality, different gasifier types have complex hydrodynamics that will cause the product gas composition to deviate from the equilibrium composition. In addition, the model assumes that reaction rates are fast enough and residence times are long enough to reach equilibrium. Gasification chemical kinetics consists of thousands of complicated chemical reactions, making it difficult to accurately represent gasification with a kinetic model. In addition, kinetic mechanisms for converting solid fuel, especially biomass, to primary products are not well known (Biagini et al., 2004). Therefore an equilibrium model allows for prediction of combustion and gasification products from complex technical fuels.

Components in Aspen Plus© are classified as either conventional or nonconventional. Conventional components are ones with property data contained in the Aspen© component database. Nonconventional components are non-homogeneous substances that do not have a consistent composition and are not contained in the Aspen©

component database. These components, which would include coal and biomass, must be given physical attributes, such as those defined by the ultimate, proximate, and sulfur analyses. Property methods must also be chosen to calculate the enthalpy and density of the substance. For this work, the property methods HCOALGEN and DCOALIGT were respectively chosen to calculate the enthalpy and density of biomass. These property methods use statistical correlations to calculate the specific heat, enthalpy, and density of coal and coal-derived substances based on the ultimate, proximate, and sulfur analyses. Because biomass can be represented as a technical fuel through these analyses, these property methods were also used for calculating the thermodynamic properties of biomass fuels. Furthermore, the property method HCOALGEN offers different options for how the enthalpy of formation of the component is calculated. For this work, the enthalpy of formation was calculated based on the higher heating value of the substance, which was specified by the user.

The equilibrium reactor RGIBBS does not accept nonconventional components as reactants. As a result, the fuel must be decomposed to conventional components so they can be used by the RGIBBS block. The conversion is accomplished with an RYIELD block, labeled DECOMP, which is a reactor model that generates products based on known yields. The fuel feed stream enters DECOMP where it is decomposed into its elemental constituents. A Fortran calculator script interacts with the RYIELD block such that decomposition of the fuel is calculated based on the proximate and ultimate analyses of the nonconventional component. The carbon content of the feed is converted to solid carbon graphite. The hydrogen, oxygen, nitrogen, chlorine, and sulfur are converted to gaseous H_2, O_2, N_2, Cl_2, and S. Finally the moisture content is converted to liquid H_2O. These species are now contained in an intermediate stream called INPROCES, which then become the reactants for the RGIBBS block. An air stream representing the gasifying oxidant also enters REACTOR, and a products stream exits it. The heat stream QDECOMP connect the DECOMP and REACTOR and represents the energy required to

decompose the solid fuel. Although QDECOMP interacts with REACTOR, the reactor is still considered to be adiabatic because DECOMP calculates the amount of heat required for decomposition and draws it from REACTOR. REACTOR is specified by a heat duty of zero and a given pressure. Because it is adiabatic, conservation of energy forces REACTOR to calculate the adiabatic reactor temperature for the products. Figure 3-1 depicts the process flowsheet for the adiabatic gasification reactor.

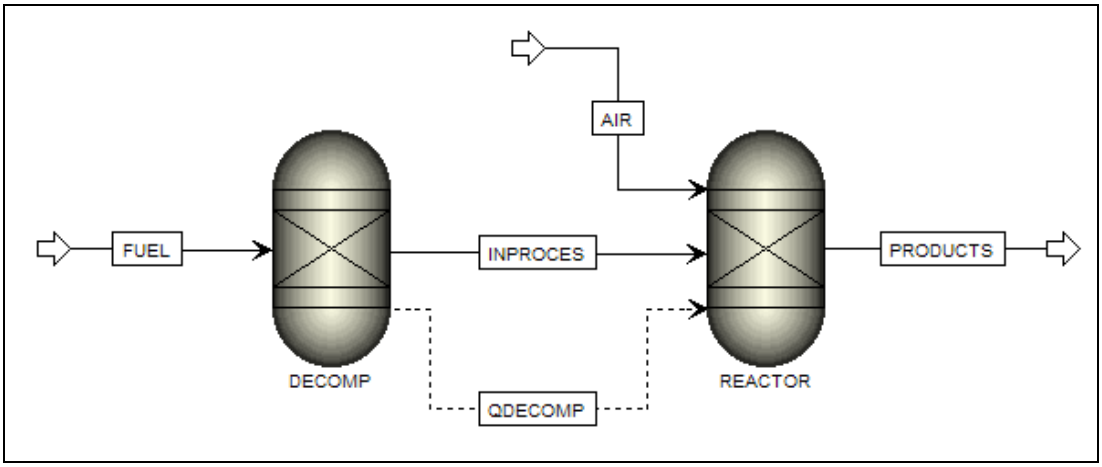

Figure 3-1: Aspen Plus© flowsheet of the adiabatic gasification model.

The gasification reactor shown in Figure 3-1 can be modified to a non-adiabatic, constant-pressure, constant-temperature reactor by adding an exiting heat stream QREACTOR to REACTOR. With pressure and temperature specified, REACTOR calculates the heat duty for the reaction. Figure 3-2 illustrates the non-adiabatic gasification reactor.

It was desired to incorporate the fuel ash into the model in a detailed manner to complete the thermodynamics of the system. Although real ash contains a mixture of individual metal elements and metal oxides, it was assumed that the ash contained only metal oxides. This assumption was made so that the mass fractions of the original ash

species could be calculated and incorporated into the model. The mass fractions were entered in the same FORTRAN calculator script that handled the decomposition of fuel into its elemental and molecular constituents. As a result, the intermediate DECOMP stream also contained metal oxides representing the fuel ash.

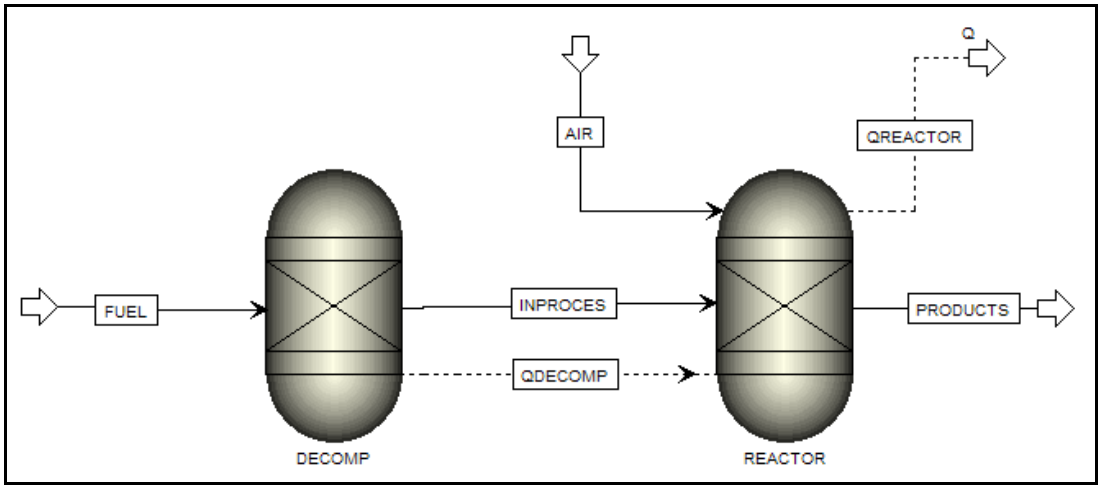

Figure 3-2: Aspen Plus© flowsheet of the non-adiabatic gasification model.

3.3 Gas Analyzer Custom Model

Aspen Plus© streams provide basic thermodynamic properties such as specific volume, enthalpy, and entropy based on the composition of the stream and property data retrieved from the Aspen Plus© property database. For simulation purposes, additional stream information was desired, including the higher and lower heating values, stoichiometric fuel-air ratio, and physical and chemical components of the flow exergy. A custom stream analyzer was built using a USER2 block, which is a blank model that allows the user to customize a unit operation block using either Fortran code or a Microsoft Excel© workbook. For this application an Excel© workbook was chosen to perform the calculations. The unit operation ANALYZE consists of one inlet stream and

one outlet stream. The model also includes a user array that contains a set of real variables which represent results calculated by the custom block. When the model is run, the USER2 block opens the specified Excel© file and transfers the inlet stream data to sheets within the workbook. The main function of the block lies within a separate worksheet in which all calculations are performed. Results are then sent to additional worksheets for output, and the Excel© file transfers the information back to Aspen Plus© to be viewed by the user. An example of the user array of results is shown in Figure 3-4.Because no manipulation of streams takes place between the inlet and outlet streams, all component mole flows and stream parameters of the inlet stream are directly copied to the outlet stream to maintain mass and energy balances.

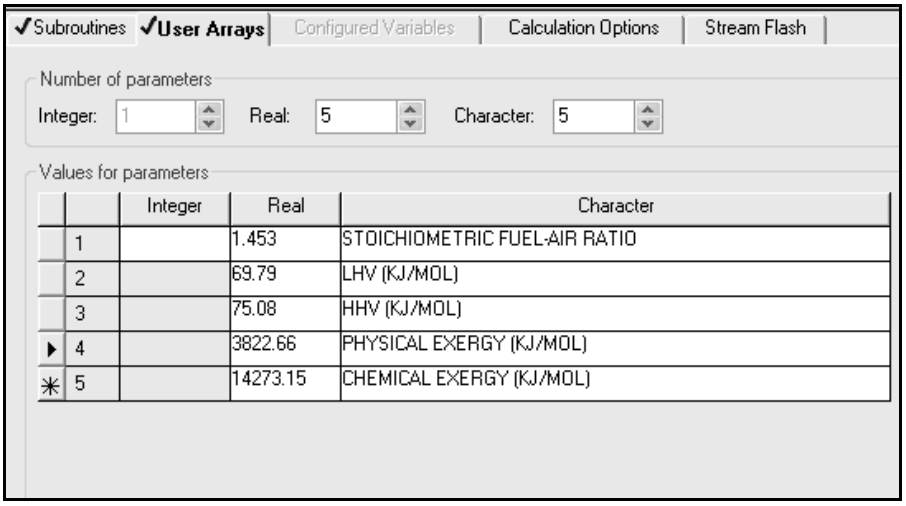

Figure 3-3: Aspen Plus© user array for ANALYZER block.

The block ANALYZER first calculates the higher and lower heating value of the stream based on the respective values of each component contained in the stream and its respective molar flow rate. ANALYZER then calculates the stoichiometric fuel-air ratio, which is the fuel-air ratio that results in complete combustion with the theoretical amount

of air. It is calculated based on the amount of carbon, hydrogen, and oxygen contained in the stream, which in turn is based on the number of carbon, hydrogen, and oxygen atoms of each component and its respective molar flow rate. Finally, the physical and chemical exergies of the stream are calculated. The physical exergy is determined based on Equation 2-1, and the chemical exergy is determined based on standard chemical exergies and Equation 2-5. After performing the calculations, the Excel© workbook passes the results back to Aspen Plus© to be viewed by the user.

3.4 Tar and Dryer Modeling

Two models not used in this work were created for the purpose of future simulation capabilities. The first was a gasification model that incorporates tar into the product gas. The purpose of this model was to allow for the capability to more accurately represent a tar-laden producer gas. The effects of the increased heating value of the gas on power production could then be simulated, or it could be used to predict tar condensation in other processes. The second model was a dryer that allowed for the capability to simulate drying solid fuels with high moisture contents.

Producer gas tar is composed of many heavy hydrocarbons that cannot be predicted by equilibrium models, including the RGIBBS block. As a result, it was desired to incorporate tar into the model so that the effects of increased heating value and tar condensation could be simulated. The basis of the model is to add a stream of tar species to the equilibrium products, and deduct that amount of mass from the original feed stream so that mass balances are satisfied. For this example, five tar species were chosen to represent the presence of tar in the product gas, although other species can be chosen as well. They included benzene, toluene, phenol, napththalene, and benz[a]anthracene.

To incorporate tar into the Aspen Plus© model, the gasification process flowsheet of Figure 3-2 was modified to add a tar stream to the gasifier products with a mixer

block, and the INPROCES stream was disconnected from the RGIBBS block. An additional material stream, FEED, was added to the flowsheet as the influent stream to block REACTOR. It was desired to take a portion of the mass of INPROCES to use as tar, leaving the remaining mass to enter REACTOR as reactants. The FEED stream reacts with the oxidant to produce equilibrium gasifier products, to which the tar stream is added to give a tar-loaded producer gas. The material disconnect between DECOMP and REACTOR is necessary to achieve an overall mass balance. The resulting flowsheet is depicted in Figure 3-4.

Stream TAR contains the representative tar species toluene, benzene, phenol, naphthalene, and benz[a]anthracene. Adding tar to the producer gas requires specification of the tar mass flow rate and the mass fractions of these five representative tar species. A Fortran calculator script was written to calculate the molar flows of carbon, hydrogen, and oxygen within the tar stream; these molar flows are subtracted from stream INPROCES in order to determine the species molar flows of stream FEED. In addition, the calculator script also set the temperature and pressure of stream TAR to be equivalent to those of stream PRODUCTS.

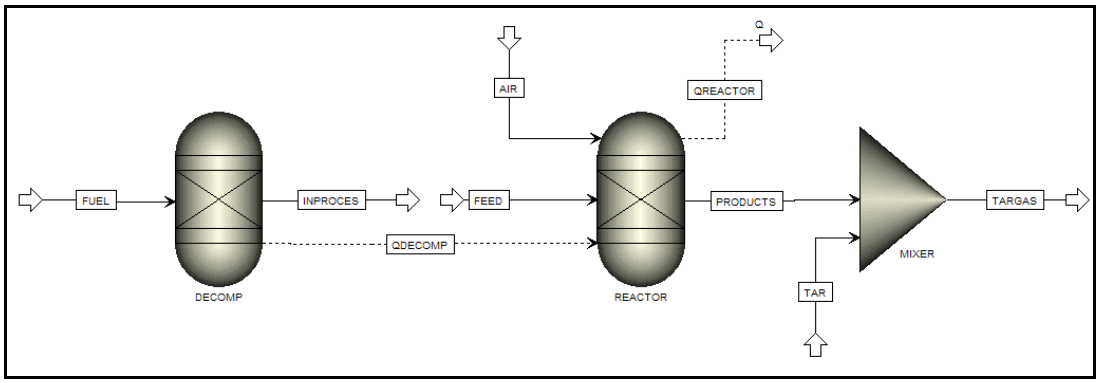

Figure 3-4: Aspen Plus© flowsheet of the gasification model with tar addition.

The dryer model is derived from one presented in a solids modeling tutorial by Aspen Technology and is based on satisfying mass and energy balances at steady state (Aspen Technology, Inc., 2000). It models the drying of a wet, nonconventional solid fuel by means of an intermediate temperature gaseous medium, and its purpose is to determine energy and flow requirements of the medium to meet moisture limits for the exiting fuel. The dryer is modeled using two unit operation blocks, RSTOICH and FLASH2, as depicted in Figure 3-5. The RSTOICH block labeled DRY-REAC serves as a reactor, in which a portion of the wet nonconventional solid reacts to form liquid water, and the moisture attribute of the fuel decreases. Stream MEDIUM is the drying medium at an elevated temperature. The stream labeled IN-DRYER that connects the two blocks contains a mixture of solid fuel and moist medium. The FLASH2 block labeled DRY-FLSH is used to flash this stream so that the dried fuel is separated from the moist exhaust. The dried fuel exits block DRY-FLSH through stream DRYFUEL, and the moist exhaust exits through stream EXHAUST. The apparent reaction that occurs within block DRY-REAC is simply a manipulation of the moisture attribute of the nonconventional solid's proximate analysis. The moisture attribute is decreased to a value input by the user, and the difference is converted to liquid water. The manipulation of the moisture attribute is accomplished via a Fortran script, and it is within this script that the user specifies the new moisture content of the dried fuel.

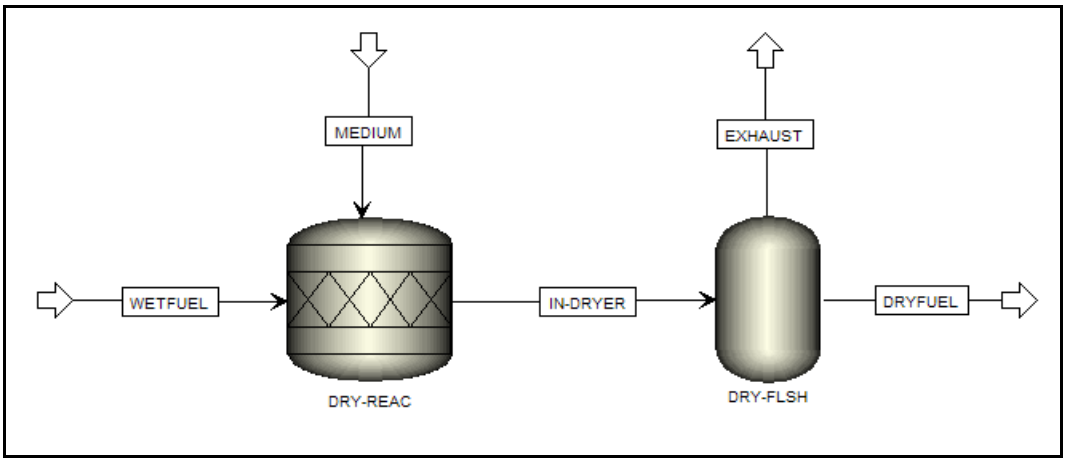

Figure 3-5: Aspen Plus© flowsheet of the dryer model.

CHAPTER 4: INTERNAL COMBUSTION ENGINE MODEL DEVELOPMENT

4.1 Introduction

Aspen Plus© is a popular tool in the energy and chemical processing industries. It contains all necessary blocks to fully simulate a combined heat and power plant, including expansion turbines for power production. However, as gas engines become more popular in the power production industry, especially for burning syngas, Aspen Plus© does not contain a standard model of this component in its library. The purpose of this chapter is to develop an internal combustion engine model based on closed-system thermodynamics and integrate it within the open-system realm of Aspen Plus©. The goal is to base this model on several gas engine parameters so that detailed operating conditions can be simulated. After explaining its development in this chapter, the model will be validated against a similar model from the literature.

4.2 Modeling Considerations

There are generally two mathematical methods for modeling internal combustion engines, fluid dynamic-based and thermodynamic-based (Bayraktar and Durgun, 2003). Fluid dynamic-based models rely on conservation of mass, energy, and species and are therefore multi-dimensional in nature. Because they require a detailed understanding of spatial distribution of fluid flow, temperature, and species composition within the cylinder, this type of model is not ideal for predicting engine performance parameters (Bayraktar and Durgun, 2003). Thermodynamic-based models are grounded on the First Law of Thermodynamics and treat the cylinder charge as a zero-dimensional system; spatial variations in fluid properties do not exist and time is the only independent variable. Because this type of model relies on thermodynamics, it is better suited for predicting engine performance parameters and emissions.

The model used in this work is thermodynamic-based and attempts to predict the performance of a commercial size spark ignition engine. The model includes the effects of heat transfer between the cylinder charge and cylinder wall but does not attempt to predict the effects of friction or mass leakage through crevices, both of which are phenomena experienced by real engines. As a result, the model predicts indicated performance parameters such as indicated power, and not brake-specific parameters, such as brake power. The cylinder charge is treated as a homogenous fuel-air mixture with no spatial variation in temperature or pressure, and all gases are assumed to be ideal. The model used in this work is also a four-stroke engine which is the type most often used in power production applications. The four-stroke engine cycle consists of two full engine revolutions in which intake, compression, expansion, and exhaust discharge occur. Work occurs during all four processes; the system performs work during the intake and expansion strokes, and work is done on the system during the compression and exhaust discharge strokes. The developed model disregards the intake and exhaust discharge strokes, because the intake and exhaust pressures are typically very comparable, and therefore the net work performed during these two processes is usually insignificant compared to the net work performed during the compression and expansion strokes.

4.3 Numerical Engine Model

The foundation of the model lies in solving for the cylinder pressure during the compression and expansion strokes. To determine the crank angle-dependant cylinder pressure, the First Law of Thermodynamics is combined with the ideal gas law to form Equation 4-1

$$\frac{dp}{d\theta} = -\gamma \frac{p}{V}\frac{dV}{d\theta} + \frac{\gamma - 1}{V}\left(\frac{dQ}{d\theta}\right) \tag{4-1}$$

where p is the pressure, V is the volume, γ is the specific heat ratio of the mixture, Q is the heat transfer interacting with the system, and θ is the crank angle.

Equation 4-1 requires equations for volume, heat release, and heat transfer as a function of crank angle. The instantaneous volume is dependent on piston-cylinder geometry as given by Equations 4-2 through 4-4.

$$V(\theta) = \frac{V_d}{r-1} + \frac{V_d}{2}\left[\left(\frac{2l}{s}\right) + 1 - \cos\theta - \left(\left(\frac{2l}{s}\right)^2 - \sin^2\theta\right)^{0.5}\right] \tag{4-2}$$

$$\frac{dV}{d\theta} = \frac{V_d}{2}\sin\theta\left[1 + \cos\theta\left(\left(\frac{2l}{s}\right)^2 - \sin^2\theta\right)^{-0.5}\right] \tag{4-3}$$

where

$$V_d = \frac{\pi}{4}b^2 s \tag{4-4}$$

In Equations 4-2 through 4-4, V_d is the displacement volume, r is the compression ratio, b is the cylinder bore, s is the stroke, and l is the connecting rod length

The heat transfer term is comprised of two parts, as shown in Equation 4-5. The first, Q_{comb}, is heat transfer to the system from combustion, and the second, Q_w, is heat transfer away from the system as a result of the temperature difference between the cylinder charge and the cylinder wall.

$$\frac{dQ}{d\theta} = \frac{dQ_{comb}}{d\theta} - \frac{dQ_w}{d\theta} \tag{4-5}$$

The rate of heat release from combustion depends on the mass burn rate, which is dependent on the chemical kinetics of the combustion process. However, a thermodynamic-based model of an internal combustion engine does not include chemical kinetics, and therefore the mass burn rate must be specified mathematically. There are two ways to define the mass burn rate, the first of which involves knowledge of the turbulent burning velocity, flame propagation area, and density of unburned mixture (Ramos, 1989). This method is difficult to use, however, because although correlations for the laminar burning velocity of fuel-air mixtures are widely available, relating the

laminar burning velocity to the turbulent velocity requires a fluid dynamic-based model. Calculation of the time-dependant flame propagation area requires detailed knowledge of the cylinder geometry and location of the spark plug. It is more common to specify the mass burn rate mathematically, for example with a Wiebe function, which is the method used for this model. The Wiebe function is defined by

$$x_b(\theta) = 1 - \exp\left[-a\left(\frac{\theta - \theta_s}{\theta_d} \right)^{\lambda} \right] \tag{4-6}$$

where x_b is the mass burn fraction, θ_s is the start of heat release (spark timing), θ_d is the duration of heat release or combustion duration, a is the Wiebe efficiency factor, and λ is the Wiebe form factor (Ferguson and Kirkpatrick, 2001). Figure 4-1 shows a typical Wiebe curve with efficiency factor of 5, form factor of 3, spark timing of -20°, and combustion duration of 30°.

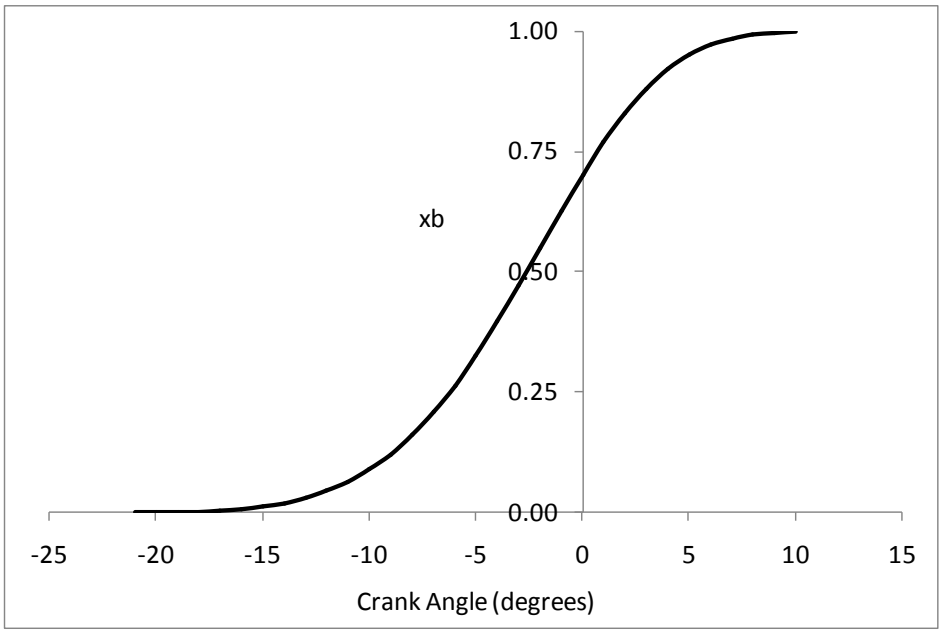

Figure 4-1: Mass burn fraction represented by a typical Wiebe curve.

The mass burn rate is the derivative of the mass burn fraction with respect to crank angle as given by Equation 4-7.

$$\frac{dx_b}{d\theta} = \frac{\lambda a}{\theta_d}(1 - x_b)\exp\left[\frac{\theta - \theta_s}{\theta_d}\right]^{\lambda-1} \tag{4-7}$$

The heat release rate is finally given by Equation 4-8

$$\frac{dQ_{comb}}{d\theta} = n^o_{fuel} LHV \frac{dx_b}{d\theta} \tag{4-8}$$

where n^o_{fuel} is the initial number of moles of fuel in the mixture and LHV is the lower heating value of the fuel.

The Wiebe parameters are usually selected to match experimental data. For the typical spark-ignited engine, Heywood (1988) recommended values of 5 and 3 for a and λ. These Wiebe parameters are important in that they determine the shape of the Wiebe curve. Steeper slopes and more compressed forms of the curve represent faster combustion. Faster combustion results in higher thermal efficiency as heat release approaches the ideal case of the Otto cycle, in which constant-volume heat release occurs. Deviations from the standard values of 5 and 3 for the Wiebe form and efficiency factors result in relatively insignificant changes in efficiency. The combustion duration has the largest effect on the Wiebe curve and thus the thermal efficiency. For a given combustion duration, the Wiebe form and efficiency factors merely change the steepest location of the Wiebe curve. Furthermore the literature does not contain any studies that have linked producer gas combustion to these two parameters. As a result, for this work the form and efficiency factors were fixed according to Heywood's recommendation of 5 and 3 respectively. This is a reasonable assumption because the thermal efficiency is much less sensitive to these two parameters compared to the combustion duration.

4.4 Combustion Duration

The combustion duration is probably the most important parameter affecting performance for an internal combustion engine model. However, it is difficult to predict, and experimental measurements of the combustion duration are preferred for engine simulation studies. The engine modeled developed in this chapter is meant to simulate combustion of producer gas. For this reason, the following is a discussion of how the combustion duration might be predicted for engines fueled by producer gas.

Combustion in a spark ignition engine results from a flame that propagates from burned products to the unburned fuel-air mixture. The process can be divided into two parts, the first of which is the flame development stage, which is initiated by the spark discharge. The two electrodes of the spark plug produce a small flame kernel which propagates outward in nearly-spherical form. The fraction of burned mass during this stage, which is also known as the ignition lag or delay, is quite small; it is usually considered to range from 1 to 5 percent of the total charge (Heywood, 1988). Once the highly turbulent flow field within the combustion chamber begins to affect the kernel, the spherical shape of the flame becomes highly distorted, and combustion proceeds at a much faster rate. This second stage of combustion is commonly referred to as the rapid-burning stage. The combustion duration comprises both stages of flame propagation, and both stages are represented well by the Wiebe curve.

The combustion duration is dependent on two factors, the distance that the flame must travel to burn the fuel-air mixture, and the speed at which it propagates. The distance the flame must travel depends on the cylinder geometry and size, including the spark plug location. Larger cylinders require that the flame propagate over a longer distance, thereby increasing the combustion duration. The speed of flame propagation is governed by the reaction kinetics occurring within the flame and the turbulent flow field within the cylinder. All the above phenomena are dependent on the mixture temperature and pressure, compression ratio, engine speed, fuel composition, and equivalence ratio.

That the combustion duration is dependent on so many factors makes it difficult to predict with a model.

Shrestha and Karim (2001) developed an analytical method to model the combustion duration of gas-fueled spark ignition engines and verified it against experimental results. The method is centered on the equivalence ratio, since the lean and rich operational equivalence ratio limits are associated with extremely long combustion periods, and there is an equivalence ratio at which the combustion duration reaches a minimum. The combustion duration was correlated to the equivalence ratio ϕ in the form of Equations 4-9 – 4-11.

$$\theta_d = C' \exp\left(\frac{\phi_{\min} - \phi}{\sqrt{\phi - \phi_l}}\right) + C'' \exp\left(\frac{\phi - \phi_{\min}}{\sqrt{\phi_r - \phi}}\right) \tag{4-9}$$

$$C' = \theta_{d,\min}\left[\frac{\sqrt{(\phi_{\min} - \phi_1)/(\phi_r - \phi_{\min})}}{1 + \sqrt{(\phi_{\min} - \phi_1)/(\phi_r - \phi_{\min})}}\right] \tag{4-10}$$

$$C'' = \frac{\theta_{d,\min}}{1 + \sqrt{(\phi_{\min} - \phi_1)/(\phi_r - \phi_{\min})}} \tag{4-11}$$

where $\phi_{\min}$ is the equivalence ratio for minimum combustion time, ϕ_l is the lean equivalence ratio limit, and ϕ_r is the rich equivalence ratio limit, and $\theta_{d,\min}$ is the minimum combustion duration. The minimum combustion duration can be observed from experimental data or can be correlated based on a number of engine operating conditions. If experimental data is not at hand, the authors report that for lean operation, even a small assumed value for $\theta_{d,\min}$ at the stoichiometric equivalence ratio can produce a reasonably accurate approximation for θ_d as a function of ϕ.

With no experimental data at hand, the minimum combustion duration can be approximated using a combination of data presented in the literature and a physical correlation. Experimental data on the combustion duration of engines fueled by alternative gaseous fuels is scarce. One of the few studies in this field is that of Li and

Karim (2006). The researchers used a single-cylinder, four-stroke, spark ignited CFR engine to examine the knock and combustion characteristics of CH_4, H_2, CO, and some of their mixtures. They reported experimental combustion duration results for CO-H_2 mixtures in the absence of diluents such as N_2 and CO_2. Because the presence of diluents prolongs the combustion duration, the results reported by Li and Karim (2006) are used as the basis for the minimum combustion duration $\theta_{d,\min}$ for the numerical engine model. These data however are not automatically transferable to the engine model because of differences in engine specifications and operational factors. The data of Li and Karim (2006) can therefore be manipulated with a correlation presented by Shrestha and Karim (2001). Shrestha and Karim (2001) proposed that the combustion duration can be approximated by Equation 4-12

$$\theta_d = C\frac{V_{st}^{1/3}}{r^{1/2}}S_F S_p^{1/3} \tag{4-12}$$

where C is a constant that depends on the cylinder geometry and spark plug location, V_{st} is the cylinder volume at spark timing, S_F is the flame speed, and S_p is the mean piston speed. Equation 4-12 can be used to predict how the combustion duration data reported by Li and Kari would transfer to the model-based engine. Several works in the literature (Hernandez et al., 2005; Natarajan et al., 2007) can be used to approximate the flame speeds required by Equation 4-12.

The literature contains a large amount of research on the equivalence ratio limits or flammability limits of alternative gaseous fuels. These define the lean and rich limits at which a flame can be sustained in a fuel-air mixture. Wierzba et al. (1996) presented lean and rich flammability limits of a variety of mixtures of diluent gaseous fuels. Fuels included CH_4, CO, and H_2, and diluents included N_2 and CO_2. Data provided by Wierzba et al. (1996) in the form of volume percent of fuel can be converted to equivalence ratio limits and used to predict the parameters of Equations 4-9 – 4-11.

Finally, the minimum combustion duration can usually be assumed to occur at the stoichiometric equivalence ratio, making $\phi_{\min}$ equal to 1.0 (Shrestha and Karim, 2001). Before proceeding, a few points should be noted about the prediction of the combustion duration. First, it should be restated that there is a significant lack of experimental data reported in the literature on the combustion duration of alternative gaseous fuels. Second, the procedure for predicting the combustion duration contains many assumptions and approximations that should not be considered to be accurate by any means. The development of this scheme serves to approximate the variation of the combustion duration with respect to changing values of key operational engine parameters such as the compressions ratio, equivalence ratio, fuel composition, and engine speed. The combustion durations calculated by these means are approximations at best. Finally, it should be restated that the purpose of this model is to determine key thermodynamic performance characteristics of an engine, particularly the indicated power produced, and the combustion duration does not drastically affect those results. An increase in the combustion duration from 20 to 40 crank angle degrees typically results in an overall efficiency decrease of about 2%. As a result, the above discussion only serves to provide a means to predict the combustion duration of producer gas for simulation purposes.

4.5 Heat Transfer

The rate of heat transfer to and from the cylinder wall is commonly defined by a Newtonian convection equation. It is defined by Equation 4-13

$$\frac{dQ_w}{d\theta} = \frac{h_Q(\theta) A_w(\theta)\left(T(\theta) - T_w\right)}{S_E} \tag{4-13}$$

where $h_Q(\theta)$ is the instantaneous heat transfer coefficient, $A_w(\theta)$ is the instantaneous cylinder wall surface area, $T(\theta)$ is the average gas temperature, T_w is the cylinder wall temperature, and S_E is the engine speed. The cylinder wall temperature is usually assumed to be constant for modeling purposes. The heat transfer coefficient is specified

using fluid dynamics through the Nusselt and Reynolds numbers. They are defined here in Equations 4-14 and 4-15

$$Nu = \frac{h_Q L}{k} \tag{4-14}$$

$$\mathrm{Re} = \frac{\rho u L}{\mu} \tag{4-15}$$

where L is a length scale, k is the fluid thermal conductivity, ρ is the fluid density, u is a velocity scale, and μ is the fluid viscosity. There are many heat transfer coefficient correlations in the literature, many of which rely on detailed modeling of the fluid dynamics within the cylinder, often dividing it into multiple zones. Because this model has a single zone, it utilizes an instantaneous, spatially averaged heat flux correlation. One such correlation that has been widely accepted to be globally applicable to all internal combustion engines is that of Woschni (Heywood, 1988). The Woschni correlation is

$$Nu = 0.035\,\mathrm{Re}^{0.8} \tag{4-16}$$

The Woschni correlation uses the bore as a constant length scale. The velocity scale, u, depends on the piston speed, the extent of combustion, amount of swirl and tumble within the cylinder, and the amount of turbulence. The characteristic gas velocity of the Woschni correlation is defined in Equation 4-17 (Heywood, 1988).

$$u = 2.28 S_p + 0.00324 T^o \frac{V_d}{V^o} \frac{\Delta p_{comb}}{p^o} \tag{4-17}$$

It relies on two terms, the first of which is attributed to the mean piston speed, S_p of Equation 4-18.

$$S_p = 2 S_E s \tag{4-18}$$

The second term of Equation 4-17 takes into account the pressure rise caused by combustion, where V^o, p^o, and T^o are the initial volume, pressure, and temperature (at

intake), and Δp_{comb} is the instantaneous pressure rise from combustion. Δp_{comb} can be approximated by the difference between the instantaneous pressure and the isentropic pressure without combustion taking place, and that is what was done for this model.

The fluid properties are those of the burned and unburned mixture and are temperature dependant. Heywood (1988) assumed the thermal conductivity to scale to $k \sim T^{0.75}$ and the viscosity to $\mu \sim T^{0.62}$. Using these relations with Equations 4-14 – 4-18, the Woschni heat transfer coefficient in dimensional form becomes Equation 4-19 (Ferguson and Kirkpatrick, 2001).

$$h_Q = 3.26 p^{0.8} u^{0.8} b^{-0.2} T^{-0.55} \tag{4-19}$$

4.6 Numerical Solution

The engine model consists of solving the coupled ordinary differential equations of Equations 4-1, 4-3, and 4-5 for the cylinder pressure p over the crank angles comprising the compression and expansion strokes. The crank angle began at bottom-dead-center, increased to top-dead-center, and decreased back to bottom-dead-center, representing the compression and expansion strokes of the engine. A 4th-order Runge-Kutta method with a step size of 0.001 rad (0.0573 crank angle degrees) was used to solve the differential equations, totaling 6284 data points. The temperature at each crank angle step was determined using the instantaneous pressure and volume according to the ideal gas law of Equation 4-20

$$T(\theta) = \frac{p(\theta)V(\theta)\overline{M}}{m\overline{R}} \tag{4-20}$$

for which the mass m remained constant throughout the combustion process. However, the molecular weight of the mixture $\overline{M}$ is a parameter that changes during the combustion process and will be discussed in Section 4.8.

4.7 Specific Heat Ratio

The specific heat ratio is that of the burned and unburned mixture; in many zero-dimensional modeling situations it is assumed to be constant or vary linearly with temperature. For this work however, steps were taken to model the specific heat ratio of the cylinder charge as accurately as possible for two reasons. First, the model does not intrinsically keep track of individual species within the burned and unburned mixture. The engine model, being based on Equation 4-1, contains only two properties which distinguish the contents of the cylinder charge: the lower heating value and the specific heat ratio γ. The lower heating value is easily accounted for based on the fuel, but the specific heat ratio is the most important parameter for three reasons. It is the only parameter that characterizes the species within the system, it affects the change in cylinder pressure even in the absence of combustion, and it is highly temperature dependant.

Definition of the specific heat ratio is divided into three subgroups comprising the unburned fuel-air mixture, an intermediate mixture containing both burned and unburned components, and finally the post- combustion products. The specific heat ratio of each subgroup is calculated at each crank angle step during the engine model solution. The specific heat ratio of each subgroup is programmed to be substituted for the overall specific heat ratio used in Equation 4-1 based on the extent of combustion. For this reason, the mass burn fraction x_b is used as a reference to determine the overall specific heat ratio. When the mass burn fraction is equal to zero, or in other words when the cylinder charge consists solely of unburned fuel and air, the overall specific heat ratio is simply that of the unburned fuel and air. When the mass burn fraction is equal to one, the overall specific heat ratio becomes that of the combustion products. Finally, when the mass burn fraction is between zero and one, the overall specific heat ratio is defined based on the mixture of burned and unburned components. Although the mass burn fraction has a curved profile governed by the Wiebe function, for simplicity the specific

heat ratio of the burned and unburned mixture was assumed to be linear and was based on the start of ignition, combustion duration, and specific heat ratios of the reactants and products. The criteria for the overall specific heat ratio γ are given in Equation 4-21

$$\gamma = \begin{cases} \gamma_{react} & x_b = 0 \\ \gamma_{react} + \dfrac{\gamma_{prod} - \gamma_{react}}{\theta_d}(\theta - \theta_s) & 0 < x_b < 1 \\ \gamma_{prod} & x_b = 1 \end{cases} \tag{4-21}$$

where γ_{react} is the specific heat ratio of the reactants (fuel-air mixture) and γ_{prod} is the specific heat ratio of the combustion products.

The specific heat ratios γ_{react} and γ_{prod} were calculated as follows. The temperature-dependant constant-pressure specific heat capacities of a number of components were first calculated. These components represented the most dominant species expected to be found in both the reactants and products. For this work, O_2, CO, H_2, CH_4, and N_2 were recognized as the most important species in the reactants and would comprise the vast majority of the fuel-air mixture. Naturally the reactants would contain other species as well, but it can be reasonably assumed that the mole fractions of these species in the fuel-air mixture are negligibly small. For the products, complete combustion would assure that the exhaust contain CO_2, H_2O, and N_2. Because spark-ignition engines are generally run lean however, there would be a finite amount of unreacted oxygen in the exhaust, but it was assumed that this small amount of oxygen would also be negligible. The specific heat ratio of the products was thus calculated based on the assumption that complete and stoichiometric combustion occurs.

After the constant-pressure specific heat capacity of each species was calculated, the constant-volume specific heat capacity $\overline{c}_{v,j}$ and specific heat ratio for each species was calculated based on ideal gas behavior using Equations 4-22 and 4-23.

$$\overline{c}_{v,j} = \overline{c}_{p,i} - \overline{R} \tag{4-22}$$

$$\gamma_j = \frac{\bar{c}_{p,j}}{\bar{c}_{v,j}} \tag{4-23}$$

Because both $\bar{c}_p$ and $\bar{c}_v$ are extensive properties, the specific heat ratio is also an extensive property and can be calculated for an ideal gas mixture using Equation 4-24.

$$\gamma = \sum_j y_j \gamma_j \tag{4-24}$$

4.8 Mixture Molecular Weight

Definition of the mixture molecular weight was divided into three subgroups in the same way that the specific heat ratio was defined. The criteria for the mixture molecular weight are given by Equation 4-25

$$\bar{M} = \begin{cases} \bar{M}_{react} & x_b = 0 \\ \bar{M}_{react} + \dfrac{\bar{M}_{prod} - \bar{M}_{react}}{\theta_d}\left(\theta - \theta_s\right) & 0 < x_b < 1 \\ \bar{M}_{prod} & x_b = 1 \end{cases} \tag{4-25}$$

where $\bar{M}_{react}$ is the molecular weight of the reactants (fuel-air mixture) and $\bar{M}_{prod}$ is the molecular weight of the combustion products. The molecular weight of the combustion products was determined based on the approximation of product species as discussed in Section 4.7.

4.9 Engine Performance Parameters

Once the pressure, volume, and temperature were solved at each crank angle step, engine performance parameters could be computed. Work for a compression or expansion process is defined by Equation 4-26. The net work produced per cycle, W, was thus determined by integrating the pressure vs. volume curve over the range of crank angles comprising the compression and expansion strokes as in Equation 4-27.

$$\partial W = p dV \tag{4-26}$$

$$W = \int p\, dV \tag{4-27}$$

Because the pressure was numerically solved based on a uniform crank angle step size, the instantaneous volume did not change uniformly. Consequently, the pressure and volume data were integrated using a middle Riemann sum. The result of Equation 4-27 was the indicated net work of the compression and expansion strokes. The indicated mean effective pressure (IMEP), a measure of an engine's ability to do work compared to its size, is determined by Equation 4-28.

$$IMEP = \frac{W}{V_d} \tag{4-28}$$

The indicated power P is determined from the net work per cycle as shown in Equation 4-29

$$P = \frac{N_c W S_E}{2} \tag{4-29}$$

where N_c is the number of engine cylinders, and the 2 in the denominator accounts for the fact that the power stroke occurs once per two full revolutions in a 4-stroke engine. The indicated torque T is determined from Equation 4-30 using the indicated power and engine speed.

$$\mathrm{T} = \frac{N_c P}{S_E} \tag{4-30}$$

The model also determines the maximum pressure and temperature of the cycle, as well as the indicated thermal efficiency based on the net work and the lower heating value of the initial fuel-air mixture. Finally, the indicated molar fuel consumption, $\dot{n}_{fuel}$, is determined with the engine speed and moles of fuel per cylinder charge through Equation 4-31.

$$\dot{n}_{fuel} = \frac{N_c n^o_{fuel} S_E}{2} \tag{4-31}$$

$$n_{fuel}^{o} = \frac{n_{tot}}{\left(1 + \frac{\overline{M}_{fuel}}{\overline{M}_{air}\phi(\phi)_{st}}\right)} \tag{4-32}$$

where $\overline{M}_{fuel}$ is the molecular weight of fuel, $\overline{M}_{air}$ is the molecular weight of air, $(\phi)_{st}$ is the stoichiometric fuel-air ratio, and n_{tot} is the total number of moles in the mixture based on the ideal gas law at initial conditions.

4.10 Integration of the Model with Aspen Plus©

The internal combustion engine model was added to the Aspen Plus© flowsheet with a USER2 block. The USER2 block is a blank model that allows the user to customize a unit operation block using either Fortran code or a Microsoft Excel© workbook. For this application, an Excel© workbook was chosen as the platform since the numerical engine model was previously set up and solved in an Excel© spreadsheet. The engine unit operation model ENGINE consists of one inlet stream labeled GASFUEL, one outlet stream labeled GASFUEL2, a heat stream labeled ICEHEAT, and a work stream labeled ICEPOWER. It is illustrated in Figure 4-2. The label of GASFUEL is meant to indicate that the inlet stream to the engine model should only contain gaseous components. The model also includes a user array that contains two sets of real parameters or variables. The first set consists of parameters that are input by the user and required by the numerical engine model. The second set of variables consists of engine performance parameters that are determined by the model and presented as results to the user.

When the model is run, the USER2 block opens the specified Excel© file and transfers the inlet stream data and user-specified real variables to sheets within the workbook. The numerical engine model is contained within a separate worksheet in which all calculations are performed. After calculations are performed, results are sent to additional worksheets for output, and the Excel© file transfers the information back to Aspen Plus©. No manipulation of streams between the inlet and outlet stream takes

place; all component mole flows and stream parameters of GASFUEL are therefore directly copied to GASFUEL2 to maintain a mass balance.

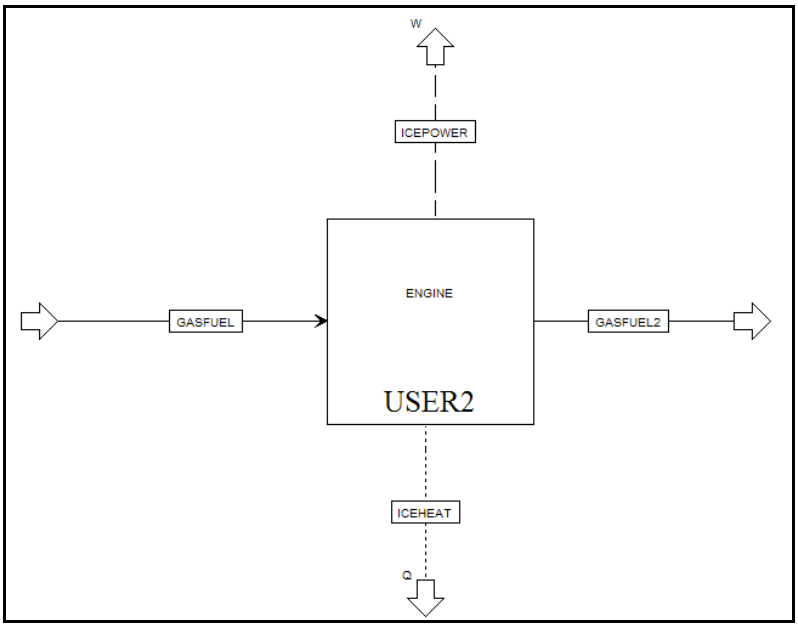

Figure 4-2: Aspen Plus© flowsheet of the custom engine model.

Specification of the engine block consists of entering the engine operating conditions into the user array of real variables. These parameters include the following: compression ratio, bore, stroke, connecting rod length, engine speed, number of cylinders, ignition timing, combustion duration, cylinder wall temperature, and equivalence ratio. A screenshot of the ENGINE user array is provided in Figure 4-3. The user array also includes the real variables of indicated work, indicated power, indicated mean effective pressure, thermal efficiency, indicated torque, maximum pressure and temperature, exhaust temperature, and required molar flow rate of fuel. These fields are blank prior to simulation because they are parameters that are solved by

the numerical engine model. All user-defined real variables and inlet stream data are sent to the Excel© workbook when the ENGINE block is initiated by Aspen Plus©.

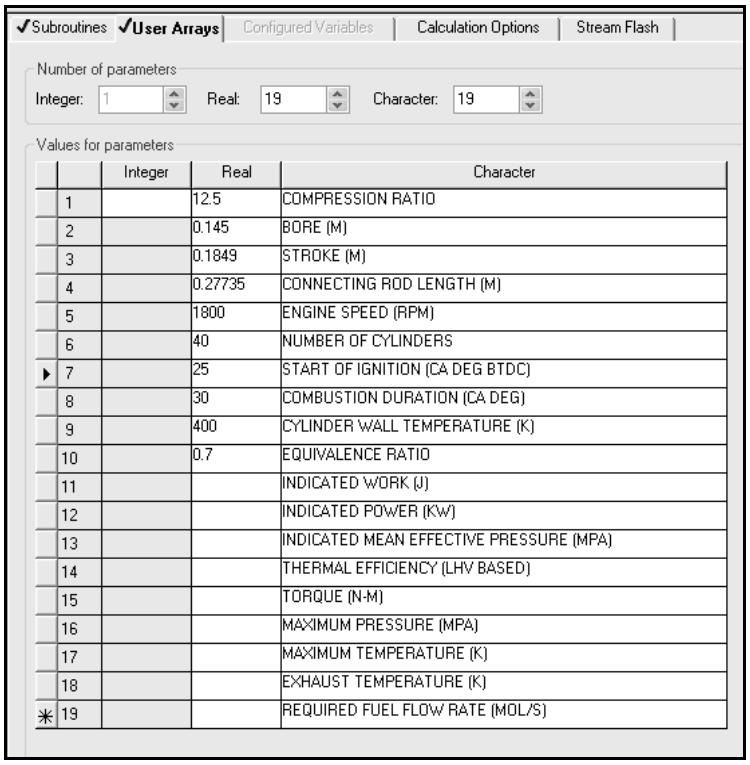

	Integer	Real	Character
1		12.5	COMPRESSION RATIO
2		0.145	BORE (M)
3		0.1849	STROKE (M)
4		0.27735	CONNECTING ROD LENGTH (M)
5		1800	ENGINE SPEED (RPM)
6		40	NUMBER OF CYLINDERS
7		25	START OF IGNITION (CA DEG BTDC)
8		30	COMBUSTION DURATION (CA DEG)
9		400	CYLINDER WALL TEMPERATURE (K)
10		0.7	EQUIVALENCE RATIO
11			INDICATED WORK (J)
12			INDICATED POWER (KW)
13			INDICATED MEAN EFFECTIVE PRESSURE (MPA)
14			THERMAL EFFICIENCY (LHV BASED)
15			TORQUE (N-M)
16			MAXIMUM PRESSURE (MPA)
17			MAXIMUM TEMPERATURE (K)
18			EXHAUST TEMPERATURE (K)
19			REQUIRED FUEL FLOW RATE (MOL/S)

Figure 4-3: Aspen Plus© user array for ENGINE block.

Once the data has been transferred to the Excel© workbook, the inlet stream data are sent to a worksheet in which the stoichiometric fuel-air ratio and lower heating value are determined in the same manner discussed in Section 3.4. The user-defined real variables are sent to a separate worksheet containing the Runge-Kutta engine model. The pressure and temperature of the inlet stream are used as the initial pressure and initial temperature of the cylinder charge. The initial pressure and temperature are used along with the initial cylinder volume at BDC to calculate the initial number of moles of mixture in the cylinder assuming ideal gas. This value is then used with the

stoichiometric fuel-air ratio and equivalence ratio to determine the initial moles of fuel within the mixture through Equation 4-32. The initial moles of fuel and lower heating value are used for the heat addition of Equation 4-8. The Runge-Kutta engine model and pressure-volume data are solved, and the engine performance parameters are calculated. These parameters are then sent back to the user array in Aspen Plus© so that the results can be displayed for the user.

Because the custom engine model does not predict engine emissions, a second unit operation was integrated to work with block ENGINE to model the combustion reaction. This was accomplished with an RGIBBS block to calculate chemical and thermodynamic equilibrium between the fuel and oxidant streams. The RGIBBS block, labeled COMBUST, was added downstream of the USER2 block, and a stream labeled ICEAIR representing the engine oxidant was added as a reactant stream, as shown in Figure 4-4. Block COMBUST was given an outlet labeled EXHAUST that represents the combustion products. The outlet stream of ENGINE, now labeled IN-ICE was connected to COMBUST and became the fuel stream for the combustion simulation. COMBUST determines equilibrium combustion products based on specified constant-pressure, constant-temperature conditions. As a result, a heat stream labeled QCOMBUST is included, and represents the heat duty from the RGIBBS reactor. The pressure and temperature of COMBUST are modeled to be those of the exhaust gas of the engine. The pressure is specified as the exhaust pressure and the temperature was specified as the exhaust temperature determined by ENGINE. A Fortran calculator script was written to transfer the calculated exhaust pressure and temperature from ENGINE to COMBUST when the model was run. A second Fortran calculator script was written to calculate the flow rate of air based on the fuel flow rate, stoichiometric fuel-air ratio of the fuel stream, and equivalence ratio specified by the user in the ENGINE block. This allowed for automatic calculation of the air flow rate based on the single specification of the equivalence ratio.

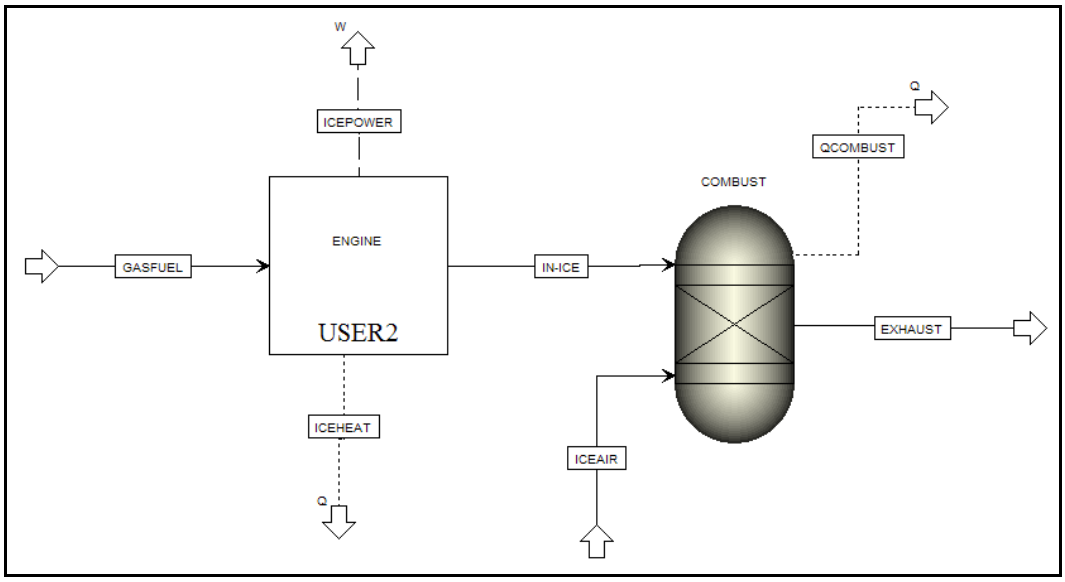

Figure 4-4: Aspen Plus© flowsheet of internal combustion engine model.

Because the custom model ENGINE works as a closed system and Aspen Plus© operates with open systems, it was important to ensure that the mass and energy balances were satisfied so its addition to the flowsheet was rational. With respect to mass balance, the two blocks ENGINE and COMBUST receive the same fuel stream; they are simply labeled differently as GASFUEL and IN-ICE. Equation 4-31 ensures that the mass of fuel of the closed system translates to a fuel flow rate that agrees with the engine speed. Block COMBUST automatically satisfies its mass balance.

The energy balances are more involved. The energy flow diagram of a simplified internal combustion engine is shown in Figure 4-5. The system inputs are the enthalpies of the fuel and air, H_{fuel} and H_{air}. The system outputs are the work produced W, heat Q, and exhaust enthalpy $H_{exhaust}$. The heat loss Q of Figure 4-5 would include heat extracted by the cooling jacket and heat lost to the environment. This quantity of heat would be equivalent to the heat stream ICEHEAT of Figure 4-4, because it is derived from the closed-system energy balance of ENGINE.

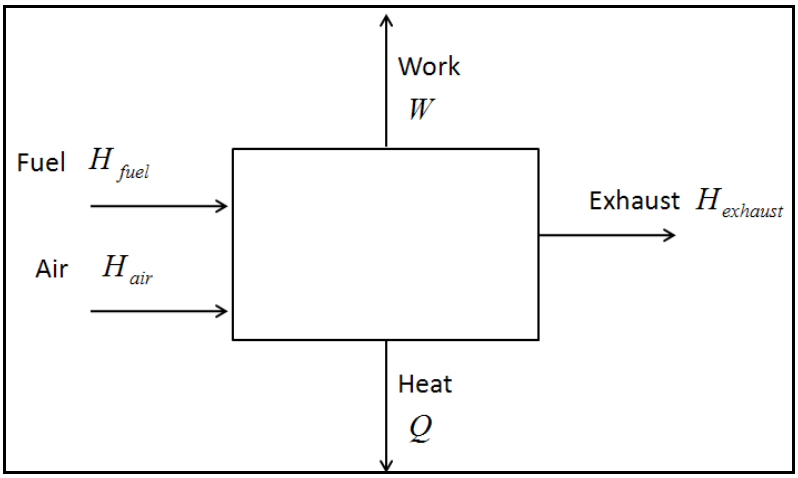

Figure 4-5: Simplified energy flow diagram of an internal combustion engine.

An energy balance on the system of Figure 4-5 gives

$$\left(H_{fuel} + H_{air}\right) - H_{exhaust} = Q + W \tag{4-33}$$

An energy balance around block COMBUST of Figure 4-4 gives

$$\left(H_{fuel} + H_{air}\right) - H_{exhaust} = QCOMBUST \tag{4-34}$$

where QCOMBUST is the heat duty of the COMBUST reactor. From comparison of Equations 4-33 and 4-34, it is apparent that in order for the energy balances of ENGINE and COMBUST to agree, the heat duty QCOMBUST must equal the sum of the heat stream and work stream generated by ENGINE (ICEHEAT and ICEPOWER).

To ensure that this was indeed the case, simple simulations of methane combustion were performed with fixed engine parameters and equivalence ratios ranging from 0.6 to 1.2 to compare the results of ICEHEAT, ICEPOWER, and QCOMBUST. It was found that the sum of ICEHEAT and ICEPOWER compared favorably to QCOMBUST. The smallest percent difference between the two values with respect to QCOMBUST was 0.9%, which occurred at an equivalence ratio of 1.0, and the largest percent difference was 2.8%, which occurred at an equivalence ratio of 0.6.

The difference between the two energy quantities can be explained with the thermodynamics of the closed and open systems. The closed system energy balance of the internal combustion engine is

$$U_{react} - U_{exhaust} = Q + W \tag{4-35}$$

where $U_{exhaust}$ is the internal energy of the exhaust, U_{react} is the internal energy of the reactants (fuel and air), and both Q and W are leaving the system.

The open system energy balance of the engine is

$$H_{react} - H_{exhasut} = QCOMBUST \tag{4-36}$$

where $H_{exhaust}$ is the enthalpy of the exhaust, H_{react} is the enthalpy of the reactants (fuel and air), and the heat duty QCOMBUST is leaving the system.

The difference between the two right-hand sides of Equations 4-35 and 4-36 is the quantity of interest.

$$QCOMBUST - (Q + W) = (H_{react} - H_{exhaust}) - (U_{react} - U_{exhaust}) \tag{4-37}$$

Upon rearranging this becomes

$$QCOMBUST - (Q + W) = (H_{react} - U_{react}) - (H_{exhaust} - U_{exhaust}) \tag{4-38}$$

Using the definition of enthalpy

$$H = U + pV \tag{4-39}$$

and the ideal gas law, Equation 4-38 reduces to

$$QCOMBUST - (Q + W) = (pV)_{react} - (pV)_{exhaust} = \overline{R}[(nT)_{react} - (nT)_{exhaust}] \tag{4-40}$$

As a result, the difference between energy values depends on the change in temperature and change in number of moles from initial state to final state. Continuity exists between the temperatures of the closed and open systems since the initial temperature of ENGINE and COMBUST are identical, and the exhaust temperatures of the closed and open systems are identical as well. However the number of moles is dependant on the molecular weight, and there is a disparity between the exhaust

molecular weight of the closed system and that of the open system. The molecular weight of the closed system is an approximation, as discussed in Section 4.8. The molecular weight of the open system is calculated by the RGIBBS block COMBUST in Aspen Plus©. As a result of the disparity between the molecular weights of the closed and open systems, relatively small differences were observed between the energy balances of the closed system and open system during the test simulations.

4.11 Model Validation

The internal combustion engine model was validated against a similar reference model from the literature. The reference model was a web-based module on the companion site of Ferguson and Kirkpatrick (2001). The reference model was also a thermodynamics-based finite heat release model that used the Woschni heat transfer correlation. The developed engine model was verified using the engine operating conditions listed in Table 4-1.

Table 4-2 compares the engine operating results between the developed and reference models. The percent differences of the indicated performance parameters, including work, power, and IMEP, were less than 1%. The percent differences of the maximum pressure and temperature were 0.34% and 0.70%, respectively. The largest percent differences occurred with the heat transfer calculations. The percent differences of the maximum heat flux, maximum heat transfer coefficient, and maximum heat rate were all less than 3%. The results verify that the developed model produces reasonably accurate simulations of engine performance parameters.

Table 4-1: Engine operating conditions used for model validation.

Parameter	Symbol	Units	Condition
Bore	b	mm	180
Stroke	s	mm	190
Rod Length	l	mm	285
Compression Ratio	r	-----	11
Speed	N	RPM	2500
Initial Pressure	p^o	bar	1
Initial Temperature	T^o	K	300
Spark Timing	θ_s	ca. deg	-25
Combustion Duration	θ_d	ca. deg	40
Cylinder Wall Temperature	T_w	K	400
Fuel	----	-----	Methane
Equivalence Ratio	ϕ	-----	1.0

Table 4-2: Results of model validation.

Parameter	Units	Reference Model	Developed Model	Percent Difference (%)
Indicated Work	J	6348	6387	0.61
Indicated Power	kW	132	133.1	0.83
IMEP	bar	13.1	13.2	0.76
Indicated Efficiency	----	0.391	0.393	0.51
Maximum Pressure	bar	88.3	88.0	0.34
Maximum Temperature	K	2557	2575	0.70
Maximum Heat Flux	kW/m^2	7400	7205	2.64
Maximum Heat Transfer Coefficient	$W/m^2 K$	3500	3437	1.80
Maximum Heat Rate	kW	460	449	2.39

CHAPTER 5: AN EXERGY ANALYSIS TO EVALUATE DIFFERENT FUELS FOR GASIFICATION

5.1 Introduction

This study endeavors to present a methodology for evaluating different solid fuels for gasification. Another purpose is to compare the effectiveness of gasifying coal and five so-called alternative solid fuels. This study goes beyond what has been similarly presented in past works in a number of ways. First, past works (Prins et al., 2007; Ptasinski et al., 2007) have focused on the evaluation of different groups of gasifier fuels represented by generalized compositions. These studies were meant to compare the effects of composition and moisture content on the gasification efficiency of these fuels. However, it will be shown here that the equivalence ratio at which the carbon boundary point occurs, which is unique to each fuel and cannot be calculated, is essential to understanding any gasification efficiency results. Past works have also used very crude representations of biomass that have only considered the carbon, hydrogen, nitrogen, and oxygen content, as well as representations that sometimes neglect ash content altogether. In contrast, this study uses exact representations of biomass feedstocks, as well as realistic compositions of ash. In addition, a disadvantage to using a popular definition of exergetic efficiency will be discussed, and a new definition will be presented that more closely relates to practical operation of the gasifier. Finally, the results presented here are meant to outline a detailed method for evaluating any particular fuel. It will be shown that the effectiveness of gasifying a fuel can be determined from basic and exact thermodynamic data instead of relying on generalized fuel characteristics such as O/C and H/C ratios.

5.2 Methodology

This study focuses on air-blown gasification at atmospheric pressure. The gasification process is simulated in Aspen Plus© as detailed in Section 3.2. The reactor is

assumed to be adiabatic with negligible heat losses, which is the ideal operating condition for real gasifiers. The fuel and air enter the reactor at environment conditions of 298.15 K and 1 atm. Since the reactor is adiabatic, the equilibrium products exit at the adiabatic reactor temperature, and the independent variable becomes the relative amount of oxidant reacting with the fuel. The amount of oxidant used in this work is represented by the fuel-air equivalence ratio, ϕ, defined by Equation 5-1

$$\phi = \frac{m_{fuel} / m_{air}}{\left(m_{fuel} / m_{air} \right)_{st}} \tag{5-1}$$

where m_{fuel} is the mass of fuel, m_{air} is the mass of air, and the subscript st denotes stoichiometric conditions, where stoichiometry is defined by complete oxidation of carbon and hydrogen to CO_2 and H_2O. The fuel-air equivalence ratio is defined such that a value of 1 corresponds to complete oxidation, values less than 1 represent fuel-lean conditions, and values greater than 1 represent fuel-rich conditions.

Ash contained in the fuel is represented by oxides of metals. Compositions of ash are based on mineral analyses when at hand (often included with proximate and ultimate analyses), or, when a mineral analysis is not known, a generic ash composition is approximated by 50% SiO_2, 25% Fe_2O_3, and 25% Al_2O_3 (Standard Laboratories, 2006). The oxygen content of these ash species is not included in the calculation of the stoichiometric fuel-air ratio because they are usually very stable components already at chemical equilibrium and do not further react with oxygen. Equilibrium product species considered by the Aspen Plus© model are those that are stable at typical gasification temperatures. They are Ar, C (carbon graphite), CO, CO_2, CH_4, CHN, COS, H_2, H_2O, H_2O_2, H_2S, HCl, N_2, N_2O, NH_3, NO, NO_2, O_2, S, SO, SO_2, SO_3, as well as any oxides of metal representing ash.

Chemical exergy of each fuel is calculated with Equation 2-9, where the multiplier ψ is based on composition according to Equations 2-7 and 2-8 and the exergy of ash is assumed to be negligible. Physical and chemical exergy of the products are calculated according to Equations 2-1 and 2-5 and using standard chemical exergies.

The fuels considered in this work are comprised of three fossil fuels and three biomass fuels, five of which (petcoke, Orimulsion, distillers dried grains, oat hulls, and switchgrass) are increasingly being considered as alternative fuels, often derived from waste streams, to conventional fossil fuels in heat and power generation systems. The fossil fuels are coal, petcoke, and Orimulsion, and the biomass fuels include distillers dried grains (DDG), oat hulls, and switchgrass. The coal selected for this work is a coal burned in the stoker boilers at the University of Iowa Power Plant (Standard Laboratories, 2006). It is mined from southern Illinois by Knight Hawk Coal, LLC. Petcoke is a solid fuel, often a waste product from processes involving coal, which contains a very high percentage of carbon and very little ash. Orimulsion is a bitumen-water emulsion produced from Venezualean bitumen (Miller and Srivastava, 2000). It has progressively become a substitute for heavy fuel oil and coal for power generation and has been proposed as a fuel for diesel engines and gasification. DDG is a byproduct of distillation processes and is produced in large quantities from ethanol plants. It is mainly sold as livestock feed, but the abundance of ethanol plants in Iowa and other Midwestern states in recent years has created saturation of this market. DDG may be a desirable gasification fuel in Iowa because of its abundant state-wide supply. Oat hulls are a cereal byproduct that has been successfully co-fired with coal at the University of Iowa Power Plant for the last few years to reduce greenhouse gas emissions and save on fuel costs (University of Iowa Facilities Management, 2009). Finally, switchgrass is a tall perennial grass that is receiving increased attention as a biomass fuel (Blevins and Cauley, 2005). It is a versatile plant which thrives in a variety of weather conditions and is expected to become a major source of ethanol in the United States in the near future.

Table 5-1 lists properties of the fuels considered, including the proximate and ultimate analyses, heating values, chemical exergy multiplier ψ, and chemical exergy values. The moisture contents ranged from 0.5% to 29%, fixed carbon from 13.7% to 80%, volatile matter from 13.1% to 81.7%, and lower heating values from 15,210 to 33,560 kJ/kg.

Table 5-1: Fuel properties.

	Coal	Petcoke	Orimulsion	DDG	Oat Hulls	Switchgrass
Moisture (%)	13.26	0.5	29	10.48	10.03	8
Proximate Analysis (% dry basis)						
FC	48.40	86.30	50.00	15.79	14.59	13.70
VM	41.93	13.10	49.70	78.75	80.28	81.70
Ash	9.67	0.60	0.30	5.46	5.13	4.60
Ultimate Analysis (% dry basis)						
C	70.78	86.60	84.50	46.49	45.93	49.00
H	5.16	4.00	10.30	6.27	5.83	4.60
O	9.56	1.20	0.40	37.86	42.42	41.00
N	1.39	1.40	0.70	3.16	0.61	0.60
S	3.40	6.20	3.80	0.40	0.08	0.20
Cl	0.04	0.00	0.00	0.36	0.00	0.00
HHV (kJ/kg) (as is)	25890	34450	33180	17430	16840	16330
LHV (kJ/kg) (as is)	24590	33560	30880	15950	15450	15210
ψ	1.065	1.054	1.067	1.125	1.130	1.120
Chemical Exergy (kJ/kg)	26820	35990	33980	18270	17750	17270

Exergetic efficiency is broadly defined as the ratio of delivered exergy to expenditures (Prins and Ptasinski, 2005). In combustion and gasification processes, there are generally two incoming streams comprised of the fuel and oxidant, and two exiting

streams comprised of the products and unconverted fuel. The efficiency can thus be defined in four different ways

$$\varepsilon_I = \frac{E_{unconv.\,fuel} + E_{gas}}{E_{fuel} + E_{gas.medium}} \tag{5-2}$$

$$\varepsilon_{II} = \frac{E_{gas}}{(E_{fuel} - E_{unconv.\,fuel}) + E_{gas.medium}} \tag{5-3}$$

$$\varepsilon_{III} = \frac{E_{unconv.\,fuel} + E_{gas} - E_{gas.medium}}{E_{fuel}} \tag{5-4}$$

$$\varepsilon_{IV} = \frac{E_{gas} - E_{gas.medium}}{(E_{fuel} - E_{unconv.\,fuel})} \tag{5-5}$$

In the equations above, E_{gas} is the total exergy of the product gas stream, which includes both physical and chemical exergy, E_{fuel} is the chemical exergy of fuel, $E_{gas.medium}$ is the exergy of the gasifying medium, and $E_{unconv.\,fuel}$ is the exergy of the unconverted solid fuel, which is defined to be the solid carbon graphite in the product stream. For this study, the oxidant is air at the environment temperature and pressure, yielding zero exergy for the gasifying medium. As a result, efficiencies ε_I and ε_{III} become identical, as do efficiencies ε_{II} and ε_{IV}. Efficiencies defined based on exergy differences generally result in lower efficiencies than those based on summation of entering and exiting streams. According to Prins and Ptasinski (2005), η_I, the most fundamental definition of efficiency based on gains and losses, has been found to over-estimate the gasification efficiency for a biomass gasifier. ε_{IV} is frequently used in other works and is deemed the rational efficiency (Prins et al. 2003). It is said to relate best to the function of the gasifier, which is to convert a solid fuel to a gaseous fuel. The difference in the denominator of ε_{IV} represents the chemical exergy of solid fuel that participates in the gasification reaction. This quantity is dependant on the amount of carbon in the products at equilibrium, which in turn is controlled by thermodynamics. The

denominator is therefore indicative of the amount of solid fuel available, as governed by thermodynamics, to produce gaseous products. It should be noted that the unconverted solid carbon exiting the gasifier contains physical exergy in addition to chemical exergy, since it will be at the same elevated temperature as the other products. This physical exergy quantity is considered unrecoverable in this work, and the term $E_{unconv.\,fuel}$ consists solely of chemical exergy. A fifth efficiency, ε_{gas}, which will be referred to as the gas efficiency in this work, is defined by Equation 5-6.

$$\varepsilon_{gas} = \frac{E_{gas}}{E_{fuel} + E_{gas.medium}} \tag{5-6}$$

which is intended to characterize the performance of gasifiers. Insufficient mixing and residence times will result in solid carbon deposits in the ash handling system, regardless of how close to the carbon boundary point the gasifier is operated. Separation of the carbon from the ash is assumed to be difficult and expensive, and the unconverted fuel is lost in most systems. Equation 5-6 is a modified version of Equation 5-2, assuming that the unconverted fuel is not recoverable. The numerator is the exergy of interest, representing availability that can be practically realized, and the denominator represents availability input to the system.

Finally, an energy efficiency, or cold-gas efficiency, can be defined based on energy content of fuel and products, as in Equation 5-7

$$\eta = \frac{LHV_{gas}}{LHV_{fuel}} \tag{5-7}$$

where LHV_{gas} and LHV_{fuel} are the lower heating values of product gas and fuel.

5.3 Results and Discussion

Table 5-2 lists the equivalence ratio and temperature at which the carbon boundary point occurs for each fuel. The carbon boundary point is the point where just enough oxidant is added to oxidize all carbon in the system, leaving no solid carbon

predicted by the equilibrium calculation. It was shown in literature that the maximum exergetic efficiency occurs at the carbon boundary point. The equivalence ratio of the carbon boundary points of the biomass fuels are much higher than those of the fossil fuels, a result that appears to be related to their higher oxygen content. The carbon boundary point equivalence ratio of petcoke is the lowest at 2.30 and is very near the carbon boundary point of 2.0 for carbon graphite, which is reasonable considering that its carbon content is almost 87%, making it nearest in composition to pure carbon graphite.

Table 5-2: Carbon boundary point of each fuel.

Fuel	Carbon Boundary Point	
	Equivalence Ratio	Temperature (K)
Coal	3.10	1620
Petcoke	2.30	1459
Orimulsion	2.90	1001
DDG	4.25	1000
Oat Hulls	4.95	1004
Switchgrass	3.80	1005

Figures 5-1 to 5-6 show the mole fractions of major gas species, as well as the fraction of unconverted carbon vs. equivalence ratio for each fuel. The carbon boundary point can be identified on the figures where the fraction of unconverted carbon becomes zero. For each fuel, the N_2 mole fraction steadily decreases as the equivalence ratio increases. The nitrogen content of each fuel is very low; almost all nitrogen in the products comes from air. As the system becomes more fuel rich, less air is added to the system, and the N_2 mole fraction decreases. The N_2 mole fraction is important because it dilutes the producer gas; its mole fraction should be kept as low as possible. There is a

noticeable change in slope of this trend at the carbon boundary point for each fuel. The N_2 mole fraction decreases more quickly as the equivalence ratio moves from lean toward the carbon boundary point, and past this point the slope decreases slightly.

The mole fractions of CO, H_2, CO_2, and H_2O follow a general trend for all fuels; mole fractions of CO and H_2 are almost absent at the equivalence ratio of 0.5 then steadily increase as the system becomes more fuel rich. Carbon and hydrogen in the system are oxidized almost completely to CO_2 and H_2O at equivalence ratios of 0.5 and 1.0. As the equivalence ratio increases, decreased availability of oxygen causes equilibrium to shift from CO_2 and H_2O to CO and H_2. This trend is expected of a system whose independent variable is the equivalence ratio, or amount of available oxygen. However, a slight yet definite digression from this trend emerges for Orimulsion and the biomass fuels. Whereas mole fractions of CO_2 and H_2O are reduced to nearly zero prior to the carbon boundary point for coal and petcoke, these species have considerable mole fractions at the carbon boundary point and beyond for Orimulsion and the biomass fuels. In fact, the mole fractions of CO_2 and H_2O actually begin to slightly increase past the carbon boundary point. In addition, the CO mole fraction of each of these four fuels shows a slight decrease on the rich side of the carbon boundary point, while the H_2 mole fraction continues a gradual increase in the same region.

At first, the stark difference between the mole fraction plots of coal and petcoke and those of Orimulsion and the biomass fuels appears to be a result of the oxygen contents of the fuels. The oxygen content of the biomass fuels is considerably larger than that of coal and petcoke. The large moisture percentage of Orimulsion adds a great quantity of oxygen to that fuel. However it must be remembered that the equivalence ratio governs the amount of oxygen in the system relative to each fuel, and the oxygen content of the fuel is considered in its calculation. Regardless, the oxygen content cannot explain the clear shifts in mole fractions of CO_2 and H_2O that occur at the carbon boundary point. Rather it may be more beneficial to consider equilibrium

thermodynamics to explain the disparity, since a definite equilibrium shift occurs in the gas phase at the carbon boundary point for Orimulsion and the biomass fuels.

Being the most important gas-phase reaction in a gasification environment, the water-gas shift reaction dictates equilibrium among CO, H_2, CO_2, and H_2O. The equilibrium constant, K_{eq}, is defined by the ratio of partial pressures of the products and reactants. Since ideal gases are assumed, partial pressures can be replaced by mole fractions, as shown in Equation 5-8.

$$K_{eq} = \frac{p_{CO_2} p_{H_2}}{p_{CO} p_{H_2O}} = \frac{y_{CO_2} y_{H_2}}{y_{CO} y_{H_2O}} \tag{5-8}$$

An equilibrium constant greater than one indicates favor toward the products (CO_2 and H_2), and a value less than one indicates favor toward the reactants (CO and H_2O). The equilibrium constant is dependent on the heat of reaction and varies with temperature according to Equation 5-9.

$$\frac{d \ln K_{eq}}{dT} = \frac{\Delta H_{rxn}}{\overline{R} T^2} \tag{5-9}$$

Thus the equilibrium constant increases with increasing temperature for an endothermic reaction, and the equilibrium constant decreases with increasing temperature for an exothermic reaction. Because the water-gas shift reaction is exothermic, the equilibrium constant will increase as the temperature decreases. A shift between products and reactants occurs when the equilibrium constant is unity, and for the water-gas shift reaction, this occurs at a temperature of about 1050 K. At equilibrium, temperatures less than 1050 K favor CO_2 and H_2, and temperatures greater than 1050 K favor CO and H_2O.

Figures 5-7 and 5-8 are plots of the adiabatic reactor temperature as a function of equivalence ratio for the fossil fuels and biomass fuels, respectively. Horizontal dashed lines indicate 1050 K and 1300 K, and vertical dashed lines indicate the carbon boundary point of each fuel. The adiabatic reactor temperatures of coal and petcoke lie clearly

above 1050 K over the range plotted. On the other hand, the temperature profiles of Orimulsion and the biomass fuels cross below 1050 K, always prior to (on the lean side of) its respective carbon boundary point. As the temperature drops below 1050 K, the equilibrium constant predicts that a shift from CO and H_2O to CO_2 and H_2 will occur. Focusing on the species profiles of Orimulsion and the biomass fuels, the mole fractions of CO_2 and H_2 do indeed increase, but CO_2 does not begin to increase until the carbon boundary point is reached. Similarly, the mole fraction of CO decreases as predicted, but likewise not until the carbon boundary point is reached. The mole fraction of H_2O also increases slightly on the rich side of the carbon boundary point. Both the equivalence ratio and water-gas shift reaction should cause the H_2O mole fraction to decrease; the fact that it does not decrease indicates that there is another reaction(s) that exerts influence on H_2O. The second major gasification reaction involving H_2O is the carbon-water reaction, $C + H_2O \leftrightarrow CO + H_2$. This is an endothermic reaction, causing the equilibrium constant to decrease with decreasing temperature, and therefore there is a shift from favoring products to favoring reactants as the temperature decreases. This trend is apparent since solid carbon forms in the products at lower temperatures, and the mole fraction of H_2O increases as well. It should also be noted that the magnitude of the standard state enthalpy of reaction of the carbon-water reaction is about three times that of the water-gas shift reaction (131 kJ/mol vs. 41 kJ/mol), which may explain why the carbon-water reaction appears to control the mole fraction of H_2O more than the water-gas shift reaction and equivalence ratio.

In summary, the composition of the producer gas in an adiabatic system is influenced by a complex relationship among the equivalence ratio, water-gas shift reaction, and carbon-water reaction. The equivalence ratio constantly seeks to shift the composition toward CO and H_2 as the system moves rich. The water-gas reaction can shift the products toward CO_2 if and when the temperature of the system drops below 1050 K, but its influence is restricted until the carbon boundary point is reached. Finally,

the carbon-water reaction can further shift the products toward H_2O, but only if the water-gas reaction has made its shift when the temperature falls below 1050 K.

There are other temperature-dependant operating factors that should be considered when evaluating a fuel for gasification. Gasifiers typically operate in the range of 700-850°C (973-1123 K). The operating temperature must be high enough to ensure sufficiently high reaction rates and for suitable conversion of primary pyrolysis products to desirable light gases. From Figures 5-7 and 5-8, Orimulsion is the only fuel that drops below this range before the carbon boundary point is reached. The ash fusion temperature is also an important parameter that influences the type of gasifier and its operation. Slagging is the partial or complete melting of ash, and ash begins to soften around 1300-1400 K (Miller, 2005). If the gasifier operating temperature is expected to be greater than 1300 K, An entrained flow gasifier, which typically operates between 1200-1500°C (1473-1773 K), is best suited to handle slagging. Here, 1300 K will be used as a lower limit for which slagging may occur. In Figure 5-7, the entire temperature profile of coal lies above 1300 K; even at an equivalence ratio of 5.0, the reactor temperature is 1525 K. The reactor temperatures of petcoke are also very high, but they drop below 1300 K around an equivalence ratio of 3.75, well past its carbon boundary point. The temperature profile of Orimulsion lies above 1300 K until an equivalence ratio of about 2.25 K, giving it some margin with respect to its carbon boundary point. In Figure 5-8, the temperature profiles of the three biomass fuels similarly lie above 1300 K for some portion of the range plotted, but these reactor temperatures drop below 1300 K prior to each carbon boundary point as well. DDG drops below 1300 K at an equivalence ratio of about 3.2, oat hulls at about 3.6, and switchgrass at about 2.9. If operation at or near the carbon boundary point is desired, these results suggest that coal and petcoke be gasified in a reactor suited to handle slag, such as an entrained flow gasifier. In contrast, the results suggest that Orimulsion and the biomass fuels can be gasified in a reactor suited to handle dry ash.

Figures 5-9 and 5-10 are plots of rational efficiency vs. equivalence ratio for the fossil fuels and biomass fuels, respectively. All fuels except coal and petcoke display a maximum rational efficiency at the carbon boundary point. For Orimulsion and the biomass fuels, the rational efficiencies almost plateau on the rich side of the carbon boundary point. Coal and petcoke are the only fuels that do not have a maximum rational efficiency; the efficiency steadily increases past the carbon boundary point. Past the carbon boundary point, both the physical and chemical exergies of the producer gas decrease, owing respectively to decreasing temperatures and exergy diverted to unconverted solid carbon. The unexpected trend displayed by coal and petcoke must be attributed to the fact that the denominator ($E_{fuel} - E_{unconv.\,fuel}$) of the rational efficiency is decreasing at a faster rate than the numerator (E_{gas}). In other words, chemical exergy of solid carbon is forming in the products at a faster rate than at which the combined exergy of the gas is decreasing. For Orimulsion and the biomass fuels, which show almost no change in rational efficiency past the carbon boundary point, the rate of change in the numerator and denominator must be about equal.

According to the results presented here, there is no limit to the rational efficiency for coal, and the equivalence ratio virtually does not affect the rational efficiency for the biomass fuels. It must be remembered that the principle behind the rational efficiency is to describe the effectiveness of converting a solid fuel to a gaseous fuel, and the denominator represents the exergy available from solid sources in supplying the exergy to the gas. In this respect, the rational efficiency is an indicator of the effectiveness of the process. However, the results presented suggest that it is not a practical definition with respect to gasifier operation.

Figures 5-11 and 5-12 are plots of gas efficiency vs. equivalence ratio for the fossil fuels and biomass fuels, respectively. Each fuel displays a maximum at the carbon boundary point, and the gas efficiency is equivalent to the rational efficiency leading up to the carbon boundary point. There is a much more prominent decrease in gas efficiency

past the carbon boundary point of each fuel in comparison to the rational efficiency because the chemical exergy of solid carbon is neglected. The gas efficiency penalizes the exergetic efficiency of the gasifier when solid carbon is deposited in the products. Whereas the rational efficiency discounts the exergy of the solid carbon, the gas efficiency considers solid carbon in the products to be a loss of availability. This is reasonable considering that deposition of solid carbon in the products is undesirable for actual gasifier operation. Therefore the gas efficiency is recommended to be used to represent the exergetic efficiency of gasifier operation.

Figures 5-13 and 5-14 are plots of cold-gas efficiency vs. equivalence ratio for the fossil fuels and biomass fuels, respectively. Even though the cold-gas efficiency is simply a ratio of energy conversion without regard to the Second Law, all six fuels show maximums at the carbon boundary point. The cold-gas efficiency decreases past the carbon boundary point due to diversion of energy availability in unconverted solid carbon as well as decreased quantity of gas flow, which in turn is caused by decreased air introduced at larger equivalence ratios. Although exergy is never conserved in irreversible processes, conservation of energy would suggest that the cold-gas efficiency should always be higher than any exergetic efficiency. However the cold-gas efficiency depends solely on the lower heating value of the product stream and does not take into account the energy attributed to the elevated temperature of the stream. At low equivalence ratios, fuel is converted to H_2O and CO_2 which have negligible lower heating values. The energy contained in the fuel is thus maintained in the temperature of the products. At richer conditions, a larger amount of fuel energy is transferred instead to CO and H_2, thereby increasing the lower heating value of the product stream. The diversion of energy results in lower product stream temperatures. This is evident in Figures 5-13 and 5-14 as the cold-gas efficiencies rise from almost 0 at an equivalence ratio of 0.5 to their maxima at the carbon boundary point.

Because the carbon boundary points of the fossil fuels differ significantly from those of the biomass fuels, it is easier to compare their maximum efficiencies. Table 5-3 lists the maximum gas and cold-gas efficiencies, which occur at the carbon boundary point of each fuel. It should be remembered that the maximum gas efficiency is equivalent to the maximum rational efficiency because no unconverted solid carbon exists at the carbon boundary point.

Table 5-3: Maximum efficiencies at the carbon boundary point.

Fuel	Maximum Gas Efficiency (%)	Maximum Cold Gas Efficiency (%)
Coal	93	87
Petcoke	82	73
Orimulsion	73	75
DDG	86	95
Oat Hulls	86	96
Switchgrass	86	92

Coal displays the highest gas efficiency, and Orimulsion displays the lowest gas efficiency of 73%, which is most likely attributed to its high moisture content. The three biomass fuels all had maximum gas efficiencies of 86%. The maximum gas efficiency of petcoke is lower than those of the three biomass fuels, despite its desirably low moisture and ash content. The lower gas efficiency of petcoke is also surprising because at the carbon boundary point, traces of CO_2 and H_2O are virtually nonexistent in the product gas, whereas for the biomass fuels, molar quantities of CO_2 are around 6% and H_2O molar quantities are around 4%. Oxidation of carbon and hydrogen to CO_2 and H_2O represents a further extent of reaction and thus larger exergy destruction, whereas a larger amount of availability results if those elements are converted to CO and H_2. It is also desirable to fundamentally understand why the gas efficiency of coal is larger than that of petcoke despite its larger moisture and ash content.

Table 5-4 lists mole fractions of the major species contained in the producer gas at the carbon boundary point for each fuel, as well as a reminder of the equivalence ratio at which it occurs.

Table 5-4: Producer gas compositions at the carbon boundary point.

Fuel	Equivalence Ratio	N_2	CO	H_2	CO_2	H_2O
Coal	3.10	0.47	0.33	0.19	0.00	0.00
Petcoke	2.30	0.59	0.32	0.08	0.00	0.00
Orimulsion	2.90	0.46	0.22	0.24	0.04	0.03
DDG	4.25	0.33	0.28	0.28	0.06	0.04
Oat Hulls	4.95	0.29	0.31	0.30	0.06	0.04
Switchgrass	3.80	0.36	0.31	0.22	0.06	0.03

Coal and petcoke contain no significant quantities of CO_2 and H_2O whereas Orimulsion and the biomass fuels do, which is desirable since these species can be considered diluents that do not add any contribution to the chemical exergy of the stream. The key difference however lies with the major stream diluent, N_2. The N_2 mole fractions of the fossil fuels range from 0.46 to 0.59, and they range from 0.29 to 0.36 for the biomass fuels. The difference in N_2 mole fractions directly results from the fossil fuels having their carbon boundary points at much lower equivalence ratios compared to the biomass fuels. This observation explains why the gas efficiencies of the biomass fuels are larger than that of petcoke and suggests that fuels with higher carbon boundary points are better suited for gasification. However, it does not explain why the maximum gas efficiency of coal is higher than those of the biomass fuels. Although the N_2 mole fraction of coal is higher than that of the biomass fuels, Table 5-4 relates only to the chemical exergy of the producer gas. Physical exergy also factors into the gas efficiency, and coal displayed the highest adiabatic reactor temperatures of all fuels. From Table 5-

2, coal had a reactor temperature of 1620 K at the carbon boundary point, and the biomass fuels had reactor temperatures around 1000 K. The higher reactor temperature of coal can most likely explain why the maximum gas efficiency is higher than those of the biomass fuels. Finally, Table 5-4 also suggests why the gas efficiency of coal is higher than that of petcoke. Not only is the N_2 mole fraction of petcoke much higher than that of coal, owing to the much lower equivalence ratio, but the producer gas of coal also contains a higher H_2 content as a direct result of the fuels' compositions.

From Table 5-3, the maximum gas efficiency is higher than the maximum cold-gas efficiency for coal and petcoke only; Orimulsion and the biomass fuels display higher cold-gas efficiencies than exergetic efficiencies. This can be explained by the fact that coal and petcoke have much higher reactor temperatures at the carbon boundary point than Orimulsion and the biomass fuels. A higher temperature lends itself to increased physical exergy of the product stream, which in turn enhances the gas efficiency. The higher temperature does not affect the cold-gas efficiency however.

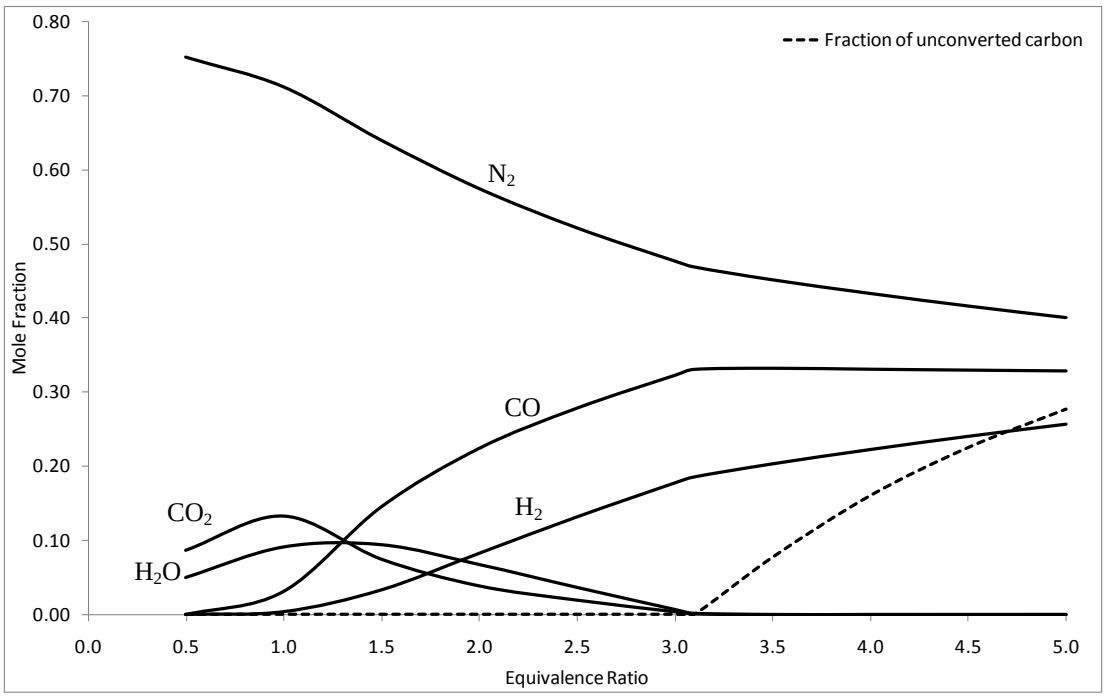

Figure 5-1: Producer gas composition - coal.

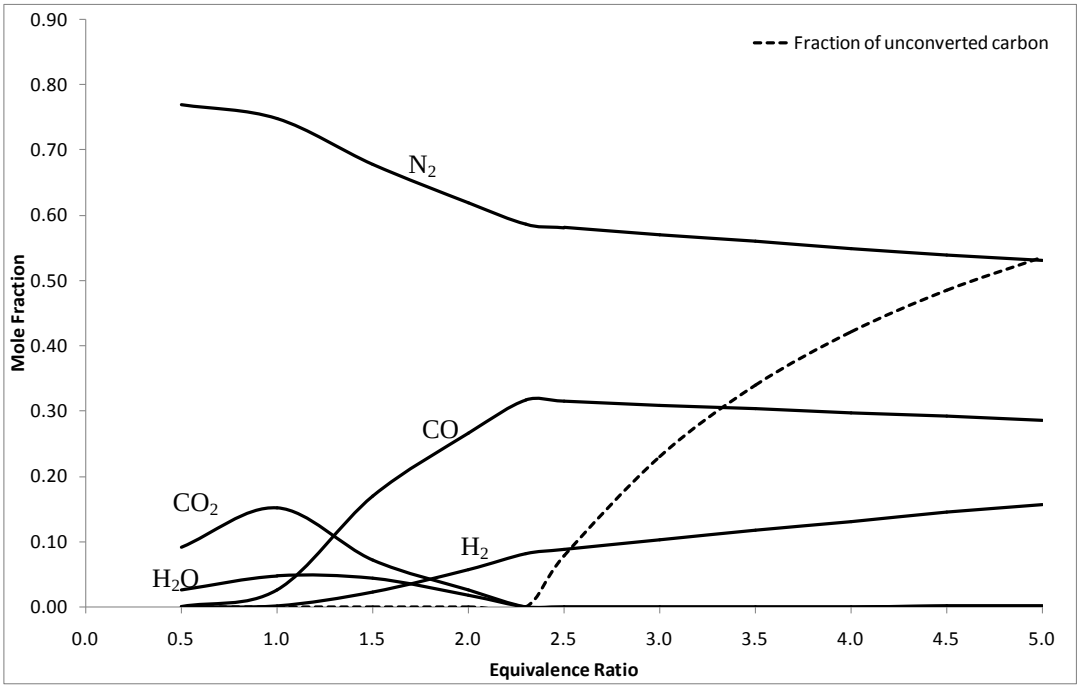

Figure 5-2: Producer gas composition - petcoke.

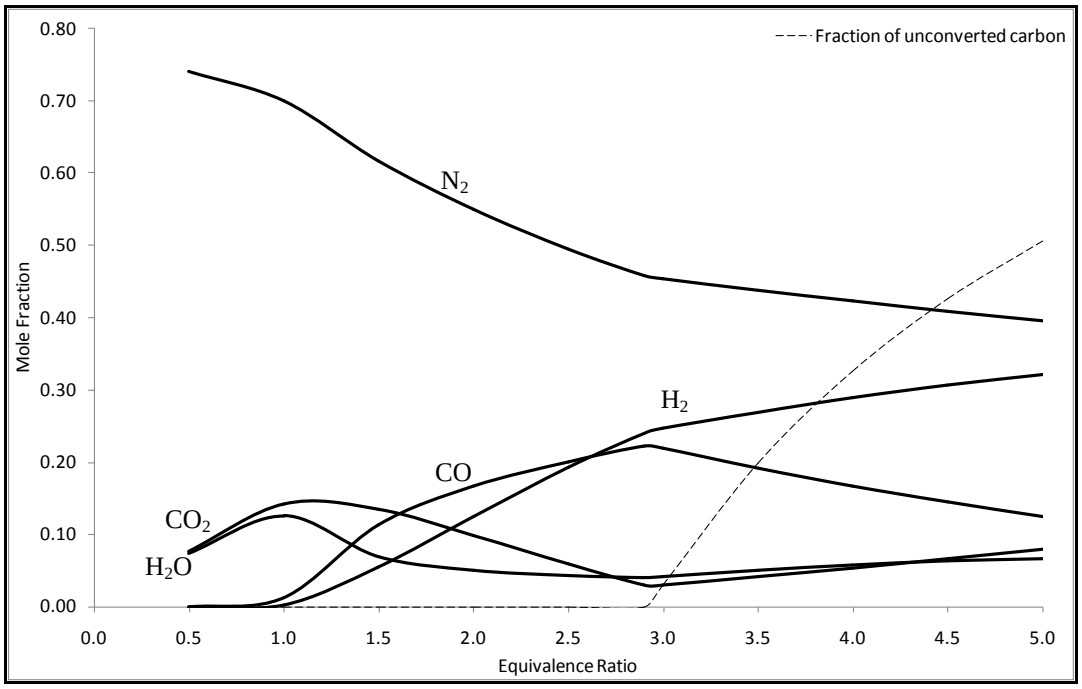

Figure 5-3: Producer gas composition - Orimulsion.

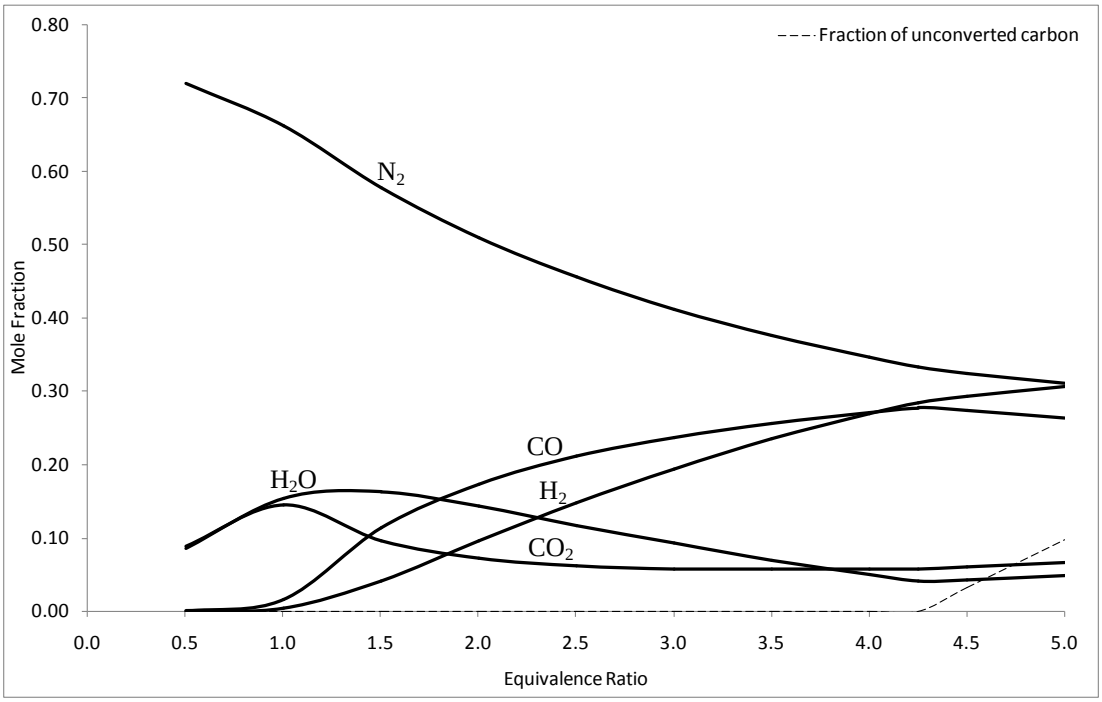

Figure 5-4: Producer gas composition - DDG.

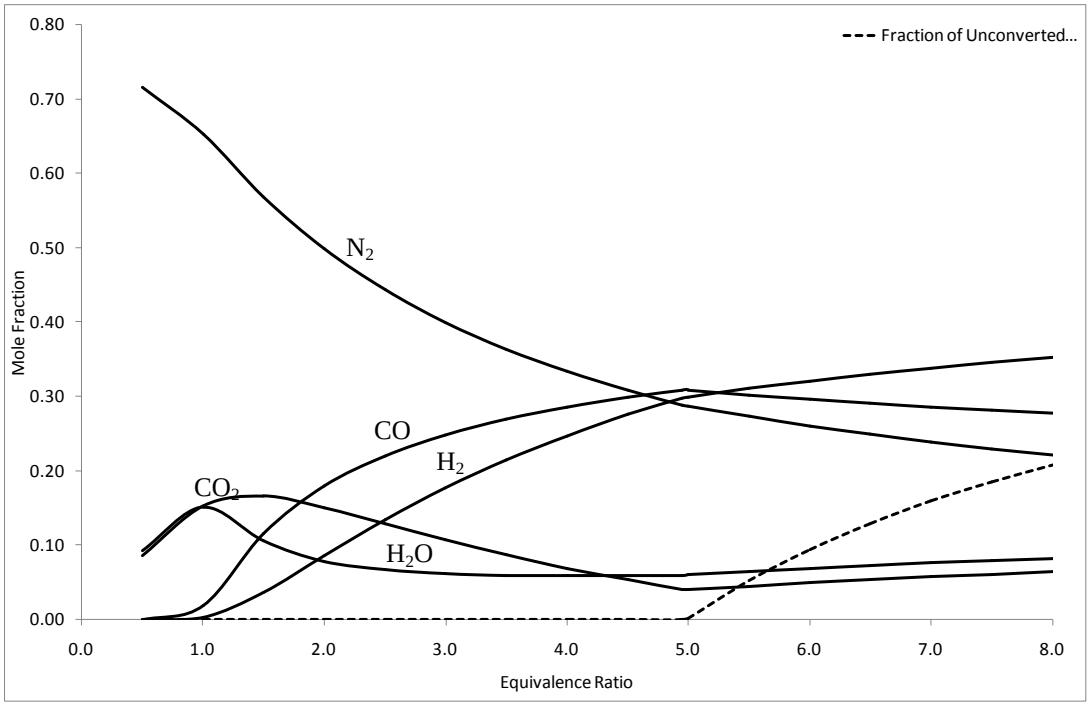

Figure 5-5: Producer gas composition - oat hulls.

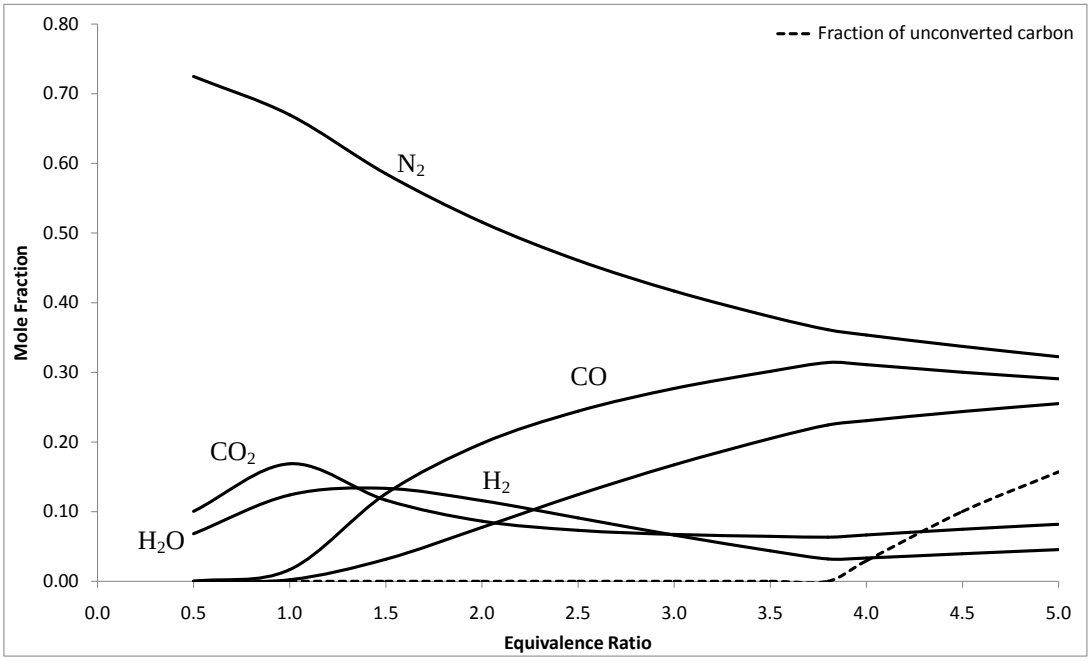

Figure 5-6: Producer gas composition - switchgrass.

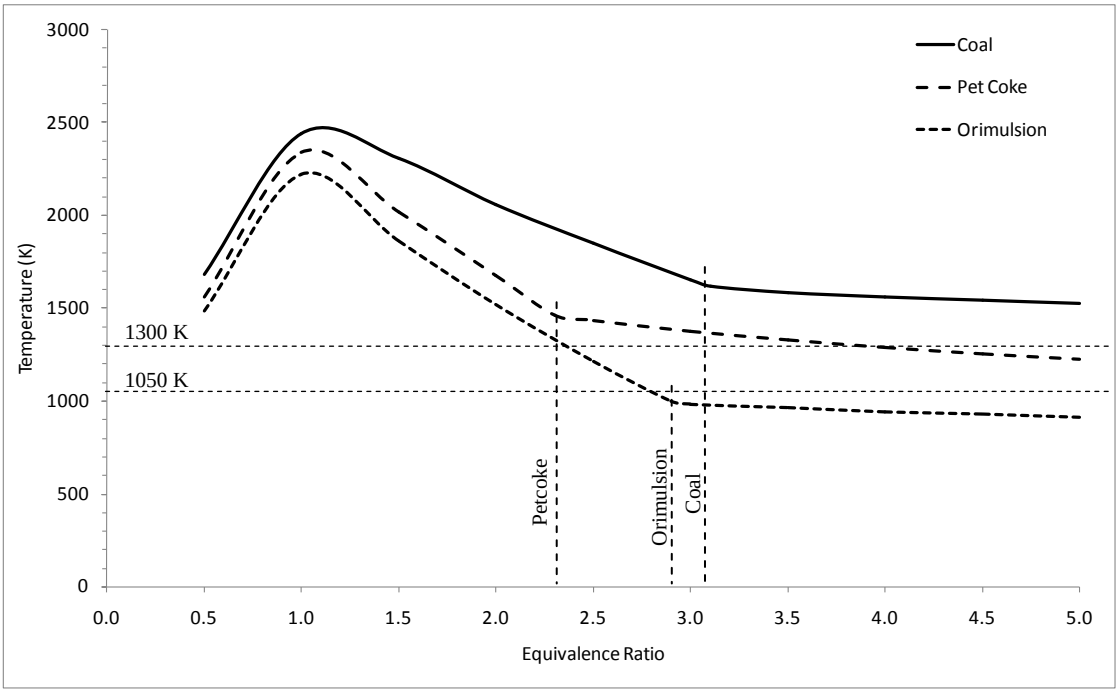

Figure 5-7: Adiabatic reactor temperatures of the fossil fuels.

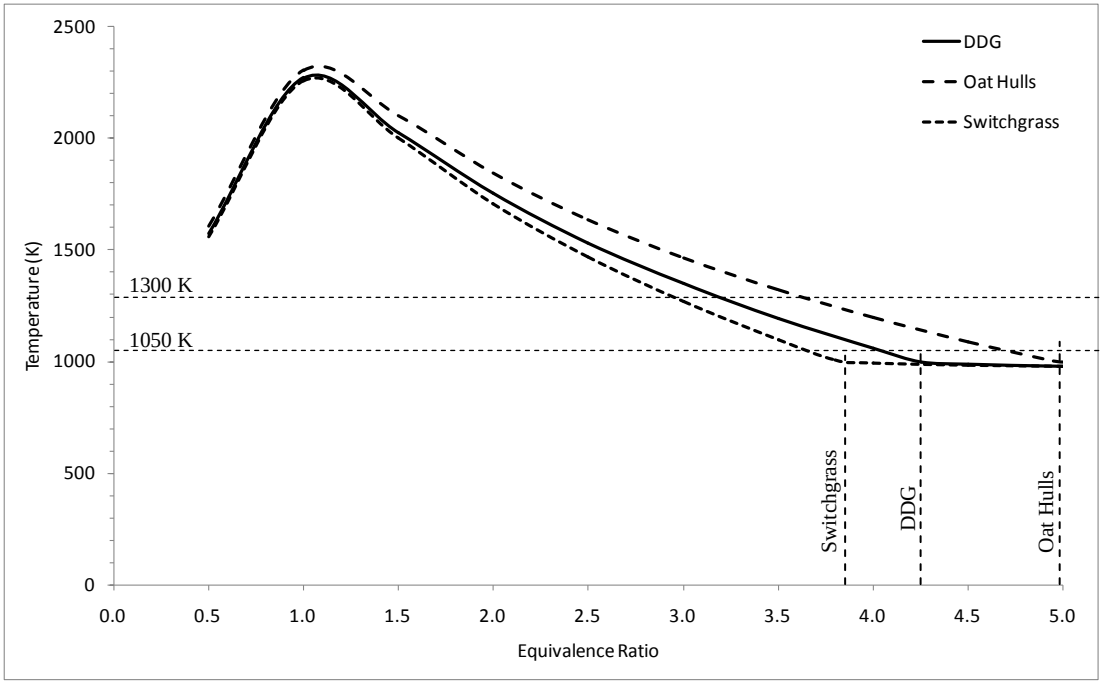

Figure 5-8: Adiabatic reactor temperatures of the biomass fuels.

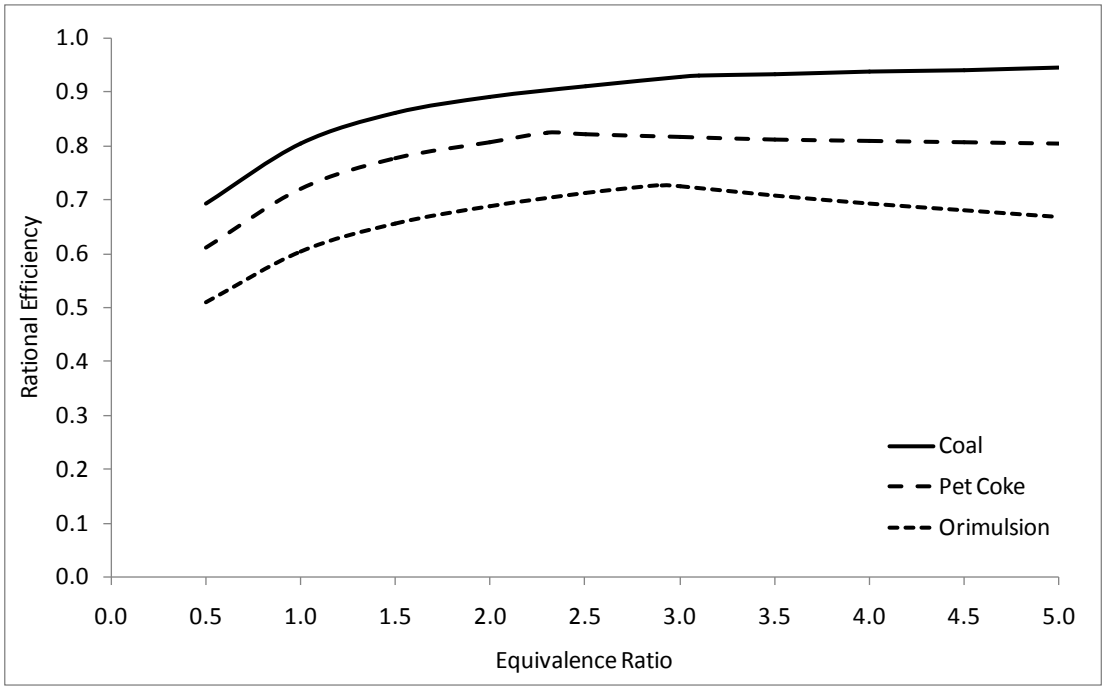

Figure 5-9: Rational efficiencies of fossil fuels.

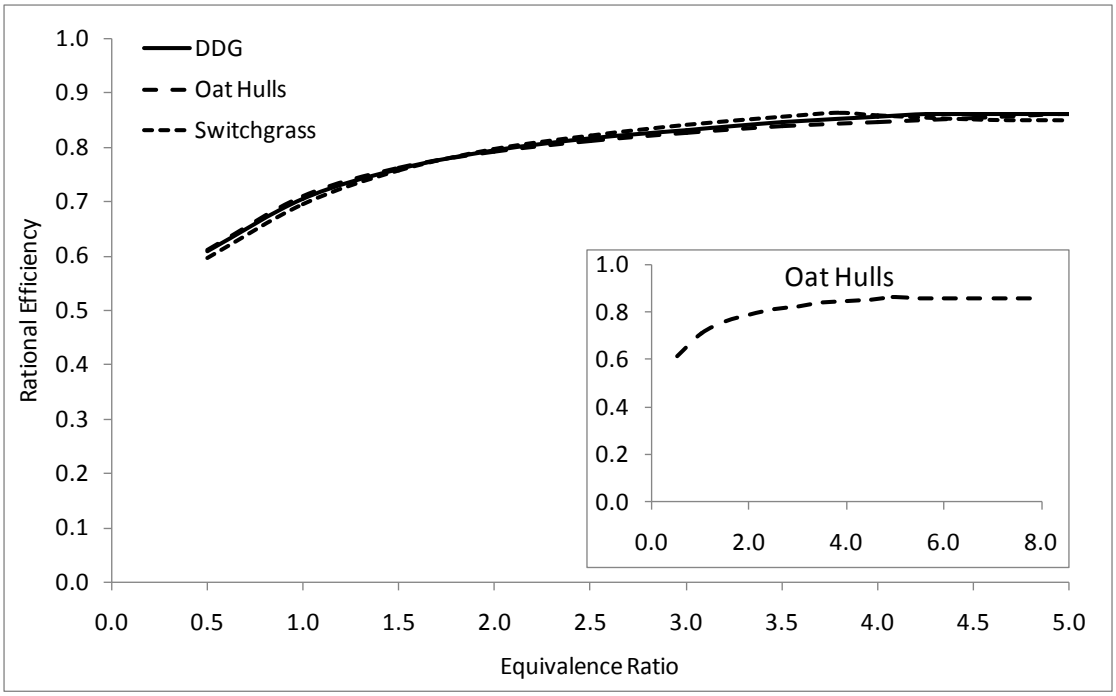

Figure 5-10: Rational efficiencies of biomass fuels.

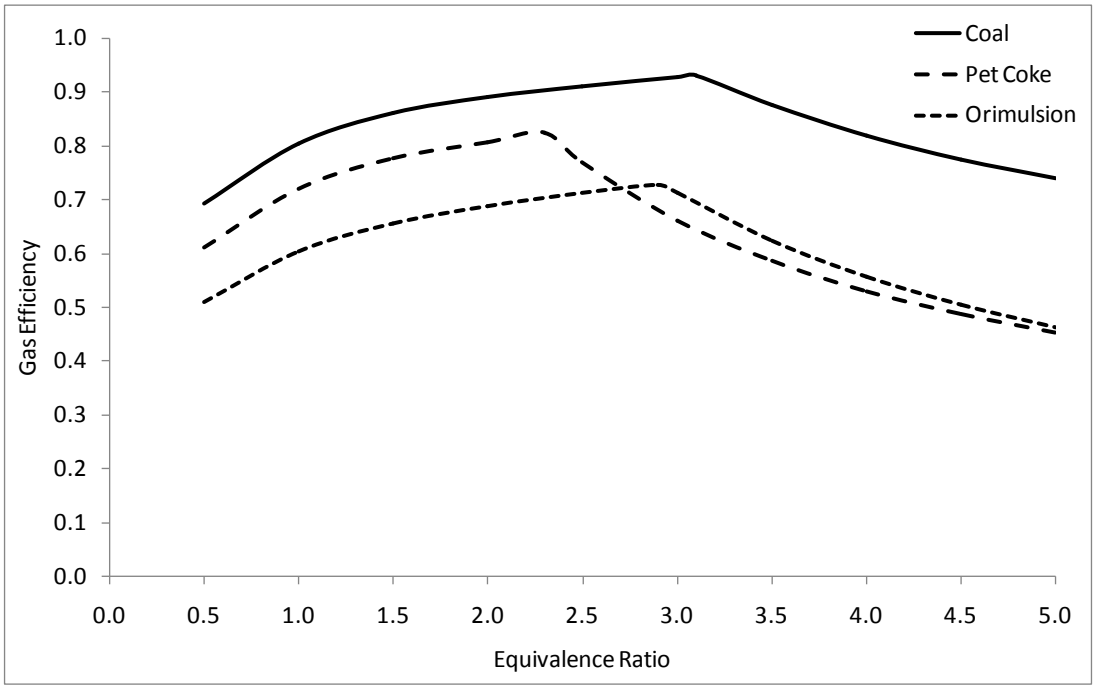

Figure 5-11: Gas efficiencies of fossil fuels.

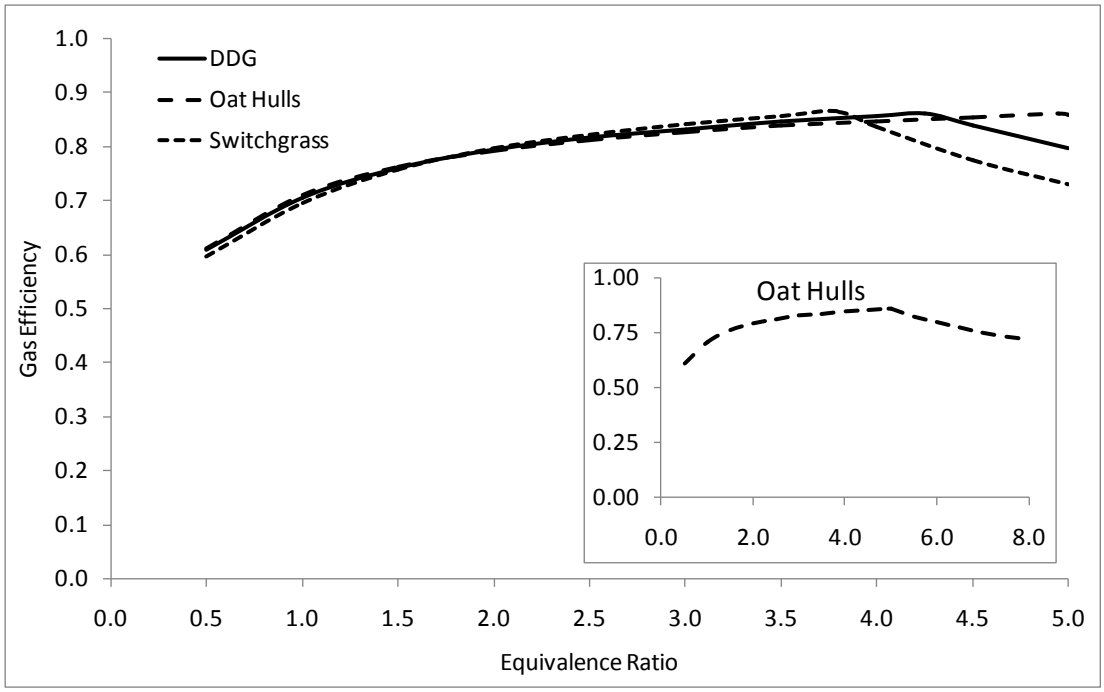

Figure 5-12: Gas efficiencies of biomass fuels.

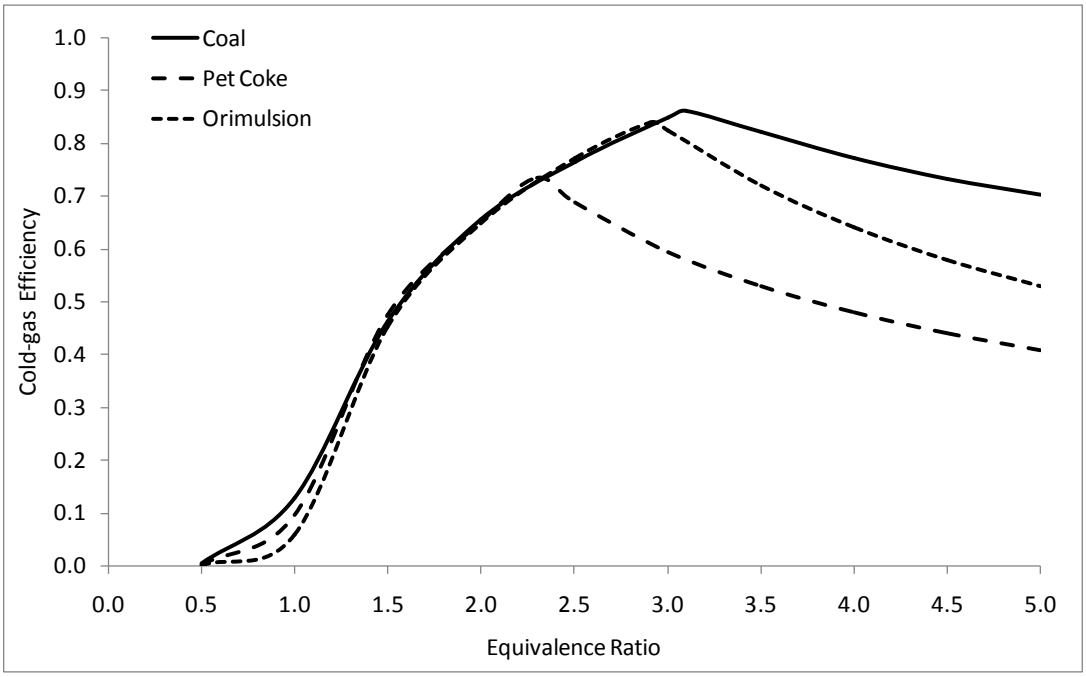

Figure 5-13: Cold-gas efficiencies of fossil fuels.

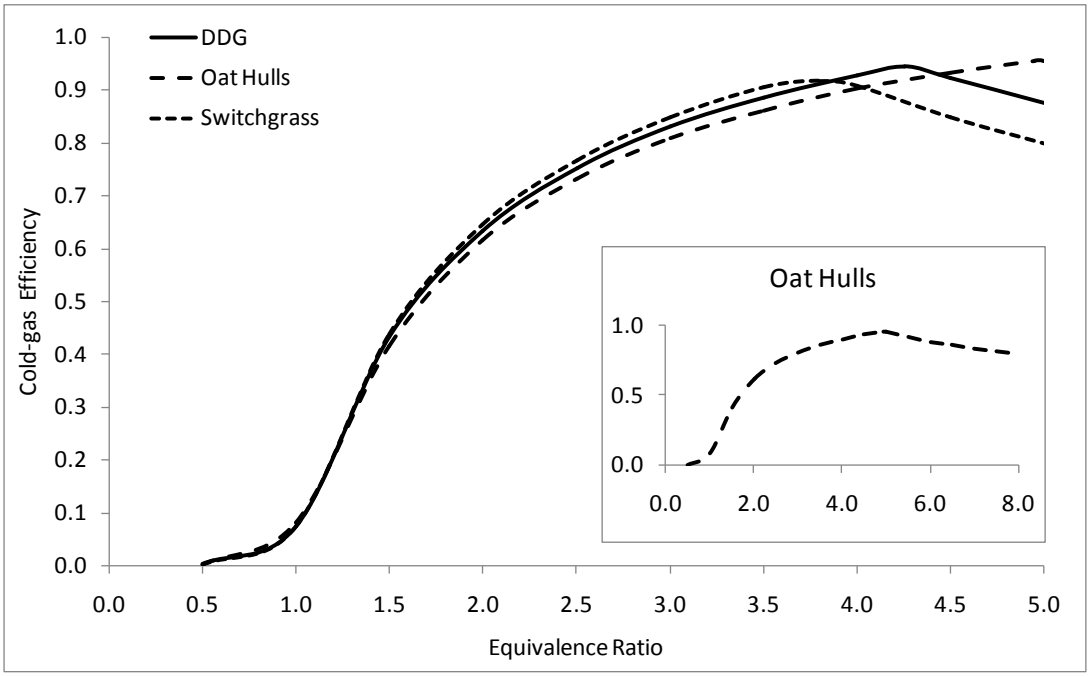

Figure 5-14: Cold-gas efficiencies of biomass fuels.

CHAPTER 6: AN EXERGY ANALYSIS OF OXYBURN PROCESSES

6.1 Introduction

As accounting and regulations of CO_2 emissions become more commonplace, CO_2 capture and storage will become higher priority in the energy industry. The aim of this chapter is to investigate using oxyburn processes for the purpose of capturing CO_2. A thermodynamic analysis of gas separation processes is presented that shows the advantages of oxidizing coal with pure oxygen with respect to CO_2 capture. The feasibility of putting that advantage into practice is then investigated by using exergy analysis to revisit the gasification considerations of Chapter 5. Attention is limited to coal because it is the fuel to be most impacted by concerns of consumption and efficiency due to its worldwide use. The reactor will first be assumed to be adiabatic, and then the implications of a non-adiabatic system will be discussed. The effects of flue gas recirculation on the gasifier will also be investigated.

6.2 A Thermodynamic Analysis of Gas Separation Processes

The purpose of this section is to use thermodynamics to derive an expression for the theoretical minimum amount of work required to separate gases in an isothermal, isobaric, non-reacting process. The result of the derivation will subsequently be used to compare the effectiveness of capturing CO_2 from two different gas separation processes.

The theoretical minimum work required for an adiabatic, isothermal, isobaric process is the negative of the change in Gibbs free energy of that process (Atkins and De Paula, 2006). Considering such a process operating at temperature T and pressure p, the change in Gibbs free energy of the process is

$$\dot{W}_{\min} = -\Delta G(T, p) = \sum_i \dot{n}_i \overline{g}_i(T, p_i) - \sum_e \dot{n}_e \overline{g}_e(T, p_e) \qquad (6\text{-}1)$$

where $\dot{n}$ is the molar flow rate, $\bar{g}$ is the molar specific Gibbs free energy, subscript i represents species entering the system, and subscript e represents species exiting the system. The molar specific Gibbs free energy is defined in Equation 6-2.

$$\bar{g}_j(T, p) = \bar{h}_j(T) - T\bar{s}_j(T, p_j) \tag{6-2}$$

where $\bar{h}_j(T)$ is the molar specific enthalpy of species j at temperature T, and $\bar{s}_j(T, p_j)$ is the molar specific entropy at temperature T and partial pressure p_j. When the molar specific enthalpy is instead evaluated at the standard pressure p_o, the molar specific Gibbs free energy is modified as in Equation 6-3.

$$\bar{g}_j(T, p) = \bar{h}_j(T) - T\bar{s}_j(T, p_o) - \bar{R}T\ln\frac{p_j}{p_o} \tag{6-3}$$

where $\bar{R}$ is the molar universal gas constant. The expression for minimum work becomes

$$\dot{W}_{\min} = \sum_i \dot{n}_i\left(\bar{h}_i(T) - T\bar{s}_i(T, p_o) - \bar{R}T\ln\frac{p_i}{p_o}\right) - \sum_e \dot{n}_e\left(\bar{h}_e(T) - T\bar{s}_e(T, p_o) - \bar{R}T\ln\frac{p_e}{p_o}\right) \tag{6-4}$$

Grouping the enthalpies, standard entropies, and logarithm terms together, the above expression takes the form of Equation 6-5.

$$\dot{W}_{\min} = \left(\sum_i \dot{n}_i\bar{h}_i(T) - \sum_e \dot{n}_e\bar{h}_e(T)\right) + \left(\sum_e \dot{n}_e T\bar{s}_e(T, p_o) - \sum_i \dot{n}_i T\bar{s}_i(T, p_o)\right) + \left(\sum_e \dot{n}_e\bar{R}T\ln\frac{p_e}{p_o} - \sum_i \dot{n}_i\bar{R}T\ln\frac{p_i}{p_o}\right) \tag{6-5}$$

If it is assumed that no chemical reactions take place across the system, then the molar flow rate of each species entering and exiting the system are equal. Then the molar flow rates can be brought outside the summations, and $\dot{n}_j$ becomes the molar flow rate of each species j involved with the process.

$$\dot{n}_i = \dot{n}_e = \dot{n}_j \tag{6-6}$$

$$\dot{W}_{\min} = \sum_j \dot{n}_j \left(\bar{h}_{j,i}(T) - \bar{h}_{j,e}(T)\right) + T\sum_j \dot{n}_j \left(\bar{s}_{j,e}(T, p_o) - \bar{s}_{j,i}(T, p_o)\right)$$

$$+ \bar{R}T\sum_j \dot{n}_j \left(\ln\frac{p_{j,e}}{p_o} - \ln\frac{p_{j,i}}{p_o} \right) \tag{6-7}$$

For an ideal gas, the specific enthalpy and specific entropy are functions of temperature only. Because the process is isothermal, the term $\left(\bar{h}_{j,i}(T) - \bar{h}_{j,e}(T)\right)$ becomes zero, and likewise for the entropy terms. The result is Equation 6-8.

$$\dot{W}_{\min} = \bar{R}T\sum_j \dot{n}_j \ln\frac{p_{j,e}}{p_{j,i}} \tag{6-8}$$

As a result, the theoretical minimum work required for an adiabatic, isothermal, isobaric, non-reacting process is a function of temperature and partial pressures of the species entering and exiting the system. As the temperature increases, the minimum work required increases. Regarding gas separation processes, more work is required to separate gases at higher temperatures than at lower temperatures. Equation 6-8 also shows that as the ratio of partial pressures increases, the minimum required work also increases. Thus as the partial pressure of the species exiting the system increases above the partial pressure at which it entered the system, the work requirement also increases. This relationship means that it will require more work to produce higher purity streams of single species in gas separation processes.

6.3 Gas Separation Study

Pressure swing absorption (PSA) air separation and monoethanolamine (MEA) chemical absorption are the leading industrial processes for N_2-O_2 and CO_2-exhaust separation, respectively (Ho et al., 2006; Kearns and Webley, 2004). Both processes occur at similar temperatures not much higher than room temperature. To illustrate the advantage of oxyburn gasification, two separation scenarios are considered. Consider

two gasification plants that have incentives to capture CO_2 as depicted in Figures 6-1 and 6-2. The plant in Figure 6-1 is an oxyburn gasification plant. Air enters the PSA separator, and pure oxygen is used for gasification and combustion. The products of combustion are primarily CO_2 and H_2O, which are easily separated by condensing the water vapor. The plant in Figure 6-2 is a gasification plant that uses air as the oxidant for gasification and combustion. The combustion products include a large fraction of N_2 as well as CO_2, H_2O, and O_2 (assuming lean combustion). After the water vapor is removed via condensation, the exhaust enters the MEA separator, and pure CO_2 is extracted from the process.

First the theoretical minimum required work to separate O_2 from air is calculated. Here, air is considered to have a molar composition of 79% N_2 and 21% O_2. Air enters the system and two streams consisting of pure N_2 and pure O_2 exit the system. The process is assumed to operate at 30°C and 1 atm.

Applying Equation 6-8 to the PSA separator in Figure 6-8 using a flow of 1 mole of air per second yields

$$\dot{W}_{\min} = \overline{R}T\sum_j \dot{n}_j \ln\frac{p_{j,e}}{p_{j,i}}$$

$$= \overline{R}T\left(\dot{n}_{N_2}\ln\frac{p_{N_2,e}}{p_{N_2,i}} + \dot{n}_{N_2}\ln\frac{p_{O_2,e}}{p_{O_2,i}}\right)$$

$$= \left(8.314\ J/mol\ K\right)\left(303.15\ K\right)\left(0.79\ mol/s\ln\frac{1.0\ atm}{0.79\ atm} + 0.21\ mol/s\ln\frac{1.0\ atm}{0.21\ atm}\right)$$

$$= 1295.4\ J/mol\ air = 6168.6\ J/mol\ O_2$$

A minimum of 6168.6 J per mole of oxygen is theoretically required to separate N_2 and O_2 from air.

To compare the CO_2 capture potential of the two systems in Figures 6-1 and 6-2, Aspen Plus was used to predict the equilibrium products of the two plants. If it is

assumed that the gasifier is operated such that all solid carbon is gasified to gaseous species, then the gasification and combustion steps can be combined to a single equilibrium reactor. The total oxidant used for both processes can be represented by an overall equivalence ratio. Adiabatic gasification and combustion are also assumed. A mass flow rate of coal of $1\,kg/s$ was the basis for each case. In calculating the minimum required work to separate CO_2 from the exhaust of the system in Figure 6-2, it was assumed that H_2O was separated from the combustion products via condensation. It was also assumed that the temperature and pressure of the MEA separator are the same as the PSA separator, so the exhaust entered the MEA separator at 30°C, 1 atm. Equation 6-8 was used to calculate the theoretical minimum work required to separate CO_2 from the exhaust. For the oxyburn process, the required feed rate of oxygen was used to calculate the minimum work using the value of 6168.6 J per mole oxygen.

Figure 6-3 is a plot of minimum work necessary to capture CO_2 for the two systems. For the oxyburn process, as the equivalence ratio increases from 0.4 to 1.0, the minimum work required to capture CO_2 decreases from 14.4 to 7.5 kJ/mol CO_2. For the process using air, the minimum work required to capture CO_2 decreases from 9.0 to 7.0 kJ/mol CO_2. The minimum required work is much higher at lean conditions for the oxyburn process because more production of oxygen is required, which subsequently requires more energy. Because pure oxygen requires a considerable amount of energy to produce, lean operation of the system results in a waste of energy.

Coal is typically burned lean to lower the combustion temperature. From Figure 6-3, if coal is to be oxidized at lean conditions, then it requires less energy to capture CO_2 using exhaust gas separation as opposed to using the oxyburn process. However, if the oxyburn process can be operated at an overall equivalence ratio closer to stoichiometric, then it has the potential to require less energy to capture CO_2. Operating closer to stoichiometric requires less production of pure oxygen, and less energy will be required to capture CO_2. If the oxyburn process can be operated closer to stoichiometric

and the process using air continues to operate at a very lean condition, then the oxyburn process becomes more competitive with the latter for capturing CO_2. If coal is oxidized by air at an overall equivalence ratio of 0.6, the oxyburn process requires less energy to capture CO_2 at an overall equivalence ratio of 0.85. If coal is oxidized by air at an overall equivalence ratio of 0.5, the oxyburn process requires less energy to capture CO_2 at an overall equivalence ratio of 0.77. If coal is oxidized by air at an overall equivalence ratio of 0.4, the oxyburn process requires less energy to capture CO_2 at an overall equivalence ratio of 0.72.

6.4 Oxidation of Coal Using Pure Oxygen – Methodology

This study focuses on the oxidation of coal using pure oxygen at atmospheric pressure. Pure oxygen is assumed to be supplied by a PSA process. PSA air separation typically occurs at temperatures not much higher than room temperature, and thus the oxygen is assumed to be supplied to the gasifier at the temperature and pressure of the environment (Kearns and Webley, 2004). For adiabatic operation, the independent variable is again the relative amount of oxidant reacting with the fuel. The equivalence ratio is used to define the relative amount of oxidant in the system, but it is modified from air to oxygen as defined in Equation 6-9

$$\phi = \frac{m_{fuel} / m_{O_2}}{\left(m_{fuel} / m_{O_2} \right)_{st}} \tag{6-9}$$

where m_{O_2} is the mass of oxygen. For non-adiabatic operation, the gas efficiency is modified to account for heat transfer to or from the reactor. The modified gas efficiency is defined by Equation 6-10.

$$\varepsilon_{gas} = \begin{cases} \dfrac{E_{gas}}{E_{fuel} + E_{gas.medium} + \left(1 - \dfrac{T_\infty}{T_b}\right)\left|Q\right|} & (\textit{heat addition}) \\ \dfrac{E_{gas} + \left(1 - \dfrac{T_\infty}{T_b}\right)\left|Q\right|}{E_{fuel} + E_{gas.medium}} & (\textit{heat extraction}) \end{cases} \tag{6-10}$$

where T_b is the boundary temperature at which heat transfer occurs and Q is the reactor heat duty. Because the reactor is uniform in temperature, the boundary temperature was taken to be the same as the reactor temperature. The gas efficiency defined by Equation 6-10 is equivalent to the gas efficiency defined by Equation 5-6 in Section 5.2 when the heat duty is zero, making the reactor adiabatic. Finally, the same sample of coal from Chapter 5 is used in this study of pure oxygen oxidation of coal.

6.5 Results and Discussion – Adiabatic Reactor

Figure 6-4 shows the adiabatic reactor temperatures of coal oxidized by air and pure oxygen. The adiabatic temperatures of the oxygen system are much higher than those of the air system. At an equivalence ratio of 1.0, the adiabatic temperature is 3574 K when oxidized by oxygen and 2438 K when oxidized by air. Even in the very rich regime, the adiabatic temperature of the oxygen system is 500 – 600 K higher than the air system.

Figure 6-5 is a plot of mole fractions of the major gas species, as well as the fraction of unconverted carbon, for pure oxygen oxidation of coal. This plot can be compared to the producer gas composition of coal oxidized by air in Figure 5-1. The carbon boundary point is apparent where the fraction of unconverted carbon becomes zero, and this occurs at an equivalence ratio of 3.25. In comparison, air oxidation of coal resulted in a carbon boundary point of 3.10. Although the two carbon boundary points could be expected to share the same equivalence ratio, the slight difference between the two can most likely be attributed to the large difference in temperatures. For the system oxidized by air, the carbon boundary point occurs at a temperature of 1620 K, whereas

for the system oxidized by oxygen, the carbon boundary point occurs at a temperature of 2401 K.

In Figure 6-5, CO_2 and H_2O almost completely disappear from the equilibrium products at the carbon boundary point. Figure 6-5 differs from Figure 5-1 in two significant ways. First, the mole fraction of CO is always higher than that of CO_2 over the range of equivalence ratios plotted. Even in the lean regime, the CO mole fraction is higher than that of CO_2. This appears to be caused by the temperature of the system. When oxidized by air, it was apparent that the equivalence ratio governed the oxidation of carbon, as CO_2 was favored over CO in the lean regime. However, when oxidized by pure oxygen, the much higher temperatures appear to have a larger influence on carbon oxidation than the equivalence ratio. The second major difference is that O_2 replaces N_2 as the major diluent. Here, the only source of N_2 is nitrogen content of the fuel. As a result, the mole fraction of N_2 in the producer gas is less than 0.005 for the range of equivalence ratios plotted and is thus not shown. In addition, the mole fraction of O_2 remains relatively high until an equivalence ratio of about 2.0. Even at stoichiometric, O_2 has a mole fraction of 0.23. The relatively high O_2 mole fraction can most likely be attributed to the fact that the temperature favors CO over CO_2. As a result, the system restricts the amount of O_2 that reacts with carbon, and leftover O_2 is available in the products. Again, the temperature appears to replace the equivalence ratio as the dominant factor in determining the equilibrium products.

Figure 6-6 compares the gas efficiencies between the systems oxidized by pure oxygen and air. The gas efficiency of the oxygen system is much higher than that of the air system in the lean regime and up to an equivalence ratio of about 1.5. At an equivalence ratio of 1.0, the gas efficiency of the oxygen system is 0.91, whereas for the air system it is only 0.80. The gas efficiencies are about equal at an equivalence ratio of 2.5 and remain comparable as the equivalence ratio increases. The maximum gas efficiency for the system oxidized by oxygen again occurs at the carbon boundary point.

At each system's respective carbon boundary points, the gas efficiencies are 0.94 for the oxygen system and 0.93 for the air system. It is interesting to note that these values do not differ much, considering that the system oxidized by air contains a considerable amount of N_2 as a diluent (a mole fraction of 0.47), whereas the system oxidized by pure oxygen has virtually no diluents at the carbon boundary point. The reason that the maximum gas efficiency of the air system is comparable to that of the oxygen system is a result of the quantity of gas exiting the reactor. The producer gas of the oxygen system contains a higher specific physical exergy as a result of higher temperatures, and the specific chemical exergy is higher because of the lack of diluents. However, overall less gas exits the reactor as a result of overall less oxidant being introduced to the reactor. These results show that using pure oxygen is much more efficient than using air when combustion of coal is desired. The results also show that using air yields comparable efficiencies to using pure oxygen when gasification of coal is desired.

6.6 Results and Discussion – Non-Adiabatic Reactor

The adiabatic reactor temperatures of coal oxidized by pure oxygen are much too high for practical material limits. The reactor temperature must be lowered before coal can be effectively oxidized by pure oxygen. One approach to lowering the reactor temperature is removing heat via a cooling jacket.

Figure 6-7 plots the heat duty required to operate the reactor over a range of temperatures, along with the gas efficiencies. Positive values of heat duty represent heat that must be extracted from the reactor, and negative values of heat duty represent heat that must be added to the reactor. The fine vertically dashed line marks 1620 K, the adiabatic temperature at which the carbon boundary point occurs for oxidation of coal by air. This temperature is used as a rough upper limit for which the reactor must be operated to avoid breakdown of reactor materials. Equivalence ratios of 3.25 and 2.50 are plotted. The equivalence ratio of 3.25 was the carbon boundary point of the adiabatic

system. At this equivalence ratio, 2840 kJ/(kg fuel) of heat must be removed from the reactor to bring the temperature down to 1620 K. This value accounts for 12% of the lower heating value of the fuel. For a fixed equivalence ratio in a non-adiabatic system, solid carbon becomes deposited in the products when the temperature becomes low enough. As a result, for a non-adiabatic system, the carbon boundary point becomes associated with a specific temperature. If the equivalence ratio is fixed at 3.25, the carbon boundary point occurs at a temperature of 2000 K, and about 3% unreacted carbon will be deposited in the products at a temperature of 1620 K.

To avoid the deposition of solid carbon while bringing the temperature down to a reasonable level, the equivalence ratio must be decreased. An equivalence ratio of 2.50 is used as an example. An equivalence ratio of 2.50 results in a much higher adiabatic reactor temperature (3110 K) than an equivalence ratio of 3.25 (2400 K). Consequently for the non-adiabatic system, much more heat must be removed to lower the temperature to 1620 K. For an equivalence ratio of 2.5, 5300 kJ/(kg fuel) must be removed from the reactor to achieve a temperature of 1620 K, almost twice the amount necessary for an equivalence ratio of 3.25. This amount accounts for 22% of the lower heating value of the fuel. Fixing the equivalence ratio at 2.50 results in a carbon boundary point occurring at a temperature of 1045 K. Therefore no solid carbon can be expected to be deposited in the products at typical operating temperatures.

The benefit to lowering the equivalence ratio from 3.25 to 2.50 is that the reactor temperature can be decreased to a more reasonable level while avoiding deposition of solid carbon in the products. Moreover, the gas efficiency is not negatively affected; in fact it increases slightly when the equivalence ratio is decreased from 3.25 to 2.50. The disadvantage to decreasing the equivalence ratio is that the amount of heat that must be removed from the reactor increases significantly. If a cooling jacket is used, an increase in heat duty requires an increased coolant flow rate. In conclusion, the carbon boundary point, heat duty, and exergetic efficiency are important considerations that must be

weighed when considering what equivalence ratio to operate the reactor. If solid carbon can be effectively captured and reintroduced into the reactor, then it may be desirable to increase the equivalence ratio. This in turn would decrease the heat duty of the cooling jacket without significantly affecting the efficiency.

6.7 Flue Gas Recirculation

The results of Section 6.6 showed that lowering the reactor temperature by removing heat may be difficult and costly. Flue gas recirculation (FGR) is another option for lowering the reactor temperature, and the effects of using it with an oxyburn gasification process are investigated.

Flue gas recirculation was simulated in Aspen Plus as follows. The solids exiting the adiabatic gasifier were separated from the gasification products. The solid-free producer gas was cooled to 50°C. It was then fed to an RGIBBS block where it reacted with either pure oxygen or air to simulate syngas combustion. The combustion took place at atmospheric pressure at an equivalence ratio of 1.0. Finally the hot combustion flue gas was isobarically cooled to 500 K before a mass splitter sent a portion of it back to the gasification reactor. Flue gas recirculation was defined by a mass percentage of the flue gas exiting the combustor. The gas efficiency of the gasification reactor was modified to account for the added physical exergy of the recirculation stream entering the gasifier, as shown in Equation 6-11

$$\varepsilon_{gas} = \frac{E_{gas}}{E_{fuel} + E_{gas.medium} + E_{rec.gas}} \tag{6-11}$$

where $E_{rec.gas}$ is the exergy of the recirculated flue gas. The recirculated flue gas contains some amount of O_2. However, equivalence ratios discussed in this section pertain only to the fuel and gasifier oxidant, and the recirculated gas is not considered in the calculation of the equivalence ratio. Effective equivalence ratios are reported that are dependent on the extent of FGR to show how they vary with FGR.

The effects of recirculating flue gas from combustion with pure oxygen will first be discussed. Figure 6-8 is a plot of adiabatic reactor temperature vs. percent FGR for gasification equivalence ratios of 3.25, 4.0, and 4.7 and flue gas from combustion with pure oxygen. The fraction of unconverted carbon is also plotted for equivalence ratios of 4.0 and 4.7. No solid carbon was deposited in the products for an equivalence ratio of 3.25 over the range plotted. The flue gas consists of almost entirely CO_2 and H_2O, and adding it to the gasifier acts to increase the specific heat of the system, thereby decreasing the adiabatic temperature. As the percentage of FGR increases, the adiabatic temperature decreases. The recirculated flue gas also increases the availability of oxidant in the gasifier which affects the deposit of solid carbon in the products. For an equivalence ratio of 4.0, as the FGR percentage increases from 0 – 10%, the fraction of unconverted carbon decreases to 0. No solid carbon is deposited in the products until 82% FGR. The reintroduction of solid carbon in the system at 82% FGR is a result of the temperature having a greater impact on the solid carbon equilibrium than the amount of oxidant. At 82% FGR, the reactor temperature is decreased to 831 K, and the low temperature begins to favor solid carbon in the products. As a result, for equivalence ratios past the carbon boundary point, flue gas recirculation introduces a window in which solid carbon disappears from the system. A similar window materializes for an equivalence ratio of 4.7, although the range in FGR is shorter than for an equivalence ratio of 4.0. Solid carbon disappears from the products at 14% FGR. Solid carbon reappears in the products at 70% FGR, at which the reactor temperature has decreased to 860 K. For equivalence ratios of 4.0 and 4.7, the disappearance of solid carbon from the products also causes a small dip and rise in the temperature profiles.

When using flue gas from combustion with pure oxygen, a significant percentage of FGR is required to achieve reasonable operating temperatures. If it is desired to bring the reactor temperature down to 1620 K, which is the carbon boundary point of the adiabatic system oxidized by air, then 48% FGR would be required for an equivalence

ratio of 3.25. 42% and 37% FGR are required to achieve a reactor temperature of 1620 K for equivalence ratios of 4.0 and 4.7, respectively.

Figure 6-9 is a plot of the gas efficiency vs. percent FGR for gasification equivalence ratios of 3.25, 4.0, and 4.7 and flue gas from combustion with pure oxygen. For an equivalence ratio of 3.25, the gas efficiency steadily decreases as the FGR percentage increases. The decrease in gas efficiency is a result of diluting the producer gas with CO_2 and H_2O. For an equivalence ratio of 4.0, the gas efficiency increases sharply from 0 – 10% FGR as a result of a decreasing amount of solid carbon being deposited in the products. The gas efficiency even surpasses the gas efficiency of an equivalence ratio of 3.25, which displayed the maximum gas efficiency (0.938) for the system without FGR. At 10% FGR, the gas efficiency reaches a maximum of 0.966, after which it decreases at a slope similar to that of the equivalence ratio of 3.25. At 82% FGR, the gas efficiency begins to decrease much more rapidly as a result of an increasing amount of solid carbon being deposited in the products. The results show that the equivalence ratio can be increased past 3.25 and attain a higher gas efficiency when FGR is used. However, there is a limit to how high the equivalence ratio can be increased while achieving a higher gas efficiency. When using flue gas from combustion with pure oxygen, this equivalence ratio limit is 4.7. At an equivalence ratio of 4.7, the maximum gas efficiency attained is 0.970, which occurs where solid carbon disappears from the products at 14% FGR. Past 14% FGR, the gas efficiency similarly decreases steadily until solid carbon forms in the products again at 70% FGR, after which it decreases more sharply. The results show that by using FGR, the equivalence ratio can be increased from 3.25 to 4.7 to increase the maximum gas efficiency from 0.938 to 0.970, representing a 3.3% increase. The main purpose of using FGR is to lower the reactor temperature to within practical material limits, and the results show that this can be achieved without sacrificing the efficiency of the gasifier.

Figure 6-10 is a plot of the effective equivalence ratio vs. percent FGR for gasification equivalence ratios of 3.25, 4.0, and 4.7. The three lines represent the fixed equivalence ratios corresponding to the original fuel and oxidant. As the percentage of FGR approaches 0%, the effective equivalence ratio approaches the corresponding fixed equivalence ratio. As the percentage of FGR increases, the effective equivalence ratio decreases. The flue gas contains a finite amount of O_2, and as the percentage of FGR increases, an increased amount of O_2 is added to the gasifier in addition to the O_2 supplied by the gasifying medium. The additional O_2 results in making the system leaner overall.

The results of recirculating flue gas from combustion with air are discussed next. Figure 6-11 is a plot of adiabatic reactor temperature vs. percent FGR for gasification equivalence ratios of 3.25, 4.0, and 4.8, and flue gas from combustion with air. The fraction of unconverted carbon is also plotted for equivalence ratios of 4.0 and 4.8. No solid carbon was deposited in the products for an equivalence ratio of 3.25 over the range plotted. Similar to Figure 6-8, equivalence ratios of 4.0 and 4.8 display windows in which solid carbon can be avoided from being deposited in the products. For an equivalence ratio of 4.0, solid carbon disappears from the products at 10% FGR. Solid carbon reappears in the products at 48% FGR, at which the temperature has decreased to 909 K. For an equivalence ratio of 4.8, solid carbon disappears from the products at 16% FGR and reappears at 24% FGR, at which the temperature has decreased to 1033 K.

The flue gas is now a dilute mixture consisting of mostly N_2, CO_2, and H_2O. Compared to Figure 6-8, Figure 6-11 shows that the reactor can be decreased to similar temperatures using a lesser amount of FGR. If it is desired to bring the reactor temperature down to 1620 K, then 21%, 10%, and 8% FGR are needed for equivalence ratios of 3.25, 4.0, and 4.8, respectively. The decrease in required amounts of FGR is a result of the flue gas containing a significant amount of N_2 (a mole fraction of about 0.65).

Figure 6-12 is a plot of gas efficiencies vs. percent FGR for equivalence ratios of 3.25, 4.0, and 4.8 and flue gas from combustion using air. For an equivalence ratio of 3.25, the gas efficiency steadily decreases in a similar manner as seen in Figure 6-9. Again this decrease is a result of dilution of the producer gas with N_2, CO_2, and H_2O. For an equivalence ratio of 4.0, the gas efficiency rises steeply from 0 – 10% FGR as a result of the decreasing fraction of unconverted solid carbon in the products. As the FGR percentage increases, more oxidant is available to convert solid carbon to gaseous products, and the gas efficiency is able to increase past the gas efficiency of an equivalence ratio of 3.25. At 10% FGR, the gas efficiency reaches a maximum of 0.962, after which it decreases at a similar slope to that of the equivalence ratio of 3.25. Again the equivalence ratio can be increased with added FGR until a maximum gas efficiency is reached. When using flue gas from combustion with air, the equivalence ratio limit is 4.8, similar to the limit of 4.7 found with using flue gas from combustion with pure oxygen. At an equivalence ratio of 4.8, the maximum gas efficiency attained is 0.968, which occurs where solid carbon disappears from the products at 16% FGR. Past 16% FGR, the gas efficiency similarly decreases steadily until solid carbon forms in the products again at 24% FGR. The results show that by using FGR, the equivalence ratio can be increased from 3.25 to 4.8 to increase the maximum gas efficiency from 0.938 to 0.962, representing a 2.6% increase.

Figure 6-13 is a plot of the effective equivalence ratio vs. percent FGR for gasification equivalence ratios of 3.25, 4.0, and 4.8. The three lines represent the fixed equivalence ratios corresponding to the original fuel and oxidant. As the percentage of FGR approaches 0%, the effective equivalence ratio approaches the corresponding fixed equivalence ratio. Similar to Figure 6-10, recirculating flue gas back to the gasifier makes the system leaner overall.

The results show that using FGR to lower the reactor temperature provides additional benefits to gasifier operation. First, the equivalence ratio can be increased past

the standard carbon boundary point. FGR provides additional oxidant to the reactor, thereby creating a window in which solid carbon can be removed from the products. At the same time, operating at a richer equivalence ratio within the solid carbon window of FGR causes the maximum gas efficiency to increase past that of the standard carbon boundary point. Finally, increasing the equivalence ratio results in decreased amounts of FGR required to lower the reactor temperature, because richer equivalence ratios naturally result in lower reactor temperatures.

Comparing the effects between using flue gas from combustion with pure oxygen and air also merits discussion. When the equivalence ratios of both systems are increased to 4.7 and 4.8, respectively, they can achieve almost identical gas efficiencies. If it is desired to bring the reactor temperature down to 1620 K, then 37% FGR is required for the system combusted with pure oxygen, and 8% FGR is required for the system combusted with air. Although 8% FGR might require less gas handling equipment than 37% FGR, it may be more desirable to use flue gas from combustion with pure oxygen for the benefit of capturing CO_2 as discussed in Section 6.2. The study of flue gas recirculation focused on gasification with pure oxygen, so pure oxygen is already available within the plant. Gasifying coal with pure oxygen does not achieve gas efficiencies much higher than gasifying with air. The benefit of gasifying with pure oxygen and recirculating flue gas from combustion with pure oxygen would have to lie in the ability to capture CO_2. Therefore it does not make sense to gasify coal with pure oxygen and recirculate flue gas from combustion with air, because energy would be used for N_2-O_2 separation at the front end and CO_2-exhaust separation at the back end. Using both forms of separation within the same plant would also require twice the amount of equipment.

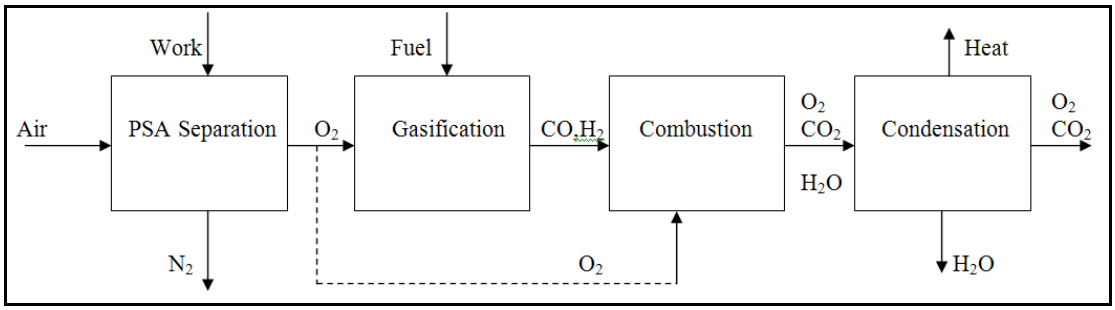

Figure 6-1: Simplified oxyburn gasification plant.

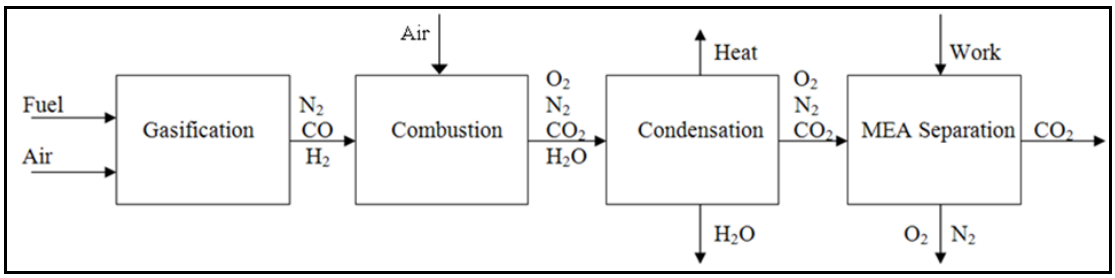

Figure 6-2: Simplified air-gasification plant.

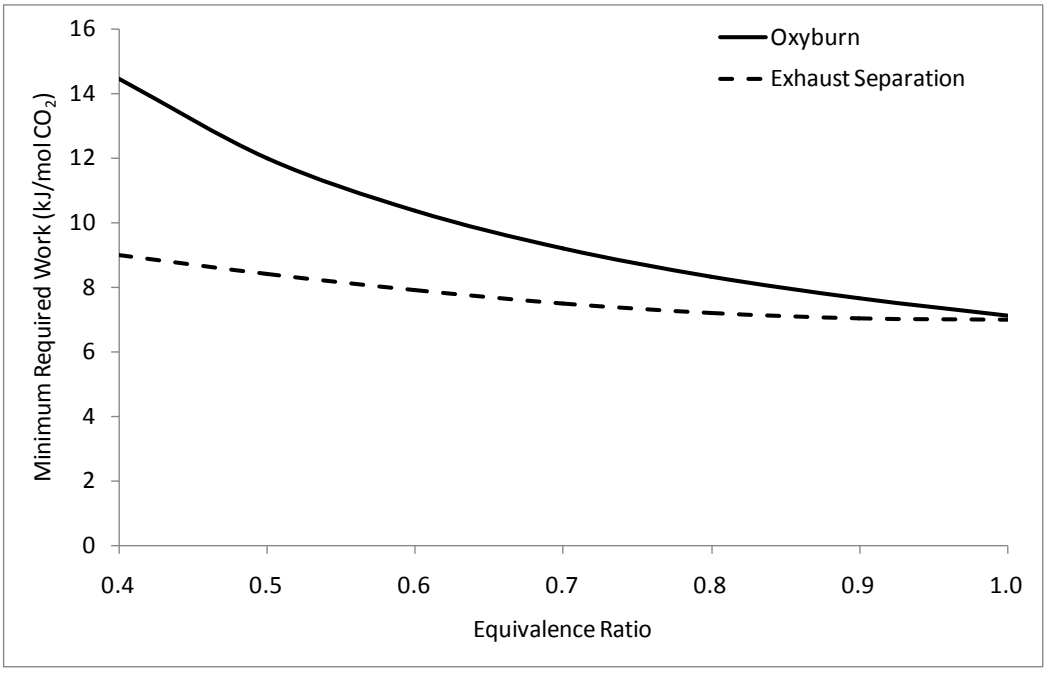

Figure 6-3: Minimum work required for gas separation processes to capture CO_2.

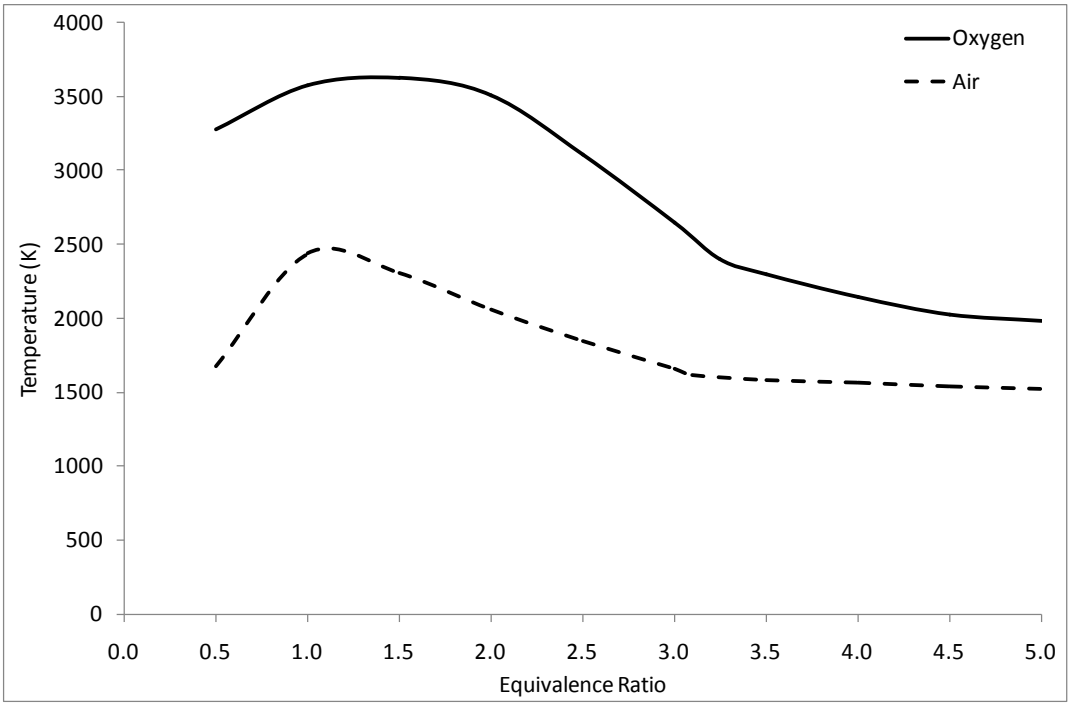

Figure 6-4: Adiabatic reactor temperatures of coal oxidized by oxygen and air.

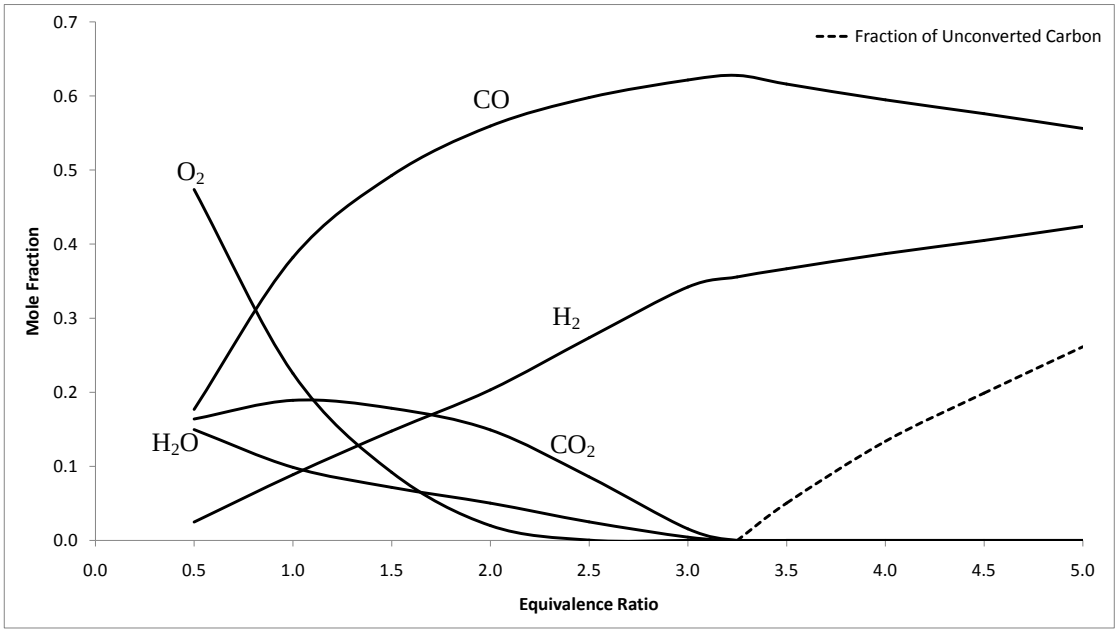

Figure 6-5: Producer gas composition – coal oxidized by pure oxygen.

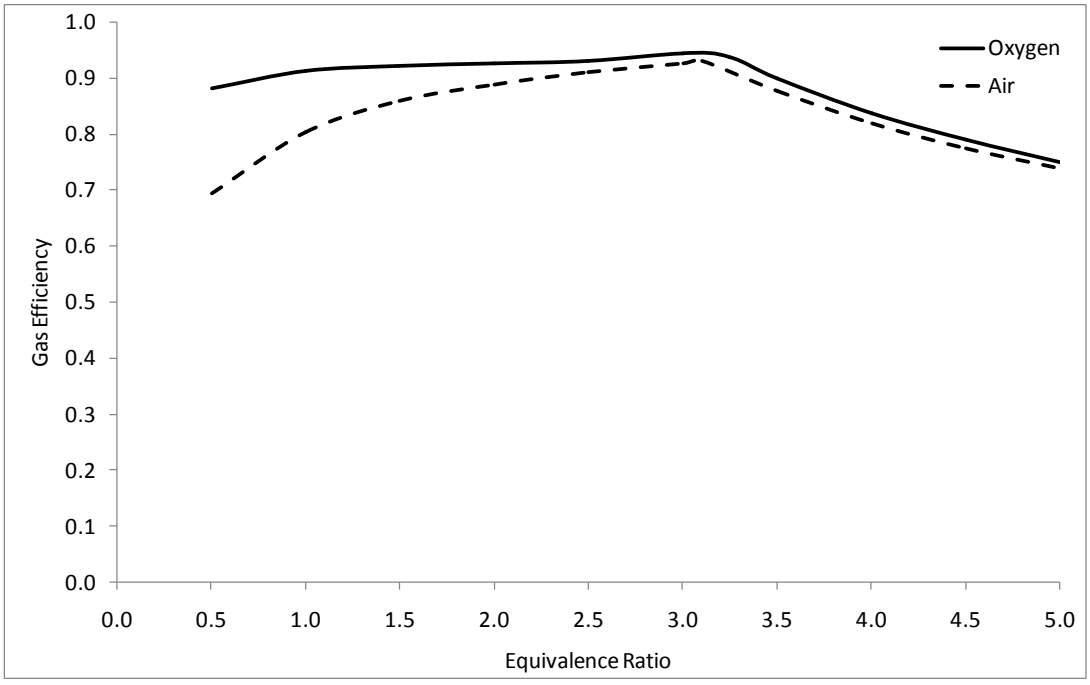

Figure 6-6: Gas efficiencies of coal oxidized by oxygen and air.

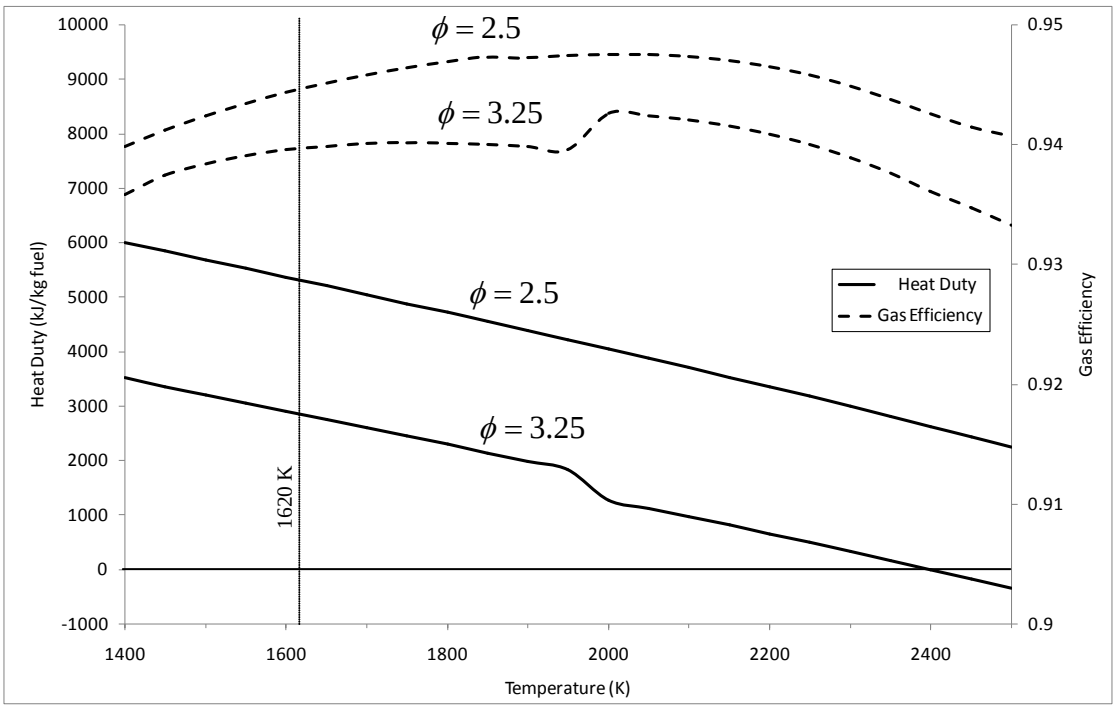

Figure 6-7: Heat duty and gas efficiency vs. temperature for coal oxidized by oxygen.

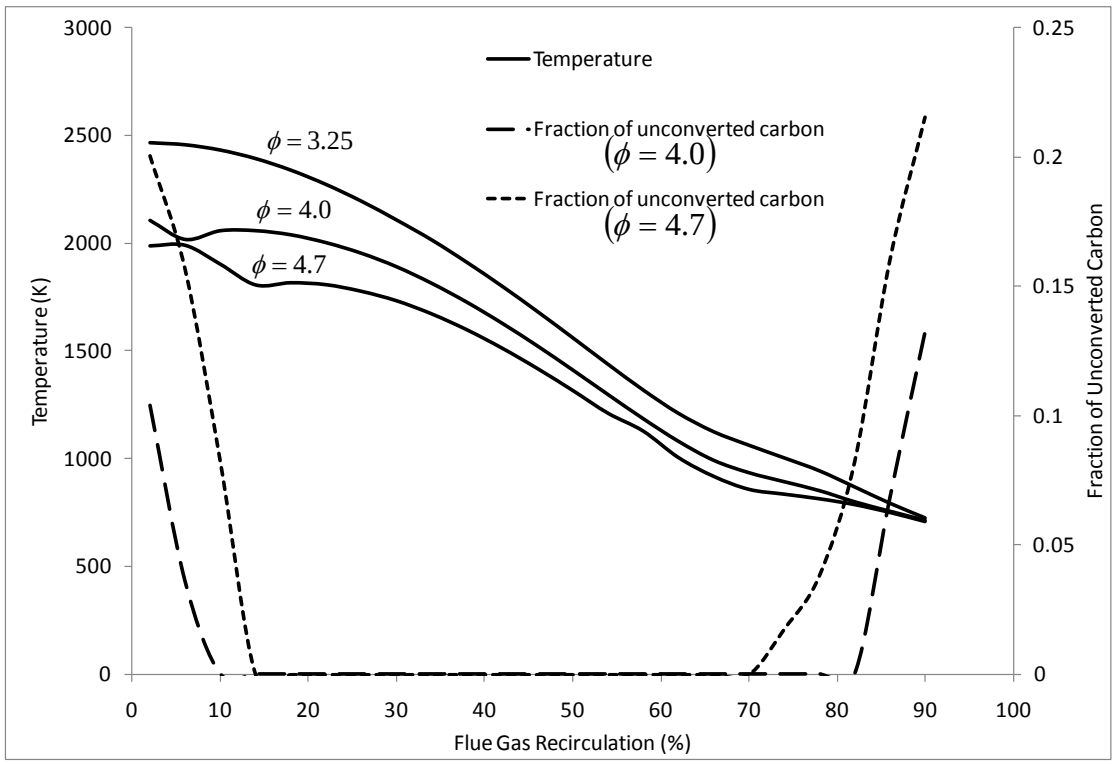

Figure 6-8: Adiabatic reactor temperature vs. percent FGR with flue gas from combustion with pure oxygen.

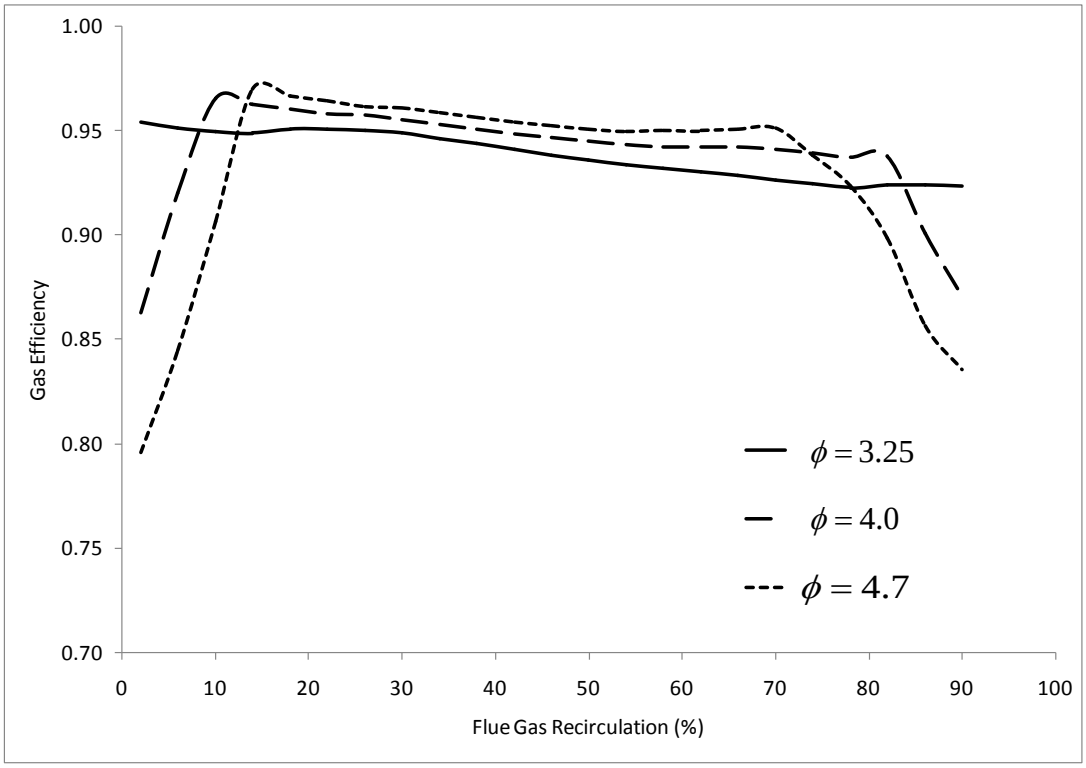

Figure 6-9: Gas efficiency vs. percent FGR with flue gas from combustion with pure oxygen.

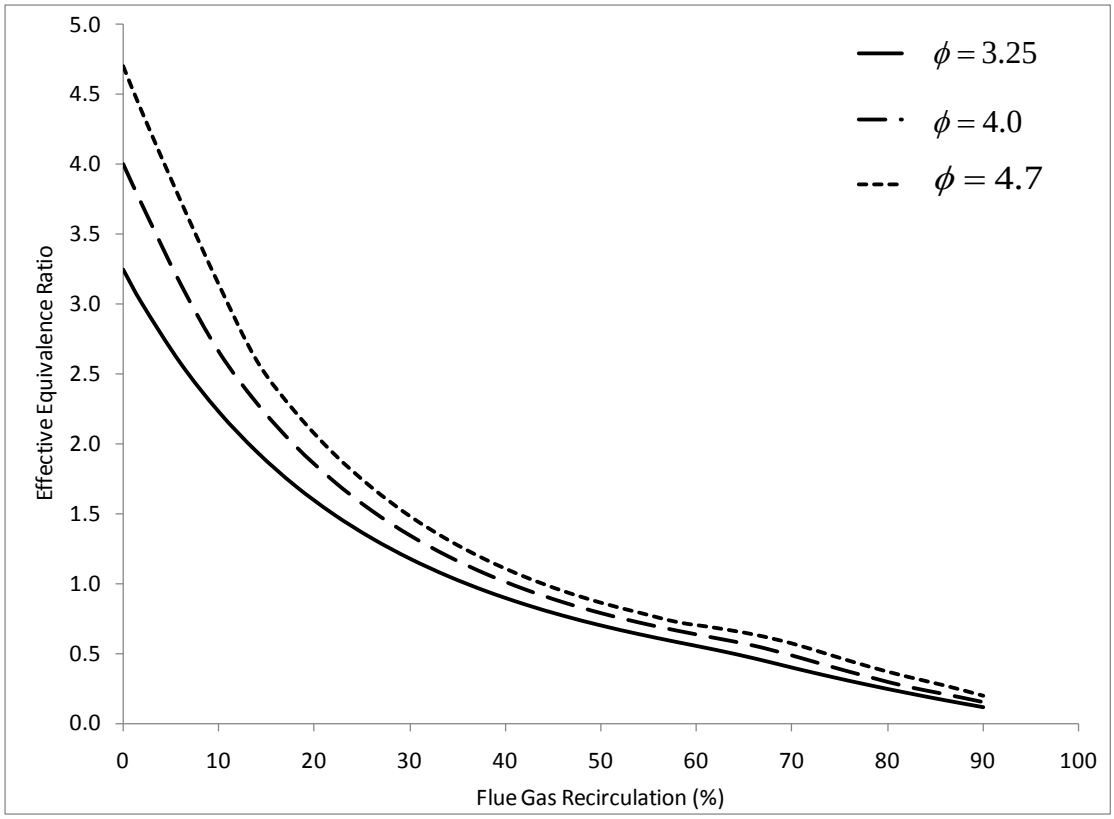

Figure 6-10: Effective equivalence ratio vs. percent FGR with flue gas from combustion with pure oxygen.

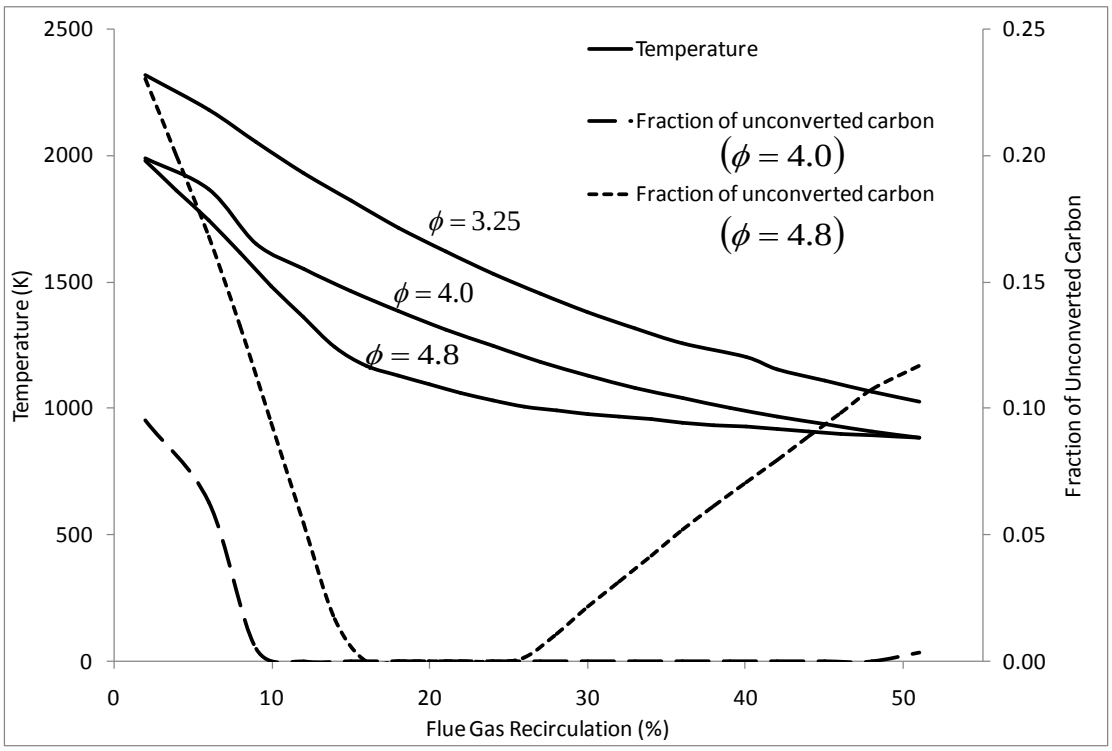

Figure 6-11: Adiabatic reactor temperatures vs. percent FGR with flue gas from combustion with air.

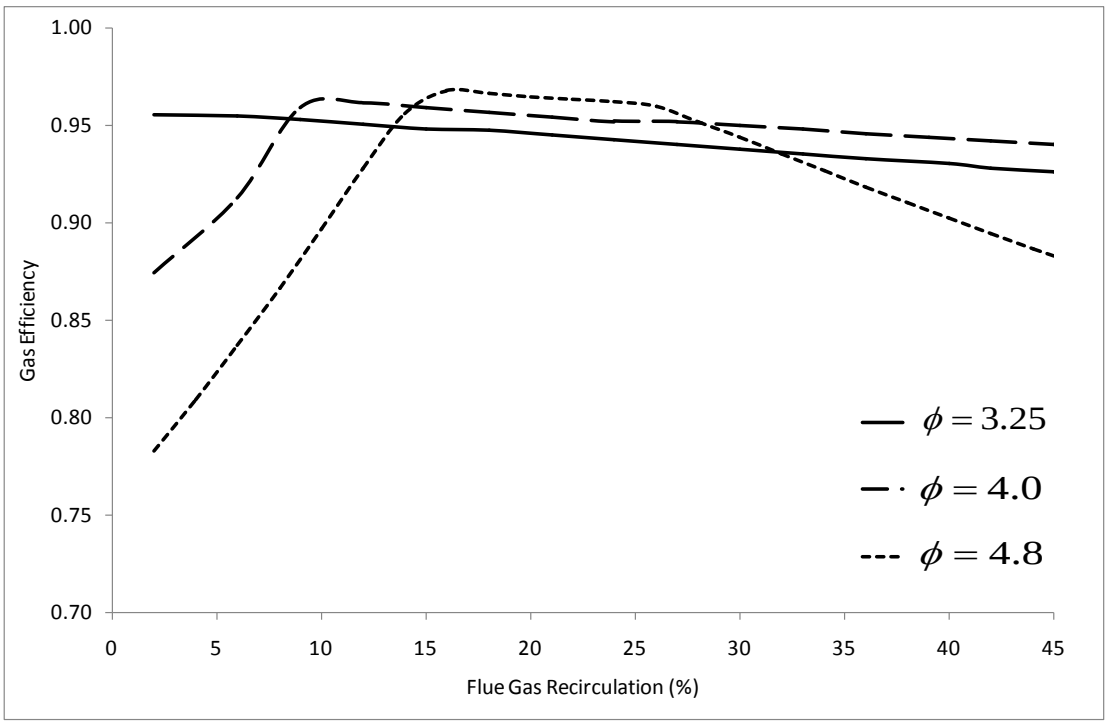

Figure 6-12: Gas efficiency vs. percent FGR with flue gas from combustion with air.

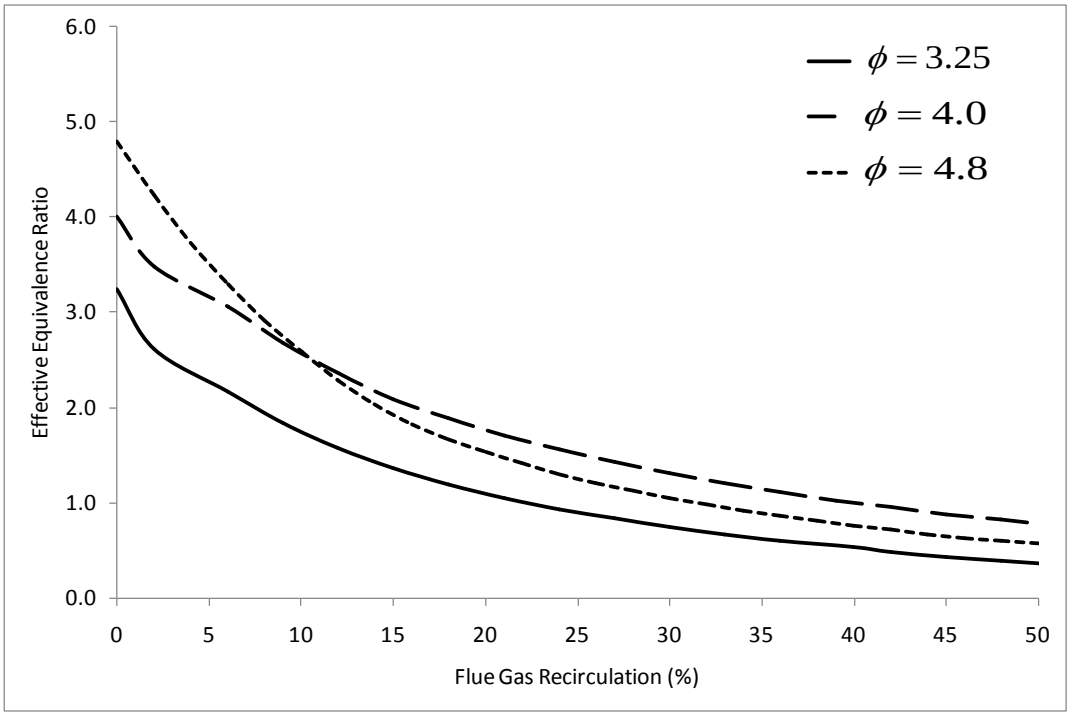

Figure 6-13: Effective equivalence ratio vs. percent FGR with flue gas from combustion with air.

CHAPTER 7: CONCLUSIONS

An investigation of gasification and oxyburn processes using exergy analysis has been conducted. Aspen Plus© was the platform used to carry out equilibrium simulations involving the conversion of solid technical fuels to producer gas. Models not used in this work were developed for the future capability of simulating tar-laden producer gas and solid fuel drying. In addition, an internal combustion engine model was developed based on closed-system thermodynamics and successfully integrated into the open-system realm of Aspen Plus©. Comparison of the developed model with a similar model from the literature verified that it produced reasonably accurate engine performance results.

A methodology has been presented to evaluate different fuels for gasification. The equivalence ratio and temperature at which the carbon boundary point occurs were confirmed to be the most important factors in determining the effectiveness of gasifying a fuel with air. When evaluating a fuel for gasification, it is important to consider if the carbon boundary point temperature falls below 1050 K, which is the transition temperature of the water-gas shift reaction. Three fossil fuels and three biomass fuels were compared to determine the effectiveness of gasifying them. Coal displayed the largest exergetic efficiency owing to its highest adiabatic reactor temperature. The three biomass fuels displayed similar exergetic efficiencies and were higher than those of petcoke and Orimulsion as a result of their carbon boundary points occurring at higher equivalence ratios. In addition, the rational efficiency was found to be an impractical indicator of gasifier performance with variation of the equivalence ratio. A new exergetic efficiency, deemed the gas efficiency, was proposed that considered solid carbon in the products as an exergy loss.

A thermodynamic study of gas separation processes was also investigated to compare the theoretical minimum work required to capture CO_2. Two systems were compared, the first being an oxyburn process that used gas separation at the front end of

the plant to produce pure oxygen for oxidation of coal, and CO_2 was separated from H_2O via condensation of combustion products. The second system used air to oxidize coal, and CO_2 was separated from combustion exhaust that included N_2. In terms of energy requirement to capture CO_2, the oxyburn process has the potential to compete with the second process. However, for the oxyburn process to be competitive, it must be operated at an overall equivalence ratio closer to stoichiometric to avoid wasting excess O_2. In addition, if the oxyburn process is to be practical, the reactor temperature must be lowered. Heat extraction via a cooling jacket may be too difficult and costly, but flue gas recirculation has the potential to effectively bring the reactor temperature down to reasonable material limits without significantly altering the performance of the gasifier. It was found that when flue gas recirculation is used, the equivalence ratio of the gasifier could be increased without depositing solid carbon in the products. Increasing the equivalence ratio also results in slightly higher exergetic efficiencies as well as decreased amounts of required flue gas recirculation to lower the reactor temperature. To effectively lower the reactor temperature, a higher percentage of flue gas must be recirculated back to the gasifier if the flue gas comes from combustion with pure O_2 instead of air. However, using pure O_2 for combustion instead of air has the advantage of requiring only one gas separation process at the front end of the plant if CO_2 capture is desired.

This work can be expanded upon in many ways. One of the more beneficial directions to which this work could lead would be a combination of exergy analysis with a zonal analysis of gasification. This work used a zero-dimensional gasifier, whereas a specific type of gasifier could be used to which a zonal analysis could be applied. Transport equations could be formed to link the different zones, and exergy analysis could be applied to each zone as well as the transport equations. In this way a more accurate model of a gasifier could be developed, and the most inefficient zones of the gasifier could be determined. Another key area in which this work can be expanded upon

would be an experimental validation of oxyburn processes with flue gas recirculation. The results presented in this work suggest that diluting the producer gas with low-exergy recirculated flue gas provides more advantages than disadvantages. However, these results were based on a zero-dimensional model, and if flue gas recirculation is feasible with oxyburn gasification, it must be determined the optimal location that the recirculated flue gas should be admitted to the gasifier. In addition it should be experimentally validated that using flue gas recirculation allows for the equivalence ratio to be increased while improving gasifier performance.

REFERENCES

Ahrenfeldt, J., Henriksen, U., Jensen, T.K., Gobel, B., Wiese, L., Kather, A., and Egsgaard, H. (2006). Validation of a continuous combined heat and power (CHP) operation of a two-stage biomass gasifier. *Energy and Fuels, 20,* 2672-2680.

Altafini, C.R., Wander, P.R., and Barreto, R.M. (2003). Prediction of the working parameters of a wood waste gasifier through an equilibrium model. *Energy Conversion and Management, 44,* 2763-2777.

Aspen Technology, Inc. (2000). Getting Started Modeling Processes with Solids.

Atkins, P.W. and de Paula, J. (2006). Physical Chemistry. New York: Oxford University Press.

Bade Shrestha, S.O. and Karim, G.A. (2001). An experimental and analytical examination of the combustion period for gas-fuelled spark ignition engine applications. Proceedings of the Institution of Mechanical Engineers; Part A; Journal of Power and Energy, 215, 63-74.

Bayraktar, H., and Durgun, O. (2003). Mathematical modeling of spark-ignition engine cycles. *Energy Sources, 25,* 651-666.

Bergman, P.C.A, van Paasen, S.V.B., and Boerrigter, H. (2002). *The novel "OLGA" technology for complete tar removal from biomass producer gas.* Presented at Pyrolysis and Gasification of Biomass and Waste Expert Meeting. 1 September 2002.

Biagini, E., Fantozzi, C., and Tognotti, L. (2004). Characterization of devolatilization of secondary fuels in different conditions. *Combustion Science and Technology, 176,* 685-703.

Blevins, L.G. and Cauley, T.H. (2005). Fine particulate formation during switchgrass/coal cofiring. *Journal of Engineering for Gas Turbines and Power, 127,* 457-463.

Brammer, J.G., and Bridgwater, A.V. (2002). The influence of feedstock drying on the performance and economics of a biomass gasifier-engine CHP system. Biomass and *Bioenergy, 22,* 271-281.

Brammer, J.G., and Bridgwater, A.V. (1999). Drying technologies for an integrated gasification bio-energy plant. *Renewable and Sustainable Energy Reviews, 3,* 242-289.

Bridgwater, A.V., Elliott, D.C., Fagernas, L., Gifford, J.S., Mackie, K.L., and Toft, A.J. (1995). The nature and control of solid, liquid, and gaseous emissions from the thermochemical processing of biomass. *Biomass and Bioenergy, 9,* 325-341.

Brown, R.C. (2003). Biorenewable Resources: Engineering New Products from Agriculture. Ames, Iowa: Iowa State Press.

Cao, Y., Wang, Y., Riley, J., and Pan, W. (2006). A novel biomass air gasification process for producing tar-free higher heating value fuel gas. *Fuel Processing Technology, 87*, 343-353.

Cummer, K.R., and Brown, R.C. (2002). Ancillary equipment for biomass gasification. *Biomass and Bioenergy, 23*, 113-128.

Devi, L., Ptasinski, K.J., and Janssen, F.J.J.G. (2003). A review of the primary measures for tar elimination in biomass gasification processes. *Biomass and Bioenergy, 24*, 125-140.

Elliot, D.C. 1988. "Relation of reaction time and temperature to chemical composition of pyrolysis oils," ACS Symposium Series 376, *Pyrolysis Oils from Biomass*. Edited by E.J. Soltes and T.A. Milne. Denver, CO. April 1987.

Evans, R.J. and Milne, T.A. (1987). Molecular characterization of the pyrolysis of biomass. 1. Fundamentals. *Energy & Fuels, 1*, 123-138.

Evans, R.J. and Milne, T.A. (1997). "Chemistry of tar formation and maturation in the thermochemical conversion of biomass," in *Developments in Thermochemical Biomass Conversion, Vol. 2.* Edited by A.V. Bridgewater and D.G.B. Boocock. London: Blackie Academic and Professional, 803-816.

Ferguson, C.R. and Kirkpatrick, A.T. (2001). *Internal Combustion Engines, Second Edition*. New York: John Wiley & Sons, Inc.

Frassoldati, A., Faravelli, T., and Ranzi, E. (2007). The ignition, combustion and flame structure of carbon monoxide/hydrogen mixtures. Note 1: Detailed kinetic modeling of syngas combustion also in presence of nitrogen compounds. *International Journal of Hydrogen Energy, 32*, 3471-3485.

Hasler, P., and Nussbaumer, Th. (1999). Gas cleaning for IC engine applications form fixed bed biomass gasification. *Biomass and Bioenergy, 16*, 385-395.

Hernandez, J., Lapuerta, M., and Serrano, C. (2005). Estimation of the laminar flame speed of producer gas from biomass gasification. *Energy & Fuels, 19*, 2172-2178.

Hernandez, J.J., Serrano, C., and Perez, J. (2006). Prediction of the autoignition delay time of producer gas from biomass gasification. *Energy and Fuels, 20*, 532-539.

Heywood, J. (1988). *Internal Combustion Engine Fundamentals*. New York: McGraw-Hill.

Higman, C. (2003). *Gasification*. Boston: Elsevier/Gulf Professional Publishing.

Ho, M.T., Allinson, G., and Wiley, D.E. (2006). Comparison of CO2 separation options for geo-sequestration: are membranes competitive? *Desalination, 192*, 288-295.

Ilbas, M., Crayford, A.P., Yilmaz, I., Bowen, P.J., Syred, N. (2006). Laminar-burning velocities of hydrogen-air and hydrogen-methane-air mixtures: An experimental study. *International Journal of Hydrogen Energy, 31*, 1768-1779.

Kearns, D.T. and Webley, P.A. (2004). Application of an adsorption non-flow exergy function to an exergy analysis of a pressure swing adsorption cycle. *Chemical Engineering Science, 59,* 3537-3557.

Kinoshita, C.M., and Zhou, Y.W. (1994). Tar formation under different biomass gasification conditions. *Journal of Analytical and Applied Pyrolysis, 29,* 169-181.

Lee, D., Yang, H., Yan, R., and Liang, D. (2007). Prediction of gaseous products form biomass pyrolysis through combined kinetic and thermodynamic simulations. *Fuel, 86,* 410-417.

Li, H., and Karim, G. (2006). Experimental investigation of the knock and combustion characteristics of CH4, H-2, CO, and some of their mixtures. *Proceedings of the Institution of Mechanical Engineers Part A-Journal of Power and Energy, 220,* 459-471.

Liao, C., Wu, C., and Yan, Y. (2007). The characteristics of inorganic elements in ashes from a 1 MW CFB biomass gasification power generation plant. *Fuel Processing Technology, 88,* 149-156.

Matheiu, P. and Dubuisson, R. (2002). Performance analysis of a biomass gasifier. *Energy Conversion and Management, 43,* 1291-1299.

Miller, B.G. (2005). *Coal Energy Systems*. Boston: Elsevier Academic Press.

Miller, C.A. and Srivastava, R.K. (2000). The combustion of Orimulsion and its generation of air pollutants. *Progress in Energy and Combustion Science, 26,* 131-160.

Milne, T.A., Evans, R.J., and Abatzoglou, N. (1998). Biomass gasifier "tars": their nature, formation, and conversion. US Department of Energy.

Moran, M.J. (1989). *Availability Analysis* (Corrected Ed.). New York: ASME Press.

Moran, M.J., and Shapiro, H.N. (2008). *Fundamentals of Engineering Thermodynamics: Fifth Edition.* New York, NY: John Wiley & Sons, Inc.

Morf, P., Hasler, P., and Nussbaumer, T. (2002). Mechanisms and kinetics of homogeneous secondary reactions of tar from continuous pyrolysis of wood chips. *Fuel, 81,* 843-853.

Munoz, M., Moreno, F., Morea-Roy, J., Ruiz, J., and Arauzo, J. (2000). Low heating value gas on spark ignition engines. *Biomass and Bioenergy, 18,* 431-439.

Natarajan, J., Lieuwen, T., and Seitzman, J. (2007). Laminar flame speeds of H_2/CO mixtures: effect of CO_2 dilution, preheat temperature, and pressure. *Combustion and Flame, 151,* 104-119.

Newby, R., Yang, W., and Bannister, R. (2000). Fuel gas cleanup parameters in air-blown IGCC. *Journal of Engineering for Gas Turbines and Power, 122,* 247-254.

Osowski, S. and Fahlenkamp, H. (2006). Regenerative energy production using energy crops. *Industrial Crops and Products, 24,* 196-203.

Phillips, S.D. (2007). Technoeconomic analysis of a lignocellulosic biomass indirect gasification process to make ethanol via mixed alcohols synthesis. *Industrial and Engineering Chemistry Research, 46*, 8887-8897.

Porpatham, E., Ramesh, A., and Nagalingam, B. (2007). Effect of hydrogen addition on the performance of a biogas fuelled spark ignition engine. *International Journal of Hydrogen Energy, 32*, 2057-2065.

Prins, M.J., Ptasinski, K.J., Janssen, F.J.J.G. (2007). From coal to biomass gasification: comparison of thermodynamic efficiency. *Energy, 32*, 1248-1259.

Prins, M.J., Ptasinski, K.J., and Janssen, F.J.J.G. (2003). Thermodynamics of gas-char reactions: first and second law analysis. *Chemical Engineering Science, 58*, 1003-1011.

Prins, M.J. and Ptasinski, K.J. (2005). Energy and exergy analyses of the oxidation and gasification of carbon. *Energy, 30*, 982-1002.

Proll, T., Siefert, I., Friedl, A., and Hofbauer, H. (2005). Industrial & Engineering Chemical Research, 44, 1576-1584.

Ptasinski, K.J., Prins, M.J., Pierik, A. (2007). Exergetic evaluation of biomass gasification. *Energy, 32*, 568-574.

Ramos, J.I. (1989). *Internal Combustion Engine Modeling*. New York: Hemisphere Publishing Company.

Rezaiyan, J. (2005). Gasification Technologies: A Primer for Engineers and Scientists. Boca Raton: Taylor & Francis.

Skjoth-Rasmussen, M.S., Glarborg, P., Ostberg, M., Johannessen, J.T., Livbjerg, J., Jensen, A.D., and Christensen, T.S. (2004). Formation of polycyclic aromatic hydrocarbons and soot in fuel-rich oxidation of methane in a laminar flow reactor. *Combustion and Flame, 136*, 91-128.

Sridhar, G., Sridhar, H, Dasappa, S., Paul, P., Rajan, N., and Mukunda, H. (2005). Development of producer gas engines. *Proceedings of the Institution of Mechanical Engineers Part D-Automobile Engineering, 219*, 423-438.

Sridhar, G., Paul, P., and Mukunda, H. (2001). Biomass derived producer gas as a reciprocating engine fuel—an experimental analysis. *Biomass and Bioenergy, 21*, 61-72.

Standard Laboratories. (2006). Knight Hawk Coal. Sample ID: 20060032308.

Szargut, J. (2005). Exergy Method: Technical and Ecological Applications. Great Britain: WIT Press.

Szargut, J., Morris, D.R., and Steward, F.R. (1988). Exergy Analysis of Thermal, Chemical, and Metallurgical Processes. New York: Hemisphere.

Tinaut, F.V., Melgar, A., Horrillo, A., and Diez de la Rosa, A. (2006). Method for predicting the performance of an internal combustion engine fuelled by producer gas and other low heating value gases. *Fuel Processing Technology, 87*, 135-142.

Torres, W., Pansare, S., and Goodwin, J. (2007). Hot gas removal of tars, ammonia, and hydrogen sulfide from biomass gasification gas. *Catalysis Reviews, 49*, 407-456.

University of Iowa Facilities Management. Utilities and Energy Management. 4 November 2008. <http://facilities.uiowa.edu/uem/uemindex.htm>

van Dyk, J.C., and Waanders, F.B. (2007). Manipulation of gasification coal feed in order to increase the ash fusion temperature of the coal enabling the gasifiers to operate at higher temperatures. *Fuel, 86*, 2728-2735.

van Paasen, S.V.B., and Kiel, J.H.A. (2004). *Tar formation in fluidized-bed gasification- impact of gasifier operating conditions.* Presentation to 2nd World Conference and Technology Exhibition on Biomass for Energy, Industry, and Climate Protection. 10 May 2004.

Wierzba, I., Bade Shrestha, S.O., and Karim, G.A. (1996). An approach for predicting the flammability limits of fuel/diluent mixtures in air. *Journal of the Institute of Energy, 69*, 122-130.